2005

Frequency Domain Independent Component Analysis Applied To Wireless Communications Over Frequency-selective Channels

Yuan Liu
University of Central Florida

FREQUENCY DOMAIN INDEPENDENT COMPONENT ANALYSIS APPLIED TO WIRELESS COMMUNICATIONS OVER FREQUENCY-SELECTIVE CHANNELS

by

YUAN LIU
B.S. Huazhong University of Science and Technology, China, 1997
M.S. Huazhong University of Science and Technology, China, 2000
M.S. University of Central Florida, 2004

A dissertation submitted in partial fulfillment of the requirements
for the degree of Doctor of Philosophy
in the Department of Electrical and Computer Engineering
in the College of Engineering and Computer Science
at the University of Central Florida
Orlando, Florida

Fall Term
2005

Major Professor: Dr. Wasfy B. Mikhael

ABSTRACT

In wireless communications, frequency-selective fading is a major source of impairment for wireless communications. In this research, a novel Frequency-Domain Independent Component Analysis (ICA-F) approach is proposed to blindly separate and deconvolve signals traveling through frequency-selective, slow fading channels. Compared with existing time-domain approaches, the ICA-F is computationally efficient and possesses fast convergence properties. Simulation results confirm the effectiveness of the proposed ICA-F.

Orthogonal Frequency Division Multiplexing (OFDM) systems are widely used in wireless communications nowadays. However, OFDM systems are very sensitive to Carrier Frequency Offset (CFO). Thus, an accurate CFO compensation technique is required in order to achieve acceptable performance. In this dissertation, two novel blind approaches are proposed to estimate and compensate for CFO within the range of half subcarrier spacing: a Maximum Likelihood CFO Correction approach (ML-CFOC), and a high-performance, low-computation Blind CFO Estimator (BCFOE).

The Bit Error Rate (BER) improvement of the ML-CFOC is achieved at the expense of a modest increase in the computational requirements without sacrificing the system bandwidth or increasing the hardware complexity. The BCFOE outperforms the existing blind CFO estimator [25, 128], referred to as the YG-CFO estimator, in terms of BER and Mean Square Error (MSE), without increasing the computational complexity, sacrificing the system bandwidth, or increasing the hardware complexity. While both proposed techniques outperform the YG-CFO estimator, the BCFOE is better than the ML-CFOC technique. Extensive simulation results illustrate the performance of the ML-CFOC and BCFOE approaches.

This work is dedicated to my parents, far away in China, and Yali Xiong.

ACKNOWLEDGMENTS

I would like to express my sincere respect and gratitude to my advisor, Dr. Wasfy B. Mikhael, for his seasoned guidance and help throughout my Ph.D. study. His great wisdom and constant encouragement helped me overcome difficulties that I have encountered through my graduate study and research.

I would also like to express my appreciation to the distinguished members of the dissertation committee: Dr. David Chester, Dr. Albert Berg, Dr. Michael Haralambous, and Dr. Thomas Xinzhang Wu.

I sincerely thank Dr. Brent Myers for his valuable comments and guidance. I express sincere appreciation to Conexant Systems, Inc. for supporting this work.

I thank faculty and staff in the Department of Electrical and Computer Engineering at the University of Central Florida. They helped me a great deal during my study period.

I am grateful to my parents for their encouragement and support during my study in the USA.

TABLE OF CONTENTS

LIST OF FIGURES

LIST OF TABLES

LIST OF ACRONYMS/ABBREVIATIONS

BER	Bit Error Rate
BSS	Blind Source Separation
CDMA	Code Division Multiple Access
CFO	Carrier Frequency Offset
CLT	Central Limit Theorem
CMA	Constant Modulus Algorithm
DAB	Digital Audio Broadcasting
DFT	Discrete Fourier Transform
DQPSK	Differential Quadrature Phase-Shift Keying
DSP	Digital Signal Processing
DVB	Digital Video Broadcasting
FEC	Forward Error Correction
FFT	Fast Fourier Transform
HiperLAN 2	High Performance Radio Local Area Networks type 2
ICA	Independent Component Analysis
ICI	Intercarrier Interference
IDFT	Inverse Discrete Fourier Transform
IFFT	Inverse Fast Fourier Transform
ISI	Intersymbol Interference
MCM	Multicarrier Modulation
MIMO	Multiple-Input Multiple-Output

MMAC	Mobile Multimedia Access Communications
OFDM	Orthogonal Frequency Division Multiplexing
PDF	Probability Density Function
QAM	Quadrature Amplitude Modulation
QPSK	Quadrature Phase Shift Keying
RF	Radio Frequency
STFT	Short Time Fourier Transform
SNR	Signal to Noise Ratio
WLAN	Wireless Local Area Networks
WMAN	Wireless Metropolitan Area Networks
WSSUS	Wide-Sense Stationary Uncorrelated Scattering

CHAPTER ONE: INTRODUCTION

The first-generation (1G) radio systems use analog communication techniques to transmit voice over radio, such as Advanced Mobile Phone Services (AMPS), Nordic Mobile Telephone (NMT) systems, and Total Access Communication Systems (TACS), which were developed in the 1970s and 1980s. The 2G systems were built in the 1980s and 1990s, and featured the implementation of digital technology, such as Global System for Mobile communications (GSM), Digital-AMPS (D-AMPS), Code Division Multiple Access (CDMA), and Personal Digital Cellular (PDC). Among them, GSM is the most successful and common 2G system.

The 3G mobile technologies, which developed rapidly in the 1990s, provide users with high-rate mobile access. Three major radio air interface standards for 3G are Wideband CDMA (WCDMA), Time Division Synchronous-CDMA (TD-SCDMA), and CDMA2000. The transmitted rate of 3G is up to 144 kb/s for high-mobility traffic, 384 kb/s for low-mobility traffic, or 2 Mb/s in good conditions. However, there are two limitations associated with 3G. One is that CDMA cannot provide very high rate service, such as 100 Mb/s, due to excessive interference between services. The other is the difficulty in providing a full range of multirate services with different Quality of Service (QoS) and performance requirements. Therefore, the future mobile communication system with features of high-rate transmission and open network architecture, called 4G, is desired to satisfy the increasing demand for broadband wireless access. The key objectives of 4G are to provide reliable transmissions with peak rates ranging from 100 Mb/s for high-mobility applications to 1 Gb/s for low-mobility applications. In addition,

4G achieves high spectrum efficiency up to 10 b/s/Hz, and provides ubiquitous services that can accommodate various radio accesses [126].

These wireless revolutions have brought unprecedented excitement into the field of Signal Processing. In recent years, Blind Signal Separation (BSS) techniques have been intensively explored. BSS requires neither prior system knowledge nor any training sequence. Moreover, BSS is usually robust to multipath fading. Consequently, the BSS techniques are promising in increasing the capacity and reliability of wireless systems [40, 41, 58].

This chapter is organized as follows. In Section 1.1, multipath fading mechanism and model are studied. Section 1.2 presents BSS via Independent Component Analysis (ICA). A popular ICA method, the natural-gradient ICA algorithm, is also introduced. In Section 1.3, the properties of ICA applied to wireless communications are discussed. Frequency-selective fading and fast fading are two major obstacles to applying ICA in wireless communications. The organization of this dissertation is summarized in Section 1.4.

The mathematical notations used throughout this research work are listed in Table 1.

Table 1
Mathematical notations

$(.)^T$	Transposition
$(.)^*$	Conjugation
$(.)^H$	Conjugate transposition
$E[.]$	Expectation
$\mathrm{Re}(.)$	Extracting real-valued scalar
$Max(.)$	Selecting maximum value
$(.) \bmod M$	Modulus after division by M
$diag(.)$	Forming a diagonal matrix whose diagonal elements are chosen from the vector
$\lvert . \rvert$	Absolute value
$\lVert . \rVert$	Norm of a vector
$\leftarrow$	Substituting the variable on the left-hand side with the value on the right-hand side
$\otimes$	Convolution
$\approx$	Approximate equal
$\delta(n)$	Dirac delta function
μ	Convergence factor used in the gradient method
I	Identity matrix

1.1 Multipath Fading Channel

Transmission in wireless communication systems is carried out in the radio wave propagation environment, which places fundamental limitations on the performance of wireless communications. An accurate characterization of the propagation channel is an essential requirement for a successful design of reliable communication systems. It is thus crucial to have a good knowledge of radio fading channels [48, 97, 100, 111].

The origin of fading mechanism for wireless channels is traced to the scattering of an electromagnetic wave by a random medium. There are three basic mechanisms that impact the electromagnetic wave propagation in wireless communications. They are reflection, diffraction, and scattering [112, 113]:

- Reflection occurs when a propagating electromagnetic wave impinges on a smooth surface with very large dimensions compared with the RF signal wavelength.
- Diffraction occurs when the radio path between a transmitter and a receiver is obstructed by a dense body with large dimensions compared with the RF signal wavelength.
- Scattering occurs when a radio wave impinges on either a large rough surface or any surface whose dimensions are on the order of the RF signal wavelength.

Large-Scale and Small-Scale Fading

Two types of fading affect signals transmitted over fading channels: large-scale fading and small-scale fading. Large-scale fading represents the average signal power attenuation or the path loss due to motion over large areas. This phenomenon is affected by prominent terrain contours between a transmitter and a receiver. The receiver is often represented as being shadowed by such prominences. The statistics of large-scale fading

provide a way of computing an estimate of path loss as a function of distance. This is described in terms of a mean-path loss and a log-normally distributed variation about the mean.

Small-scale fading refers to the dramatic changes in the signal amplitude and phase that can be experienced as a result of small changes in the spatial separation between a transmitter and a receiver. Small-fading manifests itself in two mechanisms, namely, time-spreading of the signal, and time-variant behavior of the channel. The time-spreading manifestation results from non-optimum impulse responses of fading channels. This time-spreading mechanism is characterized in the time-delay domain as a multipath delay spread, T_d. The channel is time-variant because of motions between the receiver and the transmitter, and propagation path changing. The time-variant mechanism is characterized in the time domain as a channel coherence time, T_c.

Types of Small-Scale Fading

Provided the transmitted symbol period, T_s, the transmitted signal undergoes flat fading if

$$T_s > T_d \tag{1.1.a}$$

Otherwise, the transmitted signal undergoes frequency-selective fading if

$$T_s < T_d \tag{1.1.b}$$

For the flat-fading channel, all received multipath components of a symbol arrive within the symbol time duration. Hence, these components are not resolvable. Here, there is no channel-induced Intersymbol Interference (ISI) distortion, since the time-spreading does not result in significant overlap between neighboring received symbols.

For the frequency-selective fading channel, the received multipath components of a symbol extend beyond the symbol's time duration. Such multipath dispersion yields the channel-induced ISI.

A fading channel is also classified either as fast fading or slow fading. In a fast fading channel, the channel impulse response changes rapidly within T_s, i.e., T_c is smaller than T_s as:

$$T_s > T_c \tag{1.2.a}$$

In a slow fading channel, T_c is larger than T_s as:

$$T_s < T_c \tag{1.2.b}$$

Fast fading describes a condition where the time duration in which the channel behavior in a correlated manner is short compared with the time duration of a symbol. Therefore, it can be expected that the fading character of the channel changes several times while a symbol is propagating, leading to distortion of the basedband pulse shape.

The time duration in which the slow-fading channel behaves in a correlated manner is long compared with the time duration of a transmission symbol. Thus, one can expect the channel state to virtually remain unchanged during the time in which a symbol is transmitted. The propagation symbols do not likely suffer from the pulse distortion described above.

Wide-Sense Stationary Uncorrelated Scattering (WSSUS) Channel

In wireless communications, transmitted signals travel through multiple paths; this phenomenon is referred to as multipath propagation. This effect can cause fluctuations in the received signal's amplitude, phase, and angle of arrival. Multipath

propagation is a very common phenomenon of radio communication channels, and a major source of impairment for wireless communication systems.

Bello introduced a simple, common-used fading channel model: Wide-Sense Stationary Uncorrelated Scattering (WSSUS) channel [13]. This model treats signal variations arriving with different delays as uncorrelated. Bello proved that the WSSUS channel is effectively Wide-Sense Stationary (WSS) in both the time domain and the frequency domain. Mathematically, the WSSUS channel can be regarded as a time-varying linear filter, with baseband impulse response $h(t,\tau)$ given by:

$$h(t,\tau) = \sum_{p=0}^{P-1} \rho_p(t) \exp\left(j\alpha_p(t)\right) \delta\left(\tau - \tau_p(t)\right) \tag{1.3}$$

where P is the number of multipath components, $\rho_p(t)$, $\alpha_p(t)$, and $\tau_p(t)$ are the magnitude, the phase, and the multipath delay of the pth multipath component, respectively. The variable τ represents the excess time delay of the multipath component in the channel at a specific time t.

When there is no line-of-sight path between the transmitter and the receiver, $\rho_p(t)$ is statistically described by the Rayleigh distribution. This type of fading is called Rayleigh fading. On the other hand, in the presence of the line-of-sight path, $\rho_p(t)$ is statistically described by the Rician distribution, and this fading is called Rician fading.

1.2 Blind Source Separation via Independent Component Analysis

BSS is now one of the most prominent areas in Digital Signal Processing (DSP) with solid theoretical foundations and numerous potential applications [32, 80, 81, 95, 96]. In fact, BSS has become a very important research topic in many areas, such as [24]:

- Biomedical Signal Processing; biomedical signals acquired with multi-electrode devices, such as electrocardiography (ECG), electromyography (EMG), electroencephalography (EEG) and magnetoencephalography (MEG).
- Speech and Audio Enhancement where BSS is applied to separate and deconvolve the source signals.
- Digital Communication Systems where BSS is applied to separate the source signals from the interference signals.
- Data Mining where BSS is applied to find hidden factors in available data.

Independent Component Analysis (ICA) is the most widely used method to perform BSS. In ICA, unknown source signals are extracted from sensor measurements, which are the unknown combinations of the source signals [17, 27, 53, 54]. The lack of prior knowledge about the combination is compensated by statistically strong but physically plausible assumption that the source signals are independent and non-Gaussian.

ICA Formulation

The standard ICA model assumes the existence of M source signals, $s_m(n)'s$, $m = 0,1,...M\text{-}1$, and M received signals $x_m(n)'s$. Without loss of generality, the $s_m(n)'s$ and the $x_m(n)'s$ are assumed to be zero-mean. If this is not true, then the received signals $x_m(n)'s$ can always be centered by subtracting the sample mean, which

makes the model zero-mean. For simplicity, noise terms are omitted in the problem formulation. This noise-free model is sufficient for many applications.

The source signal vector $S(n)$ and the received signal vector $X(n)$ are defined as:

$$S(n) = [s_0(n),..., s_m(n),..., s_{M-1}(n)]^T \tag{1.4.a}$$

and

$$X(n) = [x_0(n),..., x_m(n),..., x_{M-1}(n)]^T \tag{1.4.b}$$

respectively.

The $x_m(n)'s$ are the linear, instantaneous combinations of the $s_m(n)'s$. This scheme is represented compactly in the vector-matrix form as:

$$X(n) = AS(n) \tag{1.5}$$

where A is an unknown full-rank $M \times M$ matrix.

The ICA model is a generative model, which describes the received signals as being generated by a process of combining the source signals. The independent components are latent variables, meaning that they cannot be directly observed. Also, the combination matrix is assumed to be unknown. The task is to estimate the source signal vector $S(n)$ from the received signal vector $X(n)$ without knowing the combination matrix A. In general, it is very difficult. However, with some practical assumptions, the separation is feasible. The two basic assumptions are listed as following [17]:

- The columns of the combination matrix A are linearly independent so that the matrix A is invertible.
- The underlying components $s_m(n)'s$ are statistically independent and non-Gaussian.

The task of ICA is to determine the separating matrix W so that the separated signal vector $\tilde{S}(n)$ becomes an estimate of the source signal vector $S(n)$ as:

$$\begin{aligned}\tilde{S}(n) &= [\tilde{s}_0(n),...,\tilde{s}_m(n),...,\tilde{s}_{M-1}(n)]^T \\ &= WX(n)\end{aligned} \tag{1.6}$$

Since the combination matrix A is unknown, it is obvious that the two ambiguities associated with ICA hold [53, 118] as:

- The permutation ambiguity is that the order of the recovered signals $\tilde{s}_m(n)'s$ cannot be uniquely determined.
- The gain ambiguity is that the phase and amplitude of the recovered signals $\tilde{s}_m(n)'s$ cannot be determined.

In order to solve these ambiguities, additional prior information about the source signals and the combination is needed. Based on this idea, techniques to solve these two ambiguities are presented in the ICA algorithms devised in this research work.

Performance of ICA

The global system matrix C associated with the separating matrix W is defined as:

$$C = WA \tag{1.7}$$

The aim of ICA can be restated as making the global system matrix C in the form as:

$$C = PD \tag{1.8}$$

where P is the permutation matrix, and D is the diagonal matrix.

The matrix P and D are associated with the permutation ambiguity and the gain ambiguity, respectively.

The original source signals and the combination parameters are known in the simulation process. In this case, various performance indices are used to measure the performance of ICA. In this research work, crosstalk error, $CE(C)$, is used to measure the departure of the global system matrix C from the ideal case shown in (1.7) as:

$$CE(C)=\sum_{m=0}^{M-1}\left(\sum_{l=0}^{M-1}\frac{|C_{m,l}|^2}{\max\left(|C_{m,l}|^2\right)}-1\right)+\sum_{l=0}^{M-1}\left(\sum_{m=0}^{M-1}\frac{|C_{m,l}|^2}{\max\left(|C_{m,l}|^2\right)}-1\right) \tag{1.9}$$

where the $c_{m,l}$ is the $(m\ l)$ entry of the C.

In (1.9), the $CE(C)$ is zero when the source components are ideally separated as shown in (1.8). This index is invariant to permutation and gain ambiguities [81].

Principle of ICA

The principle of ICA can be explained through several different, but equivalent frameworks. Probably, the most intuitive framework is derived from the Central Limit Theorem (CLT). According to the CLT, if the source signals are non-Gaussian and independent, the distribution of their sum tends to be more Gaussian than the distribution of any individual one. That is to say that the separated signal $\tilde{s}_m(n)$ is maximally non-Gaussian if it equals one of $s_m(n)'s$. Thus, the basic ICA algorithm is based on the measurement of the non-Gaussianity of the separated signals [53].

The fourth-order cumulant, Kurtosis, is usually used to measure non-Gaussianity in ICA, because of its simplicity and useful properties [53]. Kurtosis of a complex random variables, $x_m(n)$, is defined as:

$$Kurt(x_m(n))=E\left[\left|x_m(n)\right|^4\right]-2\left(E\left[\left|x_m(n)\right|^2\right]\right)^2-\left|E\left[x_m^2(n)^4\right]\right|^2 \tag{1.10}$$

It is well known that Kurtosis of a Gaussian random variable equals zero. Generally, a random variable with a negative Kurtosis is said to be sub-Gaussian. A sub-Gaussian probability density tends to be flatter than the Gaussian one. If Kurtosis of a random variable is positive, this random variable is called super-Gaussian. A typical super-Gaussian probability density has a sharper peak and longer tails than the Gaussian one. Hence, Kurtosis measures the departure of a random variable from a Gaussian random variable.

In ICA algorithms, nonlinear functions are implicitly used to approximate Kurtosis. For sub-Gaussian and super-Gaussian signals, the nonlinear function $f(s)$ is usually chosen as:

$$f(s) = |s|^2 s \tag{1.11.a}$$

or

$$f(s) = \tanh(s) \tag{1.11.b}$$

respectively [5, 82].

In some ICA algorithms, first a cost function is set up. Then, the gradient method is used to optimize the cost function whose minimum corresponds to the separation case. In other words, using a cost function converts the ICA problem into an optimization problem. Usually, high-order statistical information about the source signals is used to build up the cost function [17, 18]. Given a cost function $J(W)$, the steepest-gradient method is given by:

$$W \leftarrow W - \mu \frac{\partial J(W)}{\partial W} \tag{1.12}$$

The steepest-gradient ICA algorithm is given by [12, 90]:

$$W \leftarrow W + \mu\left(\left(W^H\right)^{-1} + 2E\left[\tilde{S}_{non}(n)\tilde{S}^H(n)\right]\right) \tag{1.13}$$

where the nonlinear vector $\tilde{S}_{non}(n)$ is given by:

$$\tilde{S}_{non}(n) = \left[f\left(\tilde{s}_0(n)\right),..., f\left(\tilde{s}_m(n)\right),..., f\left(\tilde{s}_{M-1}(n)\right)\right]^T \tag{1.14}$$

Natural-Gradient ICA Algorithm

The gradient of the cost function $J(W)$ points in the steepest direction in the Euclidean orthogonal coordinate system. However, the parameter space is not always Euclidean but has a Riemannian metric structure. In such a case, the steepest direction is given by the so-called natural gradient. Thus, for the Riemannian parameter space, the standard gradient direction is no longer appropriate. The natural-gradient direction, on the other hand, uses the knowledge of the Riemannian distance structure of the parameter space to alter the gradient direction. Thus, the natural-gradient method provides fast and accurate adaptation behavior [3].

For any suitable smooth gradient-searchable cost function $J(W)$, the natural-gradient adaptation is defined as:

$$W \leftarrow W - \mu G^{-1}(W)\frac{\partial J(W)}{\partial W} \tag{1.15}$$

where $G(W)$ is the Riemannian metric tensor for the parameter W.

The natural-gradient ICA algorithm is given by [2, 3, 4]:

$$W \leftarrow W + \mu\left(I - E\left[\tilde{S}_{non}(n)\tilde{S}^H(n)\right]\right)W \tag{1.16}$$

Compared with the steepest-gradient ICA algorithm (1.13), the natural-gradient ICA algorithm (1.16) has the following advantages [50]:

- Low computational complexity. It is clear that no matrix inversion is needed in (1.16) compared with (1.13).

- Fast convergence.
- Equivariant property. Since the equivariant algorithm works well even if the combination matrix is ill-conditioned, the performance of the natural-gradient ICA algorithm is uniformly good for all combination matrices [19].

Fast Fixed-Point ICA Algorithm

Other than the natural-gradient ICA algorithm, there are numerous well-known, prominent ICA algorithms [42]. Among them, the Fast fixed-point ICA algorithm (FastICA) [55, 56, 57] has a number of desirable properties compared with other ICA algorithms.

- The convergence of the FastICA is cubic, or at least quadratic. This is in contrast to the natural-gradient ICA algorithm whose convergence is only linear. This means a very fast convergence.
- There are no step size parameters needed to choose, contrary to gradient-based algorithms. This means that the FastICA is easy to use.
- The performance of the FastICA can be optimized by choosing a suitable nonlinearity. In particular, one can obtain algorithms that are robust and/or of minimum variance.
- The independent components can be estimated one by one.

One iteration of the FastICA for find a row vector W_m^H of the separating matrix W is given by [14]:

$$\begin{aligned} W_m \leftarrow & E\left[X(n)\left(W_m^H X(n)\right)^* f\left(\left|W_m^H X(n)\right|^2\right)\right] \\ & - E\left[f\left(\left|W_m^H X(n)\right|^2\right) + \left|W_m^H X(n)\right|^2 f'\left(\left|W_m^H X(n)\right|^2\right)\right] W_m \end{aligned} \tag{1.17.a}$$

and

$$W_m \leftarrow \frac{W_m}{\|W_m\|} \tag{1.17.b}$$

where $f'(x)$ is the derivate of $f(x)$, and the nonlinear function $f(x)$ is chosen from one of these functions as:

$$f_1(x) = \frac{1}{2\sqrt{0.1+x}} \tag{1.18.a}$$

$$f_2(x) = \frac{1}{0.1+x} \tag{1.18.b}$$

and

$$f_3(x) = x \tag{1.18.c}$$

The one-unit algorithm in (1.17) can extended to the estimation of the whole ICA transformation. A simple way to accomplish this is a deflation scheme based on a Gram-Schmidt-like decorrelation. This decorrelation scheme is suitable for deflationary separation of the independent components. Sometimes, it is preferable to estimate all the independent components simultaneously, and use symmetric decorrelation [53].

Whitening Preprocessing

Whitening usually is the first step in ICA algorithms. The benefit of whitening is that the combination matrix becomes orthogonal. Instead of having to estimate the M^2 elements in the original combination matrix A, only $M(M-1)/2$ parameters in the orthogonal combination matrix are needed to be identified [53].

Let us define C_X as the covariance matrix of the received signal vector $X(n)$.

$$C_X = E\left[X(n)X^H(n)\right] \tag{1.19}$$

C_X can be expressed in the form of its eigenvalues $\lambda_m's$ and eigenvectors $\beta_m's$ as:

$$C_x = BDB^H \tag{1.20}$$

where D is the diagonal matrix of $\lambda_m's$ as:

$$D = diag(\lambda_0,...,\lambda_m,...,\lambda_{M-1}) \tag{1.21}$$

and B is the orthogonal matrix of $\beta_m's$ as:

$$B = [\beta_0,...,\beta_m,...\beta_{M-1}] \tag{1.22}$$

The whitening matrix of $X(n)$ can be expressed as:

$$V = D^{-1/2}B^H \tag{1.23}$$

where the matrix $D^{-1/2}$ is computed by a simple component-wise operation over $\lambda_m's$ as:

$$D^{-1/2} = diag(\lambda_0^{-1/2},...,\lambda_m^{-1/2},...,\lambda_{M-1}^{-1/2}) \tag{1.24}$$

The $X(n)$ is whitened by a linear transformation as:

$$\tilde{X}(n) = VX(n) \tag{1.25}$$

It is easy to prove

$$E[\tilde{X}(n)\tilde{X}^H(n)] = I \tag{1.26}$$

The natural-gradient ICA algorithm is summarized in Table 2.

Table 2
Outline of the natural-gradient ICA algorithm

Task: Estimate the source signals $S(n)$ from their linear mixture as:

$$X(n) = AS(n).$$

Step 1. Whiten the $X(n)$ through a linear transform given by:

$$\begin{aligned}\tilde{X}(n) &= VX(n) \\ &= D^{-1/2}BX(n)\end{aligned}$$

where D is the diagonal matrix of eigenvalues of the covariance matrix C_X, and B is the matrix of the eigenvectors of the covariance matrix C_X.

Step 2. Initialize the separation matrix $\tilde{W}$.

Step 3. Produce the $\tilde{S}(n)$ as:

$$\tilde{S}(n) = \tilde{W}\tilde{X}(n)$$

Step 4. Obtain the nonlinear vector $\tilde{S}_{non}(n)$ as:

$$\tilde{S}_{non}(n) = \left[f(\tilde{s}_0(n)),..., f(\tilde{s}_m(n))),..., f(\tilde{s}_{M-1}(n))\right]^T$$

where $f(s(n)) = |s(n)|^2 s(n)$ is used for sub-Gaussian signals, and $f(s(n)) = \tanh(s(n))$ is chosen for super-Gaussian signals.

Step 5. Update the separation matrix $\tilde{W}$ as:

$$\tilde{W} \leftarrow \tilde{W} + \mu\left(I - \tilde{S}_{non}(n)\tilde{S}^H(n)\right)\tilde{W}$$

Step 6. Normalize W using

$$\tilde{W} \leftarrow \tilde{W}\left(\tilde{W}^H\tilde{W}\right)^{-1/2}$$

Step 7. Check the convergence of $\tilde{W}$. If the convergence is not reached go back to **Step 3**, otherwise proceed to **Step 8**.

Step 8. The separating matrix corresponding to A is given by:

$$W = \tilde{W}V$$

Step 9. The recovered signal vector is given by:

$$\hat{S}(n) = V\tilde{S}(n)$$

1.3 Independent Component Analysis Applied to Wireless Communications

The wireless communication revolution has brought unprecedented excitement into the field of signal processing [49, 125]. On the other hand, communication over wireless channels presents formidable challenges to signal processing. Sophisticated signal processing techniques are necessary to cope with various issues ranging from efficient source and channel coding to modulation and receiver designs. As a powerful technique, ICA also arises in a wide variety of wireless communication applications, for example, digital radio with diversity, dually polarized radio channels, and multi-user/multi-access communications systems.

There are several reasons to apply ICA [24], such as:

- Training sequences for interference are often not available.
- In rapid time-varying channels, training may not be efficient.
- The system capacity can be increased by eliminating or reducing training sequences.
- Multi-path fading during the training period may lead to poor source or channel estimations.
- Training in distributed systems requires synchronization and/or sending a training sequence each time when a new link is to be set up. This may not be feasible in a multi-user scenario.

Both pros and cons exist when ICA is applied to wireless communications.

Pros of ICA Applied to Wireless Communications

In wireless communications, the source signals are man-made, and hence their properties are completely known in advance. There are ample structures that can be

exploited for high-performance ICA algorithms. This problem is semi-blind in the sense that certain additional prior information is available about the data model.

- The source signals are digitally modulated and discrete. In digital communications, binary or M-ary information is transmitted as discrete combinations of the amplitude and/or the phase of the carrier signal. Based on the discrete character of the source signal, computationally efficient algorithms can be realized [31, 45], and the steady-state performance of algorithms can be improved [79].
- The Probability Density Functions (PDFs) of the source signals are known. In communications, the signals are artificial; thus their properties are known exactly. Several ICA algorithms require knowledge of the PDFs of the source signals. Since the PDFs are completely predetermined, they can be exploited in these ICA algorithms. These resulting algorithms can achieve the desired performance based on a very small number of samples. Thus, adaptation to rapidly changing combination conditions, such as fast fading in mobile communications, becomes feasible [119, 120].
- The primary information about combination structure is partially available, and the combination mechanism is determined by a limited number of parameters. Prior combination information can be incorporated into the ICA algorithms to achieve low-computation and high-performance algorithms at a given number of data points [71-74].

Cons of ICA Applied to Wireless Communications

Mutlipath fading channel is the major challenge addressed by ICA in wireless communications. The relationship between types of fading and corresponding combination models is summarized in Fig. 1.

- If fading is frequency-independent, the combination model is instantaneous. Otherwise, if fading is frequency-selective, the combination model is convolutive.

- If fading is fast, the combination model is time-variant. Otherwise, if fading is slow, the combination model is time-invariant.

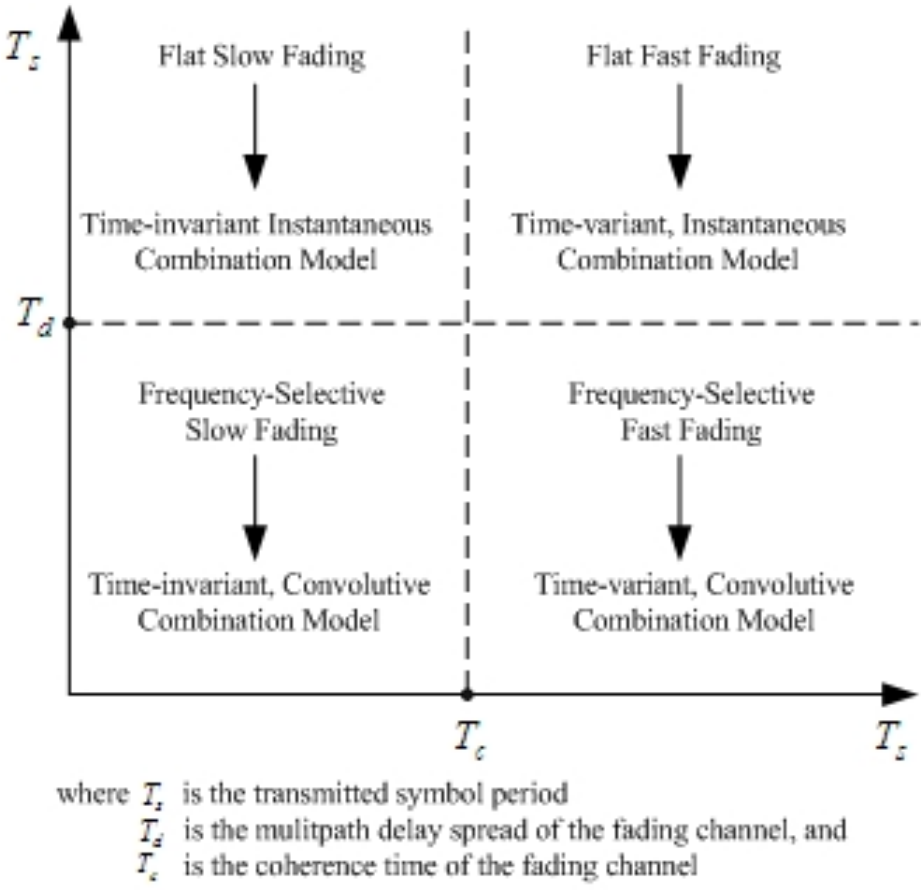

Figure 1: Types of fading experienced by the source signals and the corresponding combination models

The basic ICA model is instantaneous and time-invariant. The ICA algorithms developed in [62, 63] are proposed for this combination model, following flat, slow fading. Frequency-selective fading and fast fading result in convolutive and time-variant combinations, respectively. The convolutive or time-variant combination model is more

complicated than the basic ICA model. Thus, frequency-selective fading and fast fading are two major obstacles to applying ICA to wireless communications. Fast-convergence ICA algorithms devised in [127] are used to separate the time-variant, instantaneous combinations. The time-invariant, convolutive ICA combination is solved by the frequency-domain ICA algorithm developed in this dissertation. The most complicated situation, the time-variant, convolutive ICA combination model, remains open though.

1.4 Organization of the Dissertation

This dissertation is organized as follows:

- Chapter 2, "Frequency-Domain Independent Component Analysis," proposes a novel Frequency-Domain ICA (ICA-F) approach to separate the time-invariant, convolutive combinations of the digitally modulated signals. The ICA-F has lower computational complexity and faster convergence property than existing time-domain approaches.
- Chapter 3, "Carrier Frequency Offset in OFDM Systems," builds Carrier Frequency Offset (CFO) model in Orthogonal Frequency Division Multiplexing (OFDM) systems. In OFDM systems, transmission of data over orthogonal subcarriers results in robustness against ISI in the time domain. However, an OFDM system suffers more from CFO than the corresponding single carrier system. In this chapter, the CFO model is studied to provide some basis for the compensation approaches in the following two chapters.
- Chapter 4, "A Blind Maximum Likelihood Carrier Frequency Offset Correction Approach for OFDM Systems," proposes a novel Maximum Likelihood CFO Correction approach (ML-CFOC). The performance improvement of the ML-CFOC

has been achieved at the expense of a modest increase in the computational requirements.

- Chapter 5, “High-Performance Blind Carrier Frequency Offset Estimator for OFDM Systems”, proposes a novel Blind CFO Estimator (BCFOE) for OFDM systems. This novel approach outperforms the existing approaches [25, 128] with the same amount of computation.
- Chapter 6, “Contributions and Future Work”, summarizes the research work presented in this dissertation, and recommends further research directions.

CHAPTER TWO: FREQUENCY-DOMAIN INDEPENDENT COMPONENT ANALYSIS

In this chapter, a novel frequency-domain Independent Component Analysis (ICA-F) approach is proposed to blindly separate and deconvolve the convolutive combinations of digitally modulated signals in wireless communications. This approach relies on the fundamental observation that if signals are independent in one domain, their corresponding components in a linearly transformed domain are also independent. The proposed ICA-F lends itself to computationally efficient Fast Fourier Transform (FFT), which converts the convolutive combination in the time domain into multiple instantaneous combinations in the frequency domain. Then, the natural-gradient Independent Component Analysis (ICA) algorithm is employed in each frequency bin to separate frequency components of source signals. The permutation and gain ambiguities associated with the ICA algorithm are successfully solved. The ICA-F has lower computational complexity and faster convergence than the existing time-domain approach. Simulation results confirm the effectiveness of the proposed ICA-F [66-69].

This chapter is organized as follows. Section 2.1 formulates the convolutive combination model in the time and frequency domains. In Section 2.2, the proposed ICA-F is developed. In addition, the permutation and gain ambiguities associated with the frequency-domain ICA approach are successfully resolved. Comparison between the ICA-F and the time-domain approach is given in Section 2.3. Simulation results are presented in Section 2.4. Finally, conclusions are drawn in Section 2.5.

2.1 Convolutive Combination Model

In wireless communications, when the source signals travel through frequency-selective, slow fading channels, the received signals are the convolutive combinations of the source signals instead of the instantaneous combinations. A specific case is shown in Fig. 2, in which there are two transmitters and two receivers.

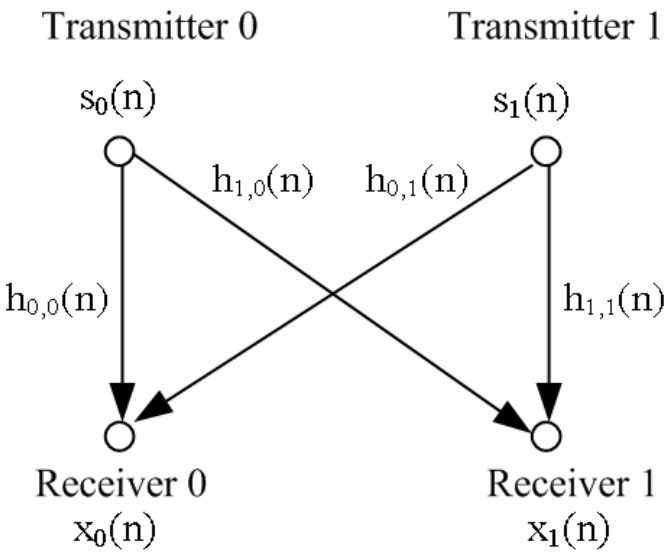

Figure 2: Convolutive combination model for the case of two transmitters and two receivers

Convolutive Combination Model in the Time Domain

There are M source signals $s_l(n)'s$, $l = 0,1,...,M-1$, and M received signals $x_m(n)'s$, $m = 0,1,...,M-1$. The $h_{m,l}(n)$ represents the impulse response of the channel from the transmitter l to the receiver m. This convolutive combination process can be expressed as:

$$x_m(n) = \sum_{l=0}^{M-1} h_{m,l}(n) \otimes s_l(n) \tag{2.1}$$

The convolutive combination model in (2.1) allows for two important propagation effects typically found in fading channels of wireless communications. First, the source signal $s_l(n)$ does not arrive at all receivers simultaneously; there are delays between the instants when the $s_l(n)$ arrives at the different receivers. Second, and more generally, the model shown in (2.1) shows that the $s_l(n)$ arrives at a receiver via more than one path. This is known as multipath propagation.

Convolutive Combination Model in the Frequency Domain

$S_l(z)$ and $X_m(z)$ are denoted as the z-transforms of $s_l(n)$ and $x_m(n)$, respectively. The equation (2.1) in the time domain can be written in the z-domain as:

$$X_m(z) = \sum_{l=0}^{M-1} H_{m,l}(z) S_l(z) \tag{2.2}$$

where $H_{m,l}(z)$ is the z-transforms of $h_{m,l}(n)$.

Define the source signal vector $S(z)$ and the received signal vector $X(z)$ as:

$$S(z) = \left[S_0(z), ..., S_l(z), ..., S_{M-1}(z)\right]^T \tag{2.3.a}$$

and

$$X(z) = \left[X_0(z), ..., X_m(z), ..., X_{M-1}(z)\right]^T \tag{2.3.b}$$

respectively.

The channel effects can be expressed as

$$H(z) = \begin{pmatrix} H_{0,0}(z) & H_{0,1}(z) & \cdots & H_{0,M-1}(z) \\ H_{1,0}(z) & H_{1,1}(z) & \cdots & H_{1,M-1}(z) \\ \vdots & \vdots & \ddots & \vdots \\ H_{M-1,0}(z) & H_{M-1,1}(z) & \cdots & H_{M-1,M-1}(z) \end{pmatrix} \tag{2.4}$$

(2.2) is written in the matrix-vector form as:

$$X(z) = H(z)S(z) \tag{2.5}$$

From (2.5), it is clear that convolutive combination in the time domain is expressed as instantaneous combinations in the frequency domain. Thus, applying discrete Short Time Fourier Transform (STFT) on the $x_m(n)'s$ is to convert the convolutive combination in time domain into instantaneous combinations in the frequency bins. For each frequency bin, the natural-gradient ICA algorithm is used to separate the source frequency components. This is the basic idea of the proposed ICA-F, which is developed in the next section.

2.2 Proposed Frequency-Domain Independent Component Analysis

The structure of the proposed ICA-F, which is comprised of five processing stages, is shown in Fig. 3. In the first stage, the discrete STFT is applied to the received signals $x_m(n)'s$. As a result, the time domain convolutive combination in (2.1) is transformed into multiple instantaneous combinations in the frequency domain in (2.5). Then, the source components in each frequency bin are recovered using the natural-gradient ICA algorithm. Since the natural-gradient ICA algorithm is applied individually to each frequency bin, the recovered signals suffer from the permutation ambiguity. This permutation ambiguity is solved by using cross-statistics between the source frequency components. In the next stage, the discrete Inverse STFT (ISTFT) is applied to obtain the $\tilde{s}_l(n)'s$. Because the $U_l(r,k)'s$ suffer from the gain ambiguity, the $\tilde{s}_l(n)$ is a filtered

version of the $s_l(n)$. The delayed version of the $s_l(n)$, $\hat{s}_l(n)$, is obtained by passing $\tilde{s}_l(n)$ through blind equalizers, Fig. 3.

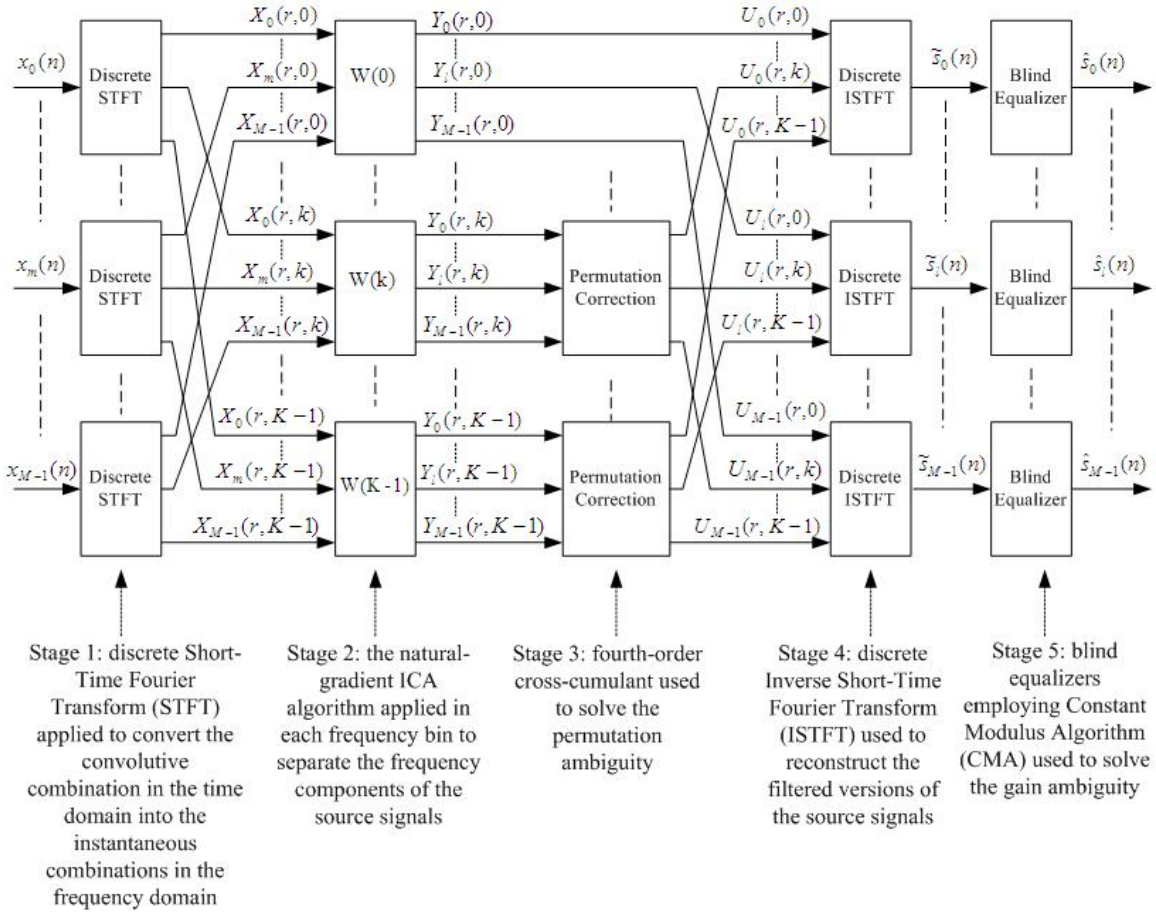

Figure 3: The proposed Frequency-Domain Independent Component Analysis (ICA-F) approach with correcting the permutation and gain ambiguities

Discrete Short-Time Fourier Transform (STFT)

In the first stage, the discrete STFT [28, 87] is applied to the received signals $x_m(n)'s$. The analysis window $win(n)$ used in the discrete STFT is a rectangular window of length L, which is given by:

$$win(n) = \begin{cases} 1, & \text{when } 0 \le n < L-1 \\ 0, & \text{otherwise} \end{cases} \tag{2.6}$$

Then, the K-point Fast Fourier Transform (FFT) is performed over the windowed section of the $x_m(n)'s$. The number K is larger than or equal to the window length L as:

$$K \ge L \tag{2.7}$$

Thus, the discrete STFT of the $x_m(n)$, $X_m(r,k)$, is expressed as:

$$X_m(r,k) = \sum_{n=0}^{+\infty} x_m(n) win(rL-n) e^{-j2\pi k(rL-n)/K} \tag{2.8}$$

where $r, (r = 1,2,...)$, is the frame number, and $k, (k = 0,1,..., K-1)$, is the frequency bin index.

In the same way as (2.8), the $S_l(r,k)$ is denoted as the discrete STFT of the $s_l(n)$. For the frame number r and the frequency bin k, the vector $S(r,k)$, and the vector $X(r,k)$ are defined as:

$$S(r,k) = [S_0(r,k),..., S_l(r,k),..., S_{M-1}(r,k)]^T \tag{2.9.a}$$

and

$$X(r,k) = [X_0(r,k),..., X_m(r,k),..., X_{M-1}(r,k)]^T \tag{2.9.b}$$

respectively.

Now, the convolutive combination in the time domain as specified in (2.1) is converted into K instantaneous combinations in the frequency domain as follows:

$$X(r,k) = H(k)S(r,k) \tag{2.10}$$

where the (m,l) entry of the matrix $H(k)$ is given by:

$$H_{m,l}(k) = H_{m,l}(z)\Big|_{z=e^{-j2\pi k/K}} \tag{2.11}$$

The source signals $s_l(n)'s$ are assumed to be complex-valued, zero-mean, stationary, non-Gaussian distributed, and statistically independent. Appendix A shows that in each frequency bin, the $S_l(r,k)'s$ are also independent, and the ICA assumptions are valid. Accordingly, the natural-gradient ICA algorithm is suitable to estimate the $S_l(r,k)'s$.

Natural-Gradient ICA Algorithm

It each frequency bin, the $X_m(r,k)'s$ are the instantaneous combinations of the $S_l(r,k)'s$. The complex natural-gradient ICA algorithm specified at Table 2 can be used to obtain $Y_l(r,k)'s$, which suffer from the permutation and gain ambiguities.

Solving Permutation Ambiguity

Since the separating systems are independently adapted in frequency bins, the source components may be extracted with arbitrary orders. The frequency component from one source signal must be grouped before the Inverse STFT (ISTFT) is performed. If $Y_l(r,k)'s$ are from different source signals, they are independent. Otherwise, they are statistically dependent. This independence is measured by the fourth-order cross-cumulant. The fourth-order cross-cumulant between $Y_l(r,0)$ and $Y_m(r,k), k \neq 0$, $CUM_{l,m}(k)$, is defined as:

$$\begin{aligned} CUM_{l,m}(k) = E\left[|Y_l(r,0)|^2 |Y_m(r,k)|^2\right] - E\left[|Y_l(r,0)|^2\right] E\left[|Y_m(r,k)|^2\right] \\ - \left|E\left[Y_l(r,0)Y_m^*(r,k)\right]\right|^2 - \left|E\left[Y_l(r,0)Y_m(r,k)\right]\right|^2 \end{aligned} \tag{2.12}$$

In principle, $CUM_{l,m}(k)$ is zero when $Y_l(r,0)$ and $Y_m(r,k)$ are from the different source signals. Otherwise, $CUM_{l,m}(k)$ is non-zero [30, 83].

From the explanation above, a method to solve the permutation ambiguity is given as following. First, the order of the $Y_l(r,0)'s$ is chosen as the reference order. Then, the order of the $Y_l(r,k)'s$, $k \neq 0$, is adjusted such that it is the same as the reference order. To do so, the recovered source components without the permutation ambiguity, $U_l(r,k)'s$, are given by:

$$U_l(r,0) = Y_l(r,0) \tag{2.13.a}$$

and

$$U_l(r,k) = Y_m(r,k), \quad k \neq 0 \tag{2.13.b}$$

where the $Y_m(r,k)$ has the maximum absolute value of $CUM_{l,m}(k)$ for $m = 0,1,..,M-1$.

Discrete Inverse Short-Time Fourier Transform (ISTFT)

In this stage, the overlap-add method [89, 98] is used to implement the discrete ISTFT. The overlapping occurs when the points of the FFT, K, is larger than the window length L.

Solving Gain Ambiguity

Due to the gain ambiguity, the $U_l(r,k)'s$ are subjected to arbitrary complex gains in frequency bins. Thus, the $\tilde{s}_l(n)'s$ are the filtered versions of the source signals, and encounter both magnitude and phase distortions. In theICA-F, blind equalizers employing Constant Modulus Algorithm (CMA) [43, 60] are used to compensate for these distortions. CMA is a blind equalization technique that restores modulus of source signals. In CMA, the FIR filter, $b_l(n)$, is used to filter the $\tilde{s}_l(n)$ to produce the $\hat{s}_l(n)$ as:

$$\hat{s}_l(n) = b_l(n) \otimes \tilde{s}_l(n) \tag{2.14}$$

The coefficients of $b_l(n)$ are updated as:

$$b_l(n) \leftarrow b_l(n) - \lambda_l E\left[\tilde{s}_l^*(n)\hat{s}_l(n)\left(\left|\hat{s}_l(n)\right|^2 - R_l\right)\right] \tag{2.15}$$

where λ_l is the convergence factor, and the constant R_l is defined as:

$$R_l = \frac{E\left[\left|s_l(n)\right|^4\right]}{E\left[\left|s_l(n)\right|^2\right]} \tag{2.16}$$

The update rule in (2.15) runs iteratively until the $b_l(n)$ converges. Consequently, the $\hat{s}_l(n)'s$ are the delayed versions of the $s_l(n)'s$, and are not subjected to the phase and amplitude distortion as the $\tilde{s}_l(n)'s$

Table 3
Outline of the proposed ICA-F

Task: Estimate the source signals $s_l(n)'s$ from their convolutive combinations as:

$$x_m(n) = \sum_{l=0}^{M-1} h_{m,l}(n) \otimes s_l(n)$$

Step 1. Perform the discrete STFT over the $x_m(n)'s$, and convert the convolutive combination in the time domain into multiple instantaneous combinations in the frequency domain as:

$$X_m(r,k) = \sum_{l=0}^{M-1} H_{m,l}(k) S_l(r,k)$$

Step 2. Separate the frequency components, $Y_l(r,k)'s$, from the above instantaneous combinations, following the steps in Table 2.

Step 3. Solving the permutation ambiguity to obtain the $U_l(r,k)'s$.

Step 4. Perform ISTFT over the $U_l(r,k)'s$ to produce the $\tilde{s}_l(n)'s$.

Step 5. Perform blind equalization over the $\tilde{s}_l(n)'s$ to produce the $\hat{s}_l(n)'s$.

2.3 Comparison Between the Proposed ICA-F and Time-Domain Approaches

Many ICA approaches have been proposed to separate the convolutive combination, and they are classified into two approaches based on the domain to apply ICA: the time-domain ICA approach [1, 5, 50] and the frequency-domain ICA approach [6, 8, 16, 23, 29, 30, 52, 59, 64, 83, 86, 92, 99, 105, 108, 109, 110, 114, 115]. In the frequency-domain ICA approach, the convolutive combination in the time domain is converted into multiple instantaneous combinations in the frequency domain. Then, these instantaneous combinations are individually separated by an instantaneous ICA algorithm. The advantage of the frequency-domain ICA approach lies in the fact that the convolutive combination with a large number of unknown parameters is decomposed into multiple, independent instantaneous combinations, each with fewer parameters to be estimated. As a result, the frequency-domain ICA approach generally has a simpler implementation and better convergence properties over the time-domain ICA approach.

The main challenges to implement the frequency-domain ICA approach, however, are the permutation and gain ambiguities, i.e., frequency components are estimated with arbitrary orders and scales in frequency bins. The permutation ambiguity leads to interference of the frequency components among the recovered signals. The gain ambiguity results in linear distortions of the recovered signals. If these two ambiguities are not properly solved, the frequency-domain ICA approach cannot work successfully.

In the existing literature, many frequency-domain ICA approaches [6, 8, 16, 52, 59, 86, 99, 105, 108, 109, 110, 114, 115, 123] are proposed to separate the convolutive combinations of speech signals. However, few references [29, 30, 83] are known for digitally modulated signals in wireless communications. Moreover, the approaches in [6,

8, 16, 52, 59, 86, 99, 105, 108, 109, 110, 114, 115] do not fully solve the gain ambiguity, that is, the recovered signals are the filtered versions of the source signals. However, the technique presented here, the ICA-F, utilizes blind equalizers to successfully solve the gain ambiguity. Thus, the signals recovered by the ICA-F are the delayed versions of the source signals.

Computational Complexity Comparison

The time-domain ICA approach is theoretically sound and achieves good separation performance once it converges. However, the time-domain approach is computationally extensive since the adaptation includes convolution operations. The time-domain ICA approach works well when convolutive combinations have short delays. However, when this approach is applied to convolutive combinations with long delays, it is unrealizable because of the computational requirements [50].

It is computationally efficient to separate the source signals in the frequency domain, as convolution in the time domain becomes computationally efficient multiplications in the frequency domain. The frequency-domain ICA approach has a computational complexity of $\mathrm{O}(F \log F)$, where F is the length of separating filters, whereas the time-domain ICA approach has $\mathrm{O}(F^2)$ [114, 115].

Separation Performance Comparison

In time-domain ICA approaches, statistical dependencies among filter taps reduce the convergence speed since updating a filter tap influences adaptation of the ones succeeding it. When the filter is very long, convergence is potentially problematic.

The frequency-domain ICA approach employs the discrete STFT, which converts the convolutive combination into multiple independent instantaneous combinations. This

means that adaptation of one parameter does not interference with other parameters, which results in fast convergence and good performance.

2.4 Simulation Results

Computer simulations are performed to confirm the effectiveness of the proposed ICA-F. The simulation setting, shown in Table 4, is used throughout this paper. The computer simulations employ the third-order convolutive combination system with the following coefficients as:

$$H(0) = \begin{pmatrix} 0.87 + 0.18j & 0.09 + 0.04j \\ 0.02 + 0.1j & 0.06 + 0.91j \end{pmatrix} \tag{2.17.a}$$

$$H(1) = \begin{pmatrix} -0.39 - 0.21j & 0.05 + 0.01j \\ 0.03 + 0.06j & -0.28 + 0.24j \end{pmatrix} \tag{2.17.b}$$

and

$$H(2) = \begin{pmatrix} 0.05 + 0.08j & 0.02 + 0.002j \\ 0.01 + 0.001j & 0.15 + 0.1j \end{pmatrix} \tag{2.17.c}$$

For the noise-free case, the crosstalk error evolutions of the instantaneous combinations in the frequency bins, from $k = 0$ to $k = 7$, are shown in Figures 4 to 11, respectively. It is obvious that the natural-gradient ICA method has successfully separated the source frequency components in each frequency bin, as shown in Fig.4 to Fig.11.

Table 4
Simulation parameters for the proposed ICA-F

Source signals	Uniformly-distributed, independent Differential Quadrature Phase Shift Keying (DQPSK)
The number of source and received signals	2
Samples of the received signals	90,000
The length of the rectangular window	3
The points of the FFT	8
The FIR filter length in blind equalizers	8
The constant in blind equalizers	$R_l = 2$

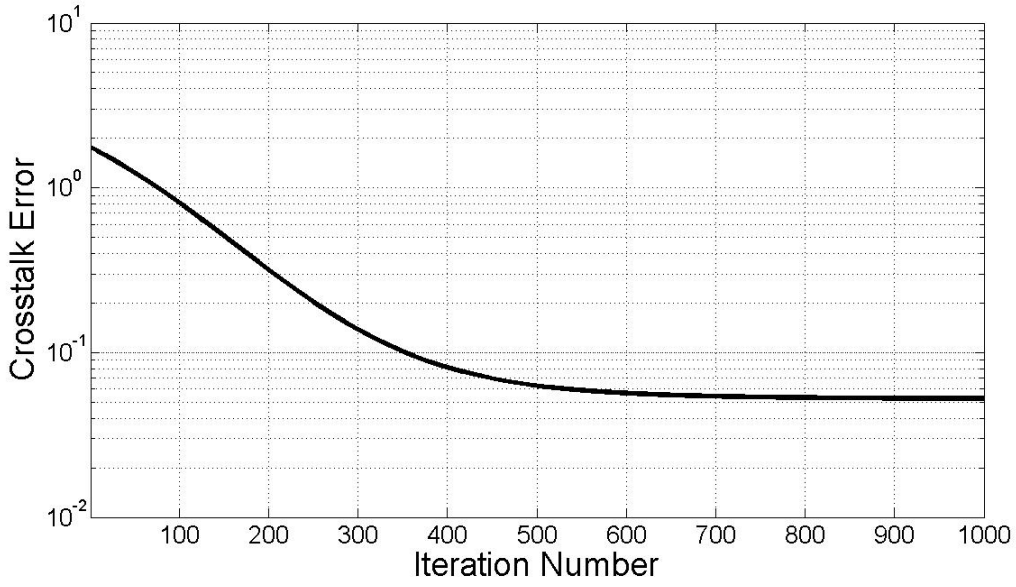

Figure 4: The crosstalk error evolution versus iteration number for the frequency bin #0 without additive noise

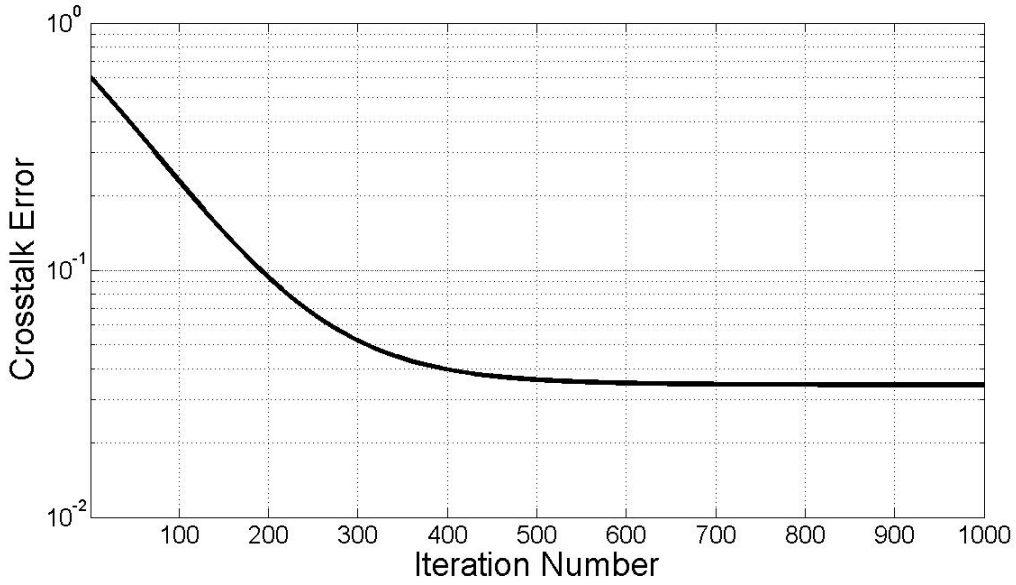

Figure 5: The crosstalk error evolution versus iteration number for the frequency bin #1 without additive noise

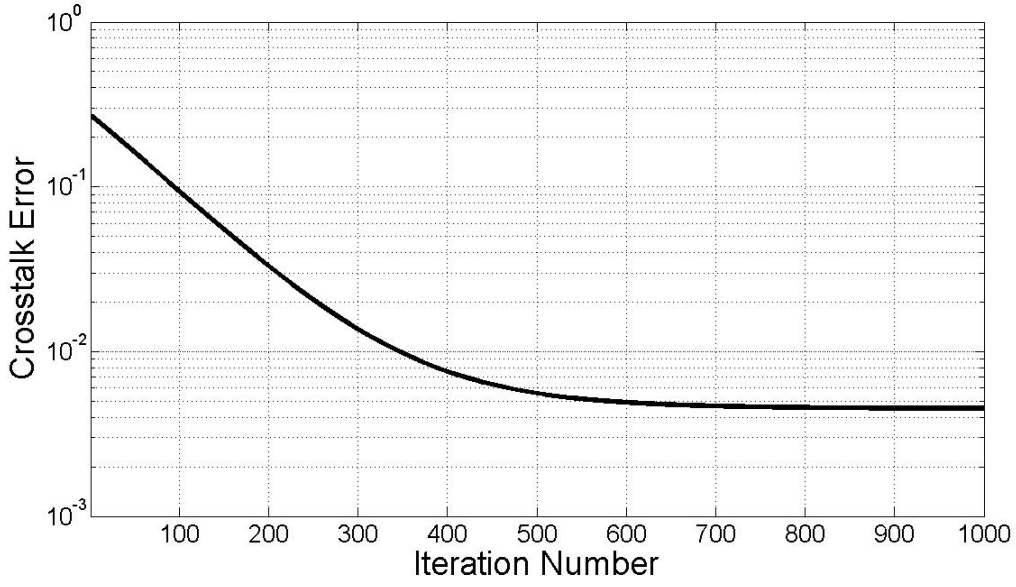

Figure 6: The crosstalk error evolution versus iteration number for the frequency bin #2 without additive noise

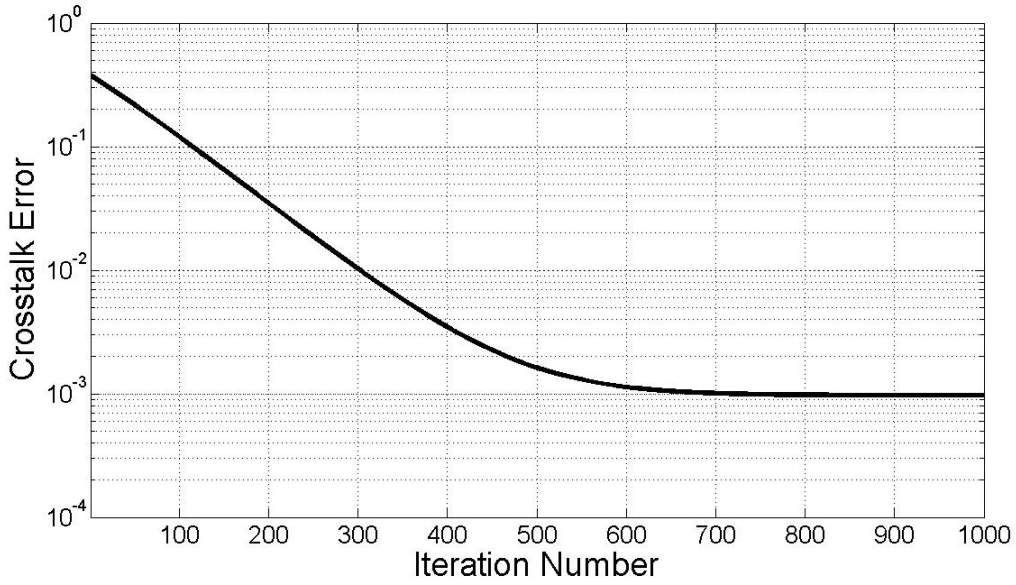

Figure 7: The crosstalk error evolution versus iteration number for the frequency bin #3 without additive noise

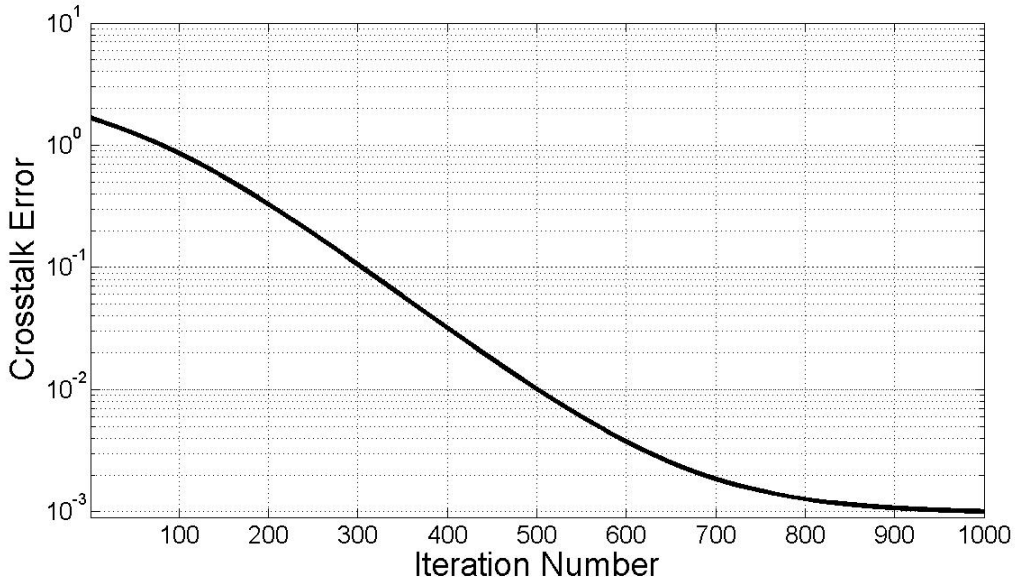

Figure 8: The crosstalk error evolution versus iteration number for the frequency bin #4 without additive noise

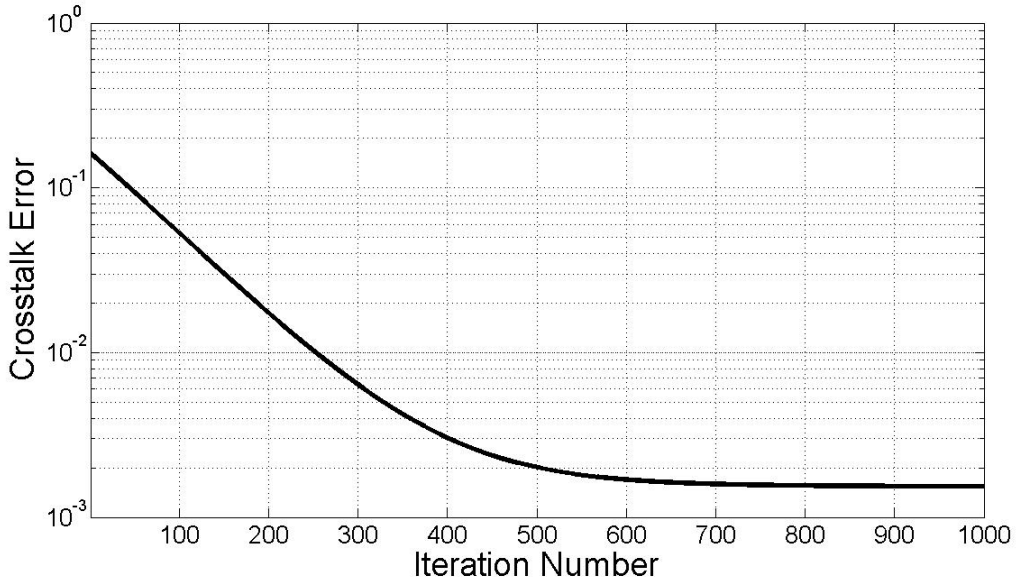

Figure 9: The crosstalk error evolution versus iteration number for the frequency bin #5 without additive noise

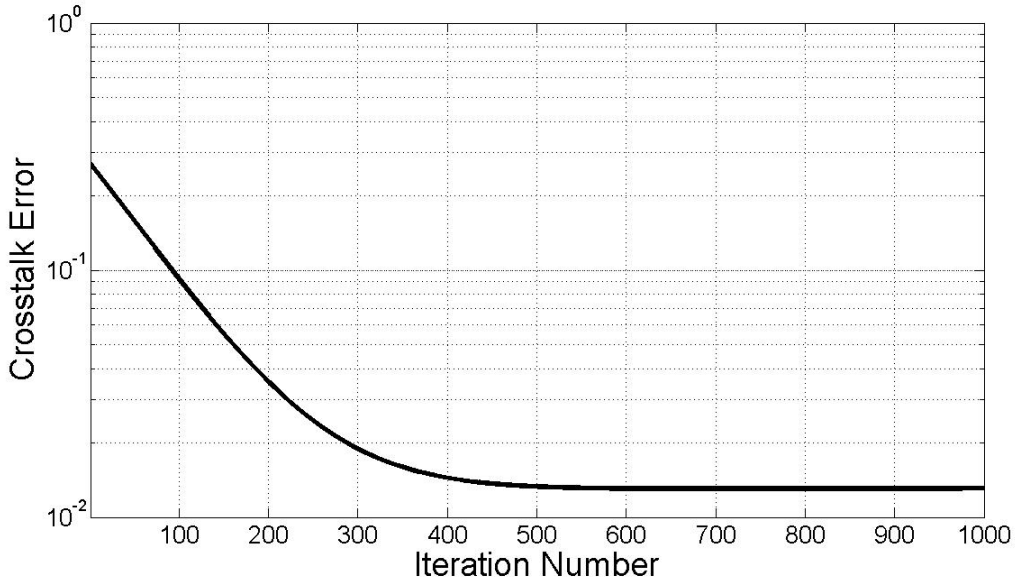

Figure 10: The crosstalk error evolution versus iteration number for the frequency bin #6 without additive noise

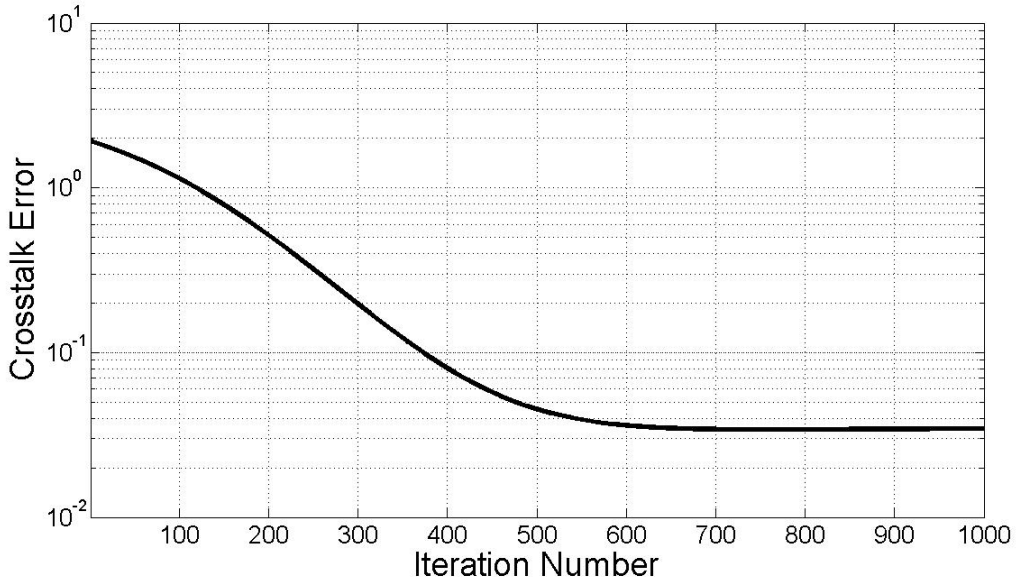

Figure 11: The crosstalk error evolution versus iteration number for the frequency bin #7 without additive noise

The space diagrams of the received signals without additive noises are shown in Fig.12a and Fig.12b, respectively. These space diagrams do not resemble characteristics of DQPSK due to the convolutive combination. The space diagrams of the recovered source signals employing the ICA-F are shown in Fig. 13a and 13b, which resemble the characteristic DQPSK constellation with easily correctable phase rotations. These space diagrams show that the proposed ICA-F successfully separates and deconvolves the convolutive combination. Figure 14a and Figure 14b present the space diagrams of the recovered signals without solving the permutation and gain ambiguities. These results demonstrate that the frequency domain ICA approach cannot achieve a good performance improvement without solving the permutation and gain ambiguities.

Figure 15 shows the Bit Error Rate (BER) of the simulated system employing the proposed ICA-F with and without solving the permutation and gain ambiguities versus SNR. For comparison, the BER of the received signals is also plotted. It suffers from error floor due to effects of the convolutive combination. It is clear that the proposed ICA-F greatly reduces the BER. However, if the ICA-F does not solve the permutation and gain ambiguities, the resulting BER is even worse than that of the received signals. This observation confirms the importance of solving the permutation and gain ambiguities in the frequency-domain ICA approach.

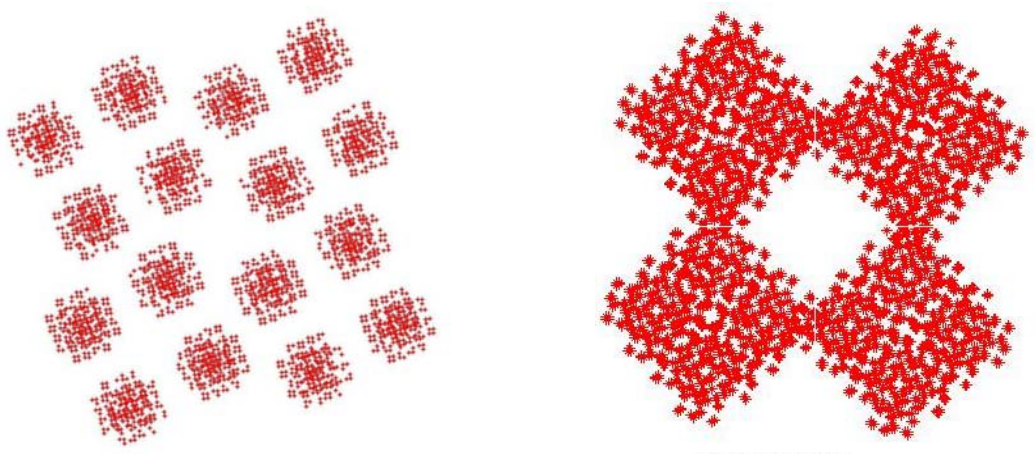

(a) (b)

Figure 12: Space diagrams of the received signals $x_0(n)$ and $x_1(n)$ without additive noises

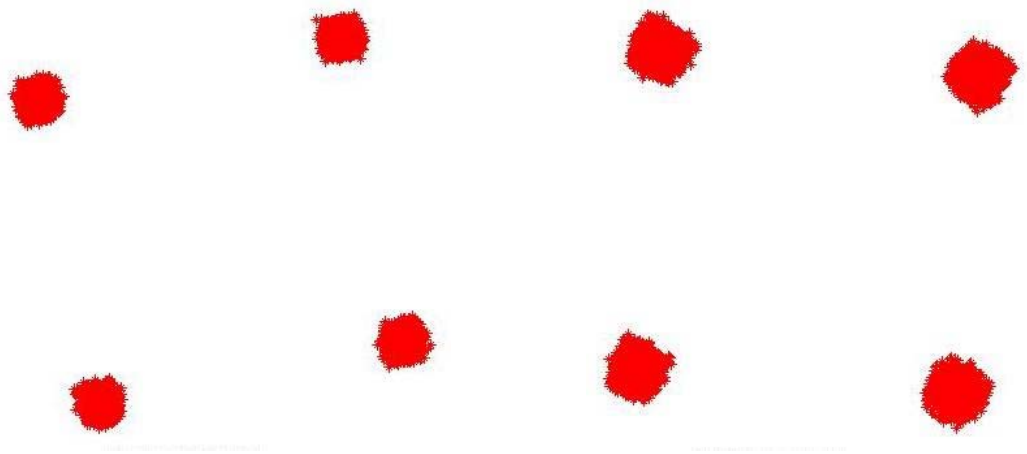

(a) (b)

Figure 13: Space diagrams of $\hat{s}_0(n)$ and $\hat{s}_1(n)$ without additive noises, where the permutation and gain ambiguities have been corrected by using the ICA-F

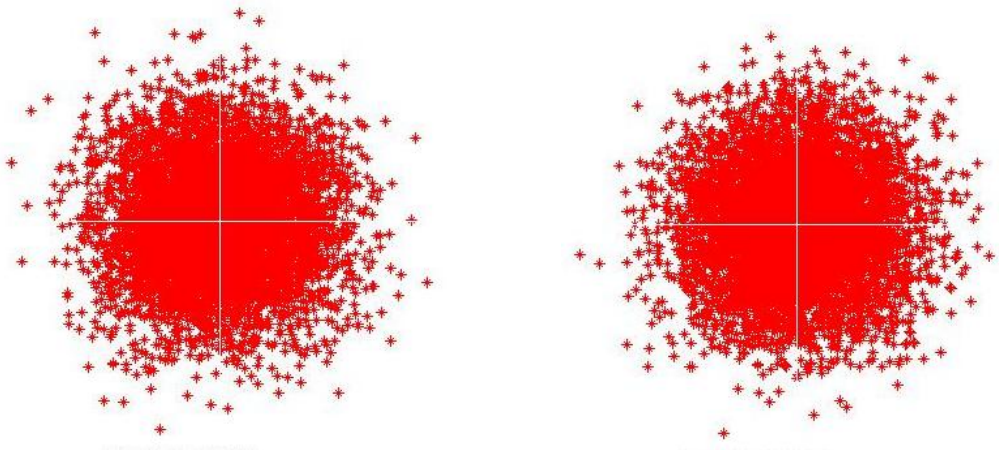

(a) (b)

Figure 14: Space diagrams of the recovered signal 1 and recovered signal 2 without additive noises, where the permutation and gain ambiguities have not been corrected

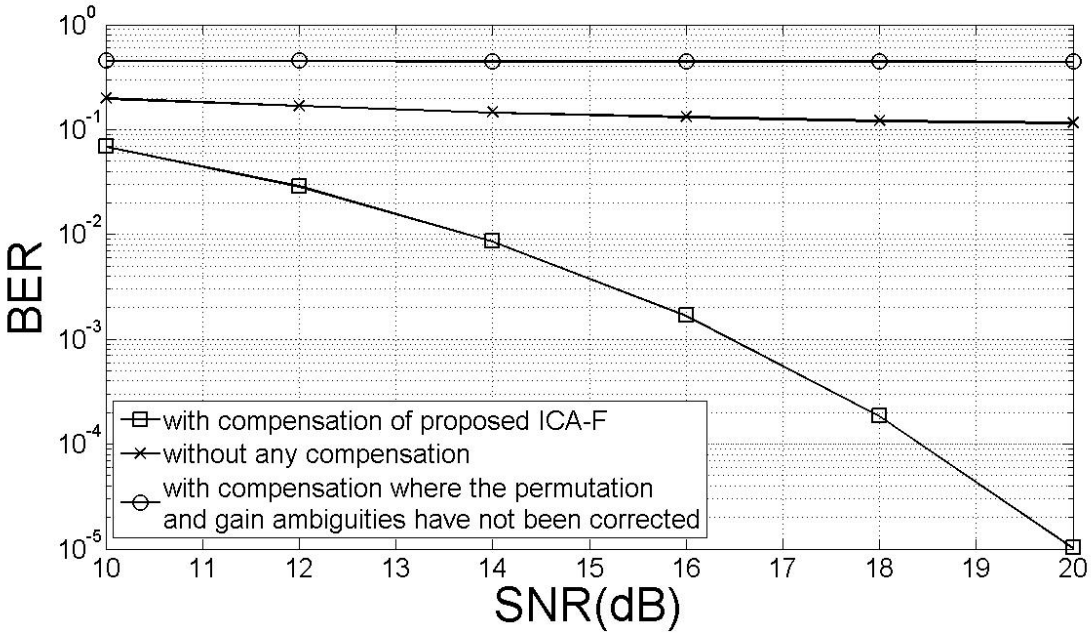

Figure 15: BER of the simulated system with compensation of the proposed ICA-F, without any compensation, and with compensation where the permutation and gain ambiguities have not been corrected versus SNR

2.5 Conclusions

In wireless communications, the received signals are the convolutive combinations of the source signals in case of slow, frequency-selective fading channels. In this contribution, a novel frequency-domain Independent Component Analysis approach (ICA-F) is proposed to blindly separate and deconvolve the source signals. In the ICA-F, the convolutive combination in the time domain is converted to multiple instantaneous combinations in the frequency domain. The proposed ICA-F is more computationally efficient and converges faster than the existing time domain approach. The ICA-F successfully solves the permutation and gain ambiguities, which are the major

obstacles to implement the frequency-domain ICA approach. Computer Simulations illustrate the performance of the proposed ICA-F.

CHAPTER THREE: CARRIER FREQUENCY OFFSET IN OFDM SYSTEMS

In Orthogonal Frequency Division Multiplexing (OFDM) systems, the wideband source signal is partitioned into multiple narrow-band signals. These narrow-band signals are transmitted simultaneously via the orthogonal, overlapping subcarriers. These subcarriers are closely spaced in frequency compared with the total channel bandwidth. Thus, the tolerable Carrier Frequency Offset (CFO) becomes a very small fraction of the channel bandwidth. In addition, the CFO causes two deleterious effects; one is the reduction of signal power, and the second is the introduction of Intercarrier Interference (ICI) from other subcarriers that are not orthogonal. Consequently, OFDM systems are very sensitive to CFO. In this chapter, CFO effects in OFDM systems are carefully investigated and modeled.

This chapter is organized as follows. Section 3.1 introduces the principle of OFDM systems. In Section 3.2, existing CFO estimation approaches are examined. The OFDM system model including CFO is given in Section 3.3. Properties of ICI coefficients are studied in Section 3.4.

3.1 OFDM Basics

In Multicarrier Modulation (MCM) systems, the transmitting data is divided into multiple parallel bit streams, which are modulated onto corresponding subcarriers. For each subcarrier in MCM systems, the influence of multipath fading is attenuation and phase rotation. Consequently, only a one-tap equalizer is needed for each subcarrier.

Thus, equalization in a MCM system is much simpler than the corresponding single-carrier system [15, 26, 88].

In earlier MCM systems, the total bandwidth is divided into multiple non-overlapping subcarriers between which a frequency guard-band is inserted. It seems reasonable to avoid spectral overlap of subcarriers in order to eliminate Intercarrier Interference (ICI). However, this scheme leads to inefficient utilization of the available spectrum. To cope with this inefficiency, an overlapping MCM technique, Orthogonal Frequency Division Multiplexing (OFDM), was proposed [21]. OFDM systems differ from the original MCM systems in that spectra of the subcarriers are overlapped and mutually orthogonal.

In OFDM, each subcarrier has an integer number of cycles within a given time interval, and the number of cycles by which each adjacent subcarrier differs is exactly one. This property ensures orthogonality between OFDM subcarriers. These subcarriers are modulated using Phase Shift Keying (PSK) or Quadrature Amplitude Modulation (QAM). The amplitude spectrum of each modulated subcarrier using either PSK or QAM has a sinc shape. At the peak spectral response of each subcarrier, all other subcarrier spectral responses are identically zero.

Following data modulation, symbols are fed through a serial-to-parallel conversion process. Each PSK or QAM symbol is assigned into a subcarrier. QAM is the most popular type of modulation in combination of OFDM. Rectangular constellations are especially easy to implement as they can be split into independent Pulse Amplitude Modulation (PAM) components for both the in-phase and quadrature parts.

An Inverse Fast Fourier Transform (IFFT) is performed to produce a time domain signal. A guard time is introduced to eliminate Intersymbol Interference (ISI) caused by the delay spread of fading channels. As a rule, the guard time is usually two or four times larger than the expected delay spread. This can take care of ISI, but ICI, crosstalk between subcarriers, remains an issue. To reduce ICI, OFDM symbols are cyclically extended into the guard interval. This cyclic extension ensures that an OFDM symbol has an integer number of cycles in the FFT interval as long as the delay is less than the guard time.

At the receiver after Radio Frequency (RF) and Analog-to-Digital (A/D) conversion stages, time and frequency synchronization between the transmitter and receiver is very crucial to the performance of an OFDM link. Next, a Fast Fourier Transform (FFT) operation is used to demodulate all subcarriers. To demodulate the subcarriers using PSK or QAM modulation, the reference phase and amplitude of the constellation on each subcarrier are required. To overcome the unknown phase and amplitude ambiguities, two techniques, coherent and differential detection, are used. The complete block diagram of the transceiver for OFDM systems is given in Fig.16.

In summary, the OFDM transmission scheme has the following key advantages:

- OFDM is an efficient way to deal with multipath. For a given delay spread, the implement complexity is significantly lower than that of a single-carrier system with an equalizer.
- OFDM is robust against narrowband interference, since such interference affects only a small percentage of the subcarriers.

- In relatively slow time-varying channels, an OFDM system is capable of significantly enhancing the capacity by adapting the data rate per subcarrier according to the Signal-to-Noise Ratio (SNR) of that particular subcarrier.
- OFDM makes single-frequency networks possible, which is especially attractive for broadcasting applications.

On the other hand, OFDM also has drawbacks compared with single-carrier systems:

- OFDM is more sensitive to frequency offset and phase noise.
- OFDM has a relatively large peak-to-average power ratio, which tends to reduce the power efficiency of the RF amplifier.

Much of the research focuses on the high efficient implementation of OFDM systems. Weinsten and Ebert were the first to suggest using the Discrete Fourier Transform (DFT) and Inverse Discrete Fourier Transform (IDFT) to perform baseband modulation and demodulation. The use of DFT and IDFT eliminates arrays of sinusoidal generators and coherent demodulation required in parallel data systems, making implementation of OFDM systems cost effective [124]. An efficient implementation of DFT and IDFT can be obtained by any available Fast Fourier Transform (FFT) algorithm. Recent advances in Very-Large-Scale Integration (VLSI) technology make high-speed, large-scale FFT chips commercially affordable.

OFDM has been successfully applied to a wide variety of digital communications applications over the past several years. Some applications of OFDM are:

- Terrestrial Digital Audio Broadcasting (DAB) and Digital Video Broadcasting (DVB) in Europe [104].

- Wireless Local Area Network (WLAN), such as IEEE 802.11a [131], High Performance Radio Local Area Networks type 2 (HiperLAN 2), and Mobile Multimedia Access Communications (MMAC) [117].
- Wireless Metropolitan Area Networks (WMAN), such IEEE 802.16 [34, 39, 132] and 3G wireless communication systems. The Wireless World Research Forum (WWRF) considers OFDM the most important technology for a future public cellular radio access technology.
- High-bit-rate Digital Subcarrier Lines (HDSL) and Asymmetric Digital Subcarrier Lines (ADSL), and Very-high-speed Digital Subscriber Lines (VDSL) [10].

3.2 Existing Carrier Frequency Offset Estimation Approaches

In an OFDM link, subcarriers are orthogonal only if the transmitter and the receiver use the exactly same frequencies. However, CFO actually exists in a practical OFDM system. CFO destroys orthogonality between subcarriers, and results in ICI. Consequently, CFO decreases the Signal-to-Noise Ratio (SNR) of the desired signal, and hence increases Bit Error Rate (BER) [94]. In order to achieve the acceptable performance, the CFO must be estimated and corrected.

In practice, the value of CFO can be several times larger than the subcarrier spacing. Thus, the CFO value is expressed as an integer part and a fractional part with respect to the subcarrier spacing. The integer part of the CFO causes a circular shift of the desired signals, but does not introduce ICI, i.e., the orthogonality of the subcarriers is still maintained. The fractional part, however, destroys orthogonality between

subcarriers, and causes ICI [74, 85]. In the literature, a few CFO estimation approaches can recover the CFO up to half the distance of the subcarriers. If the CFO is larger, what they estimate is just the fractional part of the CFO, and an ambiguity of an integer number subcarrier intervals is left.

A number of techniques have been proposed to estimate or correct the CFO in OFDM systems. These existing CFO estimation techniques are categorized as data-aided estimation approaches [7, 51, 77, 103, 129] or blind estimation approaches [9, 11, 22, 25, 37, 38, 58, 65, 78, 121, 122, 128], according to the requirement of training sequences. The data-aided technique requires a known pilot symbol. The blind technique does not need any training sequence but need some statistical properties, such as independence and identically distribution of source signals. The data-aided CFO estimator has two limitations: the reduction of the bandwidth efficiency and the introduction of additional system delay since estimators can only identify CFO after receiving the training sequence. The blind CFO estimator, however, is free from these two drawbacks. It does not need training sequences, and is hence bandwidth efficient. In addition, the blind CFO estimator can identify CFO in real-time from the received data. In general, the blind estimation approach is more attractive than the data-aided estimation approach for future wireless communications.

Data-Aided CFO Estimators

The ICI self-cancellation scheme has been proposed to mitigate ICI effects [129]. Its main idea is to modulate one data symbol into a group of subcarriers with predefined weight coefficients. This results in cancellation of most ICI effects.

The windowing method has been presented to reduce ICI effects [7]. Hamming window and Kaiser window both are able to reduce sensitivity to the CFO. However, these two approaches can correct only the fractional part of the CFO.

The Maximum Likelihood algorithm, working on two identical OFDM symbols, has been developed to estimate CFO [84]. This estimate is conditionally unbiased and consistent. Moreover, a method to resolve the integer part of the CFO is proposed, where ad hoc shortened symbols are periodically transmitted in the OFDM symbol stream, forcing the subcarrier spacing to be locally larger than twice the maximum CFO value. However, this method does not seem very attractive, since it requires a signal structure strictly matched to the range of possible CFO.

In [105], a rapid synchronization method works on a two-symbols training sequence, which is placed at the start of the frame. The CFO is found in two steps, by finding the fractional part and then the integer part. The resulting CFO estimator is very accurate and provides a very wide acquisition range for the CFO.

Blind CFO Estimators

The blind CFO estimator identifies the CFO via two steps; first the fractional part of the CFO is estimated, and then the integer part of CFO is solved by using a slide window [85]. The resulting strategy is to compute the energy of the samples belonging to a sliding window that follows the FFT in the OFDM receiver, and to locate the relevant energy peak. Considering the selectivity of the channel leads to the use of weighted window instead of a rectangular one [76].

The blind CFO estimator in [107] has two limitations, namely, the constellation on each subcarrier must have points equally spaced in phase, and the length of the guard time must be chosen from a subset of allowed values.

The Maximum Likelihood CFO estimator in [11] is proposed for flat channels, and is affected by the error floor in the case of multipath channels.

The blind CFO estimation approach in [22] oversamples the received signals by a factor of two. This blind CFO estimator improves the system performance at the expense of the hardware complexity.

The techniques proposed in [9, 37, 38, 65, 121, 122] take advantage of virtual subcarriers existing in many OFDM systems. These estimators are robust against multipath fading, but have relatively high computational costs.

The blind CFO estimator in [25, 76, 128], called the YG-CFO estimator in this research work, utilizes fourth-order statistics to identify CFO. Exploitation of fourth-order statistics has proven to be beneficial to estimate the CFO in OFDM systems. Thus, the YG-CFO estimator has low computational complexity, and is free from the limitations of other blind CFO estimators. However, the YG-CFO estimator does not consider noise effects, and its performance suffers greatly from noise.

3.3 OFDM System Model with Carrier Frequency Offset

Forward Error Correction and Interleaving

In OFDM systems, subcarriers arrive at a receiver with different amplitudes due to multipath fading. In the worst case, some subcarriers may be completely lost. Hence, even though most subcarriers may be detected without errors, the overall BER will be largely dominated by several subcarriers with small amplitudes. To avoid the weak subcarriers from dominating performance, and to achieve an acceptable performance with a reasonable signal power level, Forward Error Correction (FEC) coding is essential [35,

130]. The goal of FEC coding is to improve the BER performance of power-limited and/or bandwidth limited channel by adding structured redundancy to the transmitted data.

Convolutional coding is one commonly used FEC scheme. In the convolutional coding, the input bits are convolved with a binary impulse response to produce the output bits. The convolutional encoding can be implemented by simple shift registers and modulo-2 adders. Decoding of convolutional codes is more often performed using the Viterbi algorithm, which is an efficient way to obtain the optimal maximum likelihood estimate of the encoded sequence. The complexity of the Viterbi algorithm grows exponentially with the constraint length. Hence, practical implementations of Viterbi algorithm do not go further than a constraint length of about 10.

FEC coding is not designed to deal with error bursts. Therefore, interleaving is applied to spread bit errors, which occur in bursts rather than being randomly scattered. Interleaving randomizes the occurrences of bit errors prior to decoding. At the transmitter, the coded bits are arranged in a certain way such that adjacent bits are separated by several bits after interleaving. At the receiver, the reverse permutation is performed before FEC decoding. A commonly used interleaving scheme is block interleaving, where input bits are written in a matrix column by column and read out row by row.

OFDM is a two-dimensional system, where interleaving can be performed in both time and frequency domains. Applying time-frequency interleaving in OFDM systems distributes bit errors over the whole signal bandwidth and the time interleaving depth.

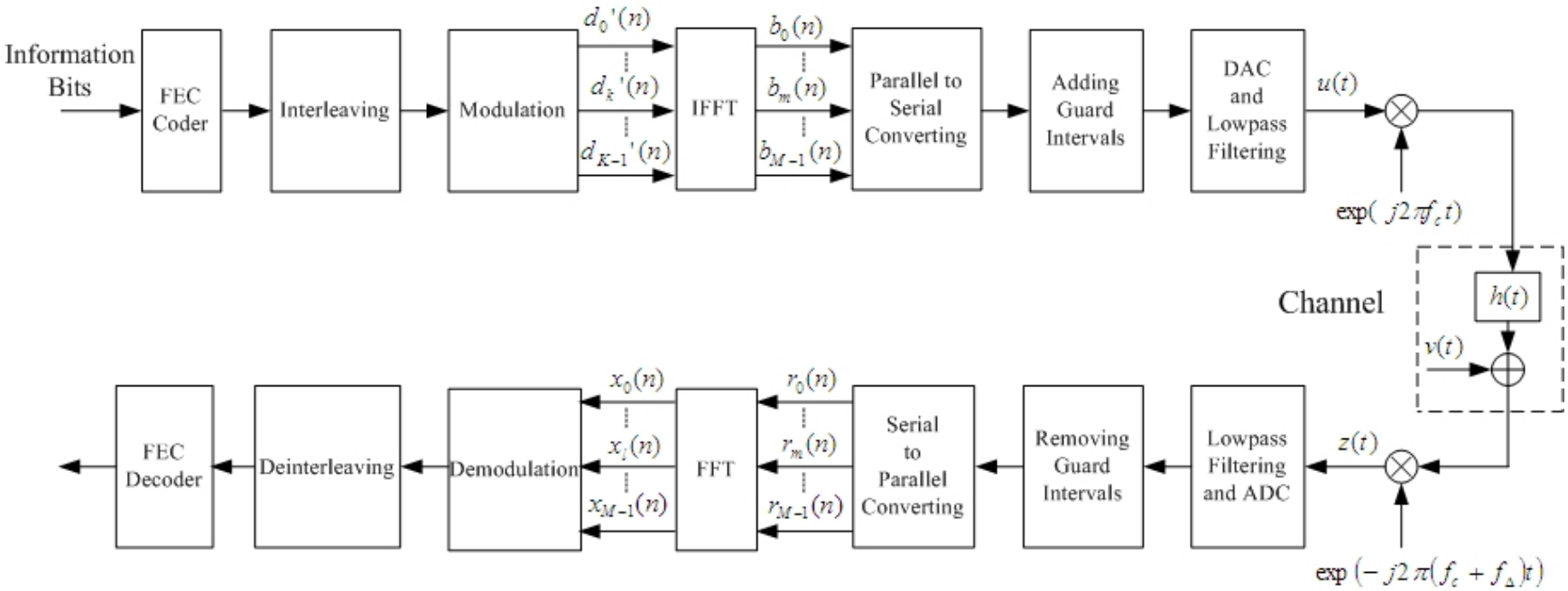

Figure 16: The block diagram of an OFDM system suffering Carrier Frequency Offset. In the OFDM system, the modulated signals $d_k'(n)'s$, $k = 0,1,...,K-1$, are mapped to orthogonal subcarriers by an M-point IFFT operation. The number of data-carrying subcarriers is generally fewer than the number of IFFT points, i.e., $M > K$. The guard time is added between the OFDM symbols. In practice, there exists a frequency offset f_Δ between the local oscillators of the transmitter and the receiver

Modulation

There are two modulation schemes in OFDM systems: coherent modulation and differential modulation. In coherent modulation, the data symbols to be transmitted are directly mapped to the modulation symbols. Differential modulation occurs when the transmitted information is contained in the quotient of two successive modulation symbols. Since OFDM is a two-dimensional scheme, differential modulation can be applied either in time direction, embedded in different OFDM symbols, or in the frequency direction, inserted in different subcarriers [101, 102].

In differential modulation, no channel estimation procedure is necessary, and hence demodulation is quite simple to implement. Due to its low complexity, differential modulation is widely employed in OFDM systems. The main disadvantage associated with differential modulation is the performance loss in terms of SNR compared with coherent modulation.

In [46], a novel two–dimensional differential demodulation scheme was proposed that for the most part overcomes the degrading effects of differential demodulation compared with coherent modulation. For this scheme, neither a change in the transmitter nor knowledge about the transmitted information is necessary. The efficiency of the algorithm can be adjusted by the iteration depth and the chosen criteria.

Consider that the OFDM system has K parallel information symbols, $d_k(n)'s$, $k = 0,1,...,K-1$. For the subcarrier k, the information symbol $d_k(n)$ is differentially modulated to produce the transmitted signals $d_k'(n)$ in time direction as:

$$d_k'(n) = d_k'(n-1) \times d_k(n) \tag{3.1.a}$$

or in the frequency direction as:

$$d_{k+1}'(n) = d_k'(n) \times d_k(n) \tag{3.1.b}$$

For differential modulation in time direction, the channel coherence time must be larger than the symbol duration to ensure the channel transfer factors are approximately equal in two successive symbols. Thus, differential modulation in the time direction is suitable for slow-fading channels.

For differential modulation in frequency direction, the channel coherent bandwidth has to be larger compared with the subcarrier spacing. However, if there are a large number of subcarriers in OFDM systems, small difference exists between the respective attenuations and phase rotations of two successive subcarriers. Differential modulation in the frequency direction works well for flat-fading channels.

IFFT Operation

In the OFDM system, the transmitted signals $d_k'(n)'s$ are mapped to M orthogonal subcarriers by an M-point IFFT. The number of the transmitted signal, K, is fewer than or equal to the number of orthogonal subcarriers, M, i.e.

$$M \geq K \tag{3.2}$$

Without loss of generality, the $d_k'(n)'s$ are modulated onto the first K subcarriers, and the remaining $M - K$ subcarriers are virtual subcarriers. Thus, the transmitted signals in the time domain, $b_m(n), m = 0,1,...,M-1$, are expressed as:

$$b_m(n) = \frac{1}{\sqrt{M}} \sum_{k=0}^{K-1} d_k'(n) \exp\left(\frac{j2\pi km}{M} \right) \tag{3.3}$$

Inserting Guard Time

The guard time, which is cyclically extended, is added in between adjacent OFDM symbols. The length of the guard time is longer than the maximum delay of the fading channel in order to avoid Intersymbol Interference (ISI).

The OFDM symbol duration is T_s, and the guard time is T_g. The ADC sampling in Fig.15 is defined as T. The following relations are valid.

$$T_s = MT \tag{3.4.a}$$

and

$$T_g = GT \tag{3.4.b}$$

where G is the number of guard samples.

Transmitted Signals

The transmitted signal $u(t)$ is given by:

$$u(t) = \frac{1}{\sqrt{M}} \sum_{n=0}^{+\infty} \sum_{k=0}^{K-1} d_k'(n) \exp\left(\frac{j2\pi k}{T_s} t \right) win\left(t - n\left(T_s + T_g\right)\right) \tag{3.5}$$

where $win(t)$ is the window function defined as:

$$win(t) = \begin{cases} 1, & 0 \le t < \left(T_s + T_g\right) \\ 0, & \text{otherwise} \end{cases} \tag{3.6}$$

Fading Channels

The multipath fading channel is assumed to be quasi-stationary, i.e., channel variances are negligible during the transmission of one OFDM symbol, but channel variances are present at the successive OFDM symbols. The fading channel is modeled as:

$$h(t) = \sum_{p=0}^{P-1} \rho_p \delta\left(t - pT\right) \tag{3.7}$$

where P is the total number of fading paths, and ρ_p are independent Rayleigh-distributed time-variant complex amplitude.

The channel transfer factor is defined as:

$$h_k = \sum_{p=0}^{P-1} \rho_p \exp\left(\frac{j2\pi k}{M} p \right) \tag{3.8}$$

Relative Carrier Frequency Offset

Before an OFDM receiver can demodulate subcarriers, it has to perform at least two synchronization tasks. First, it has to find out where the symbol boundaries are and what the optimal timing instants are, in order to minimize the effects of ISI. Second, it has to estimate and correct for the Carrier Frequency Offset (CFO) of the receive signal, because any CFO introduces ICI. In this dissertation, only CFO is discussed.

In practice, there exists a frequency offset f_Δ between the local oscillators of the transmitter and the receiver, as in Fig. 15. The relative CFO with respect to the subcarrier spacing is defined as:

$$e = f_\Delta T_s \tag{3.9}$$

Received Signals in the Time Domain

The baseband received signal $z(t)$ is expressed as:

$$\begin{aligned} z(t) &= \exp(-j2\pi f_\Delta t)(u(t) \otimes h(t)) + v(t) \\ &= \exp(-j2\pi f_\Delta t) \sum_{p=0}^{P-1} \rho_p u(t - pT) + v(t) \end{aligned} \tag{3.10}$$

where $v(t)$ is white Gaussian noise.

The received signals in the time domain before the FFT demodulation, $r_m(n)'s$, are given by:

$$r_m(n) = \exp\left(-j2\pi f_\Delta T\left(n(M+G)+m\right)\right)\sum_{p=0}^{P-1}\rho_p u(T\left(n(M+G)+m\right)-pT) + v_m(n) \tag{3.11}$$

where the $v_m(n)'s$ are the independent, complex circular, and white Gaussian noise.

Since the guard time is longer than the maximum delay of the fading channel, expressed as:

$$G \geq P \tag{3.12}$$

(3.11) can be simplified as:

$$\begin{aligned} r_m(n) &= \frac{1}{\sqrt{M}}\exp\left(-j2\pi f_\Delta T\left(n(M+G)+m\right)\right) \\ &\quad \sum_{p=0}^{P-1}\rho_p\sum_{k=0}^{K-1}d_k'(n)\exp\left(j2\pi f_k T\left(nM+m-p\right)\right)+v_m(n) \\ &= \frac{1}{\sqrt{M}}\exp\left(\frac{-j2\pi en\left(M+G\right)}{M}\right)\exp\left(\frac{-j2\pi em}{M}\right) \\ &\quad \sum_{k=0}^{K-1}d_k'(n)\exp\left(\frac{j2\pi m}{M}k\right)\left[\sum_{p=0}^{P-1}\rho_p\exp\left(-\frac{j2\pi kp}{M}\right)\right]+v_m(n) \\ &= \frac{1}{\sqrt{M}}\exp\left(\frac{-j2\pi en\left(M+G\right)}{M}\right)\exp\left(\frac{-j2\pi e}{N}m\right) \\ &\quad \sum_{k=0}^{M-1}h_k d_k'(n)\exp\left(\frac{j2\pi m}{M}k\right)+v_m(n) \end{aligned} \tag{3.13}$$

Received Signals in the Frequency Domain

The frequency-domain received signals after FFT processing, $x_l(n)'s$,are given by:

$$\begin{aligned} x_l(n) &= \frac{1}{\sqrt{M}}\sum_{m=0}^{M-1}r_m(n)\exp\left(\frac{-j2\pi m}{M}l\right) \\ &= \frac{1}{M}\exp\left(\frac{-j2\pi en\left(M+G\right)}{M}\right)\sum_{k=0}^{M-1}h_k d_k'(n)\sum_{m=0}^{M-1}\exp\left(\frac{j2\pi m}{N}(k-l-e)\right) \\ &\quad +\frac{1}{\sqrt{M}}\sum_{m=0}^{M-1}v_m(n)\exp\left(\frac{-j2\pi m}{M}l\right) \end{aligned} \tag{3.14}$$

Define the ICI coefficient $a_{l.k}$ as:

$$\begin{aligned} a_{l.k} &= \frac{1}{M}\sum_{m=0}^{M-1}\exp\left(\frac{j2\pi m}{M}(k-l-e)\right) \\ &= \frac{\sin(\pi(k-l-e))}{M\sin\left(\pi\frac{k-l-e}{M}\right)}\exp\left(j\pi\left(\frac{M-1}{M}\right)(k-l-e)\right) \end{aligned} \tag{3.15}$$

The independent Gaussian noise $v_l'(n)'s$ are given by:

$$v_l'(n) = \frac{1}{\sqrt{M}}\sum_{m=0}^{M-1} v_m(n)\exp\left(\frac{-j2\pi m}{M}l\right) \tag{3.16}$$

(3.14) can be rewritten as:

$$x_l(n) = \sum_{k=0}^{M-1} a_{l.k}h_k d_k'(n) + v_l'(n) \tag{3.17}$$

The received signal vector $X(n)$, the transmitted signal vector $D'(n)$, and the noise vector $V(n)$ are defined as:

$$X(n) = \left[x_0(n),...,x_l(n),..,x_{M-1}(n)\right]^T \tag{3.18.a}$$

$$D'(n) = \left[d'_0(n),...,d'_k(n),..,d'_{K-1}(n)\right]^T \tag{3.18.b}$$

and

$$V'(n) = \left[v_0'(n),...,v_l'(n),...,v_{M-1}'(n)\right]^T \tag{3.18.c}$$

respectively.

The received signal vector $X(n)$ is expressed in term of the transmitted signal vector $D'(n)$ in matrix form as:

$$X(n) = AHD'(n) + V'(n) \tag{3.19}$$

where H is a K by K diagonal matrix as:

$$H = diag\left(h_0,...,h_k,...,h_{K-1}\right) \tag{3.20}$$

and A is the ICI matrix of the form as:

$$A = \begin{pmatrix} a_{0,0} & \cdots & a_{0,M-1} \\ \vdots & \ddots & \vdots \\ a_{M-1,0} & \cdots & a_{M-1,M-1} \end{pmatrix} \tag{3.21}$$

The desired signal vector $S(n)$ is defined as:

$$\begin{aligned} S(n) &= \left[s_0(n),...,s_k(n),...,s_{K-1}(n)\right]^T \\ &= HD'(n) \end{aligned} \tag{3.22}$$

Substituting (3.22) into (3.19) yields

$$X(n) = AS(n) + V'(n) \tag{3.23}$$

3.4 Properties of Intercarrier Interference Coefficients

If there are no frequency offsets, $e = 0$, the following properties are valid.

$$a_{l.k} = 1, \quad l = k \tag{3.24.a}$$

and

$$a_{l.k} = 0, \quad l \neq k \tag{3.24.b}$$

Thus, no ICI occurs. On the other hand, if $e \neq 0$, then

$$\left|a_{l.k}\right| \leq 1, \quad l = k \tag{3.25.a}$$

and

$$a_{l.k} \neq 0, \quad l \neq k \tag{3.25.b}$$

In this case, subcarriers are no longer orthogonal, and ICI exists. It is necessary to study properties of the ICI coefficient $a_{l,k}$ in order to develop the compensation approaches developed in chapter four and five.

Summations of ICI Coefficients

The following formulae about $a_{l,k}$ can be derived.

$$\sum_{l=0}^{M-1}\left|a_{l,k}\right|^2=\sum_{k=0}^{M-1}\left|a_{l,k}\right|^2=1 \tag{3.26}$$

$$\sum_{l=0}^{M-1}\left|a_{l,k}\right|^4=\sum_{k=0}^{M-1}\left|a_{l,k}\right|^4=\frac{M^2-1}{3M^2}\cos(2\pi e)+\frac{2M^2+1}{3M^2} \tag{3.27}$$

$$\sum_{l=0}^{M-1}\left|a_{l,k}\right|^2\left|a_{l,m}\right|^2=\frac{1-\cos(2\pi e)}{M^2\sin^2\left(\frac{k-m}{M}\pi\right)},\quad k\neq m \tag{3.28}$$

Refer to Appendix B for the detailed derivation of the above formulae. In (3.26), the summation of $\left|a_{l,k}\right|^2$ equals one, a constant unrelated to the CFO. In fact, the summations of $\left|a_{l,k}\right|^4$ and $\left|a_{l,k}\right|^2\left|a_{l,m}\right|^2, k\neq m$ are the unimode functions of CFO, shown in (3.27) and (3.28). Intuitively, the properties in (3.27) and (3.28) indicate that the fourth-order statistical properties can be used to estimate the CFO.

ICI Matrix

In the case of no virtual subcarriers in OFDM systems, i.e. $K = M$, the ICI matrix A is square. Let us define the first row of A as:

$$A_1=\left[a_{0,0},...,a_{0,k},...,a_{0,M-1}\right] \tag{3.29}$$

Note that the (l,k) entry of the A is given by:

$$a_{l,k}=a_{0,(k-l)\bmod M} \tag{3.30}$$

Hence, the ICI matrix A is circulant [44]. The eignvalues of the ICI matrix A, $\psi_m's$, are given by:

$$\begin{aligned}\psi_m &= \sum_{k=0}^{N-1} a_k e^{-j2\pi mk/M} \\ &= \frac{1}{M}\sum_{k=0}^{N-1} e^{-j2\pi me/M} \\ &= e^{-j2\pi me/M}\end{aligned} \tag{3.31}$$

It is clear that the $\psi_m's$ are simply the DFT of the sequence a_m. The eignvectors of the ICI matrix A, $U_m's$, are given by:

$$U_m = M^{-1/2}\left(1, e^{-2\pi m/M}, ..., e^{-2\pi m(M-1)/M}\right)^T \tag{3.32}$$

Consequently, the ICI matrix A can be expressed as:

$$A = U\Psi U^H \tag{3.33}$$

where the matrix U is given by:

$$\begin{aligned}U &= \left(U_0, U_1, ..., U_{M-1}\right) \\ &= \frac{1}{\sqrt{M}}\begin{pmatrix} 1 & 1 & ... & 1 \\ 1 & e^{-2\pi/M} & \ddots & e^{-2\pi(M-1)/M} \\ \vdots & \vdots & \ddots & \vdots \\ 1 & e^{-2\pi(M-1)/M} & \cdots & e^{-2\pi(M-1)(M-1)/M} \end{pmatrix}\end{aligned} \tag{3.34}$$

and the matrix Ψ is given by:

$$\Psi = diag\left(\psi_0, ..., \psi_m, ..., \psi_{M-1}\right) \tag{3.35}$$

As shown in (3.33), the A is similar to a diagonal matrix.

The inverse matrix of the A is expressed as:

$$\begin{aligned}A^{-1} &= \left(U\Psi U^H\right)^{-1} \\ &= U^H\Psi^{-1}U\end{aligned} \tag{3.36}$$

[44] states that inverses, products, and sums of circulant matrices are also circulant. Thus, the inverse matrix of A is also circulant. The conjugate transpose matrix of A is given by:

$$\begin{aligned} A^H &= \left(U\Psi U^H\right)^H \\ &= U\Psi^H U^H \end{aligned} \tag{3.37}$$

From (3.36) and (3.37), it is easy to obtain the following equation as:

$$A^{-1} = A^H \tag{3.38}$$

Thus, A is unitary. When $|e| < 0.5$, the magnitude of the diagonal element of A is larger than any off-diagonal element as:

$$|a_{0,0}| > |a_{l,k}|, \qquad \text{for } l \neq 0 \text{ or } k \neq 0 \tag{3.39}$$

CHAPTER FOUR: A BLIND MAXIMUM LIKELIHOOD CARRIER FREQUENCY OFFSET CORRECTION APPROACH FOR OFDM SYSTEMS

In this chapter, a Maximum Likelihood Carrier Frequency Offset Correction (ML-CFOC) approach is proposed for Orthogonal Frequency Division Multiplexing (OFDM) systems. The ML-CFOC exploits the independence between the desired signals, and is based on a simplified Independent Component Analysis (ICA) algorithm. The proposed ML-CFOC approach is implemented successfully for OFDM systems over multipath fading channels without requiring a training sequence. Computer simulations are given, which illustrate the optimal performance of the ML-CFOC [70-72].

This chapter is organized as follows. Section 4.1 proposes the ML-CFOC, which can greatly enhance the system Signal-to-Noise Ratio (SNR). In Section 4.2, the simplified natural-gradient ICA algorithm is used to compensate for the CFO. Simulation results are presented in Section 4.3. Finally, conclusions are drawn in Section 4.4.

4.1 Proposed Maximum Likelihood Carrier Frequency Offset Correction Approach

Maximum Likelihood Analysis

In (3.17), the $v_l'(n)'s$ are modeled as identically-distributed, independent Gaussian random variables with zero mean and variance σ_v^2. Thus, the $x_l(n)'s$ are also

independent and Gaussian-distributed. Consequently, the maximum likelihood function of the A and the $S(n)$ is given by [61]:

$$L(A,S(n)) = \frac{1}{\left(2\pi\sigma_v^2\right)^{M/2}} \exp\left\{-\frac{1}{\sigma_v^2}\left(X(n)-AS(n)\right)^H\left(X(n)-AS(n)\right)\right\} \tag{4.1}$$

Equivalently, the Maximum Likelihood estimate for $X(n)$ is the minimum of $L'\left(A,X(n)\right)$ with respect to $X(n)$, where

$$\begin{aligned} L'(A,S(n)) &= \left(X(n)-AS(n)\right)^H\left(X(n)-AS(n)\right) \\ &= X^H(n)X(n) - S^H(n)A^HX(n) - X^H(n)AS(n) + S^H(n)S(n) \end{aligned} \tag{4.2}$$

The derivation of $L'(A,S(n))$ respect to $S(n)$ is given by:

$$\frac{\partial L'(A,S(n))}{S(n)} = 2S(n) - 2A^HX(n) \tag{4.3}$$

Let (4.3) to be zero, and the maximum likelihood estimate of $S(n)$ is computed as:

$$S(n) = A^HX(n) \tag{4.4}$$

It is clear that the maximum likelihood solution to (4.1) is to find A^H. However, (3.38) states

$$A^H = A^{-1} \tag{4.5}$$

Substituting (4.5) into (4.4) yields

$$\hat{S}(n) = A^{-1}X(n) \tag{4.6}$$

The effectiveness of the ML-CFOC can be measured by the Signal-to-Noise Ratio (SNR) enhancement, which is described in the following.

SNR Enhancement Using the ML-CFOC

The application of the ML-CFOC does not enhance noise power but increases the signal power. Consequently, the system SNR increases greatly. The desired signals $s_k(n)'s$ are assumed to have the same signal energy σ_s^2. The SNR of the received signal $x_l(n)$ at the input of the ML-CFOC block is given by:

$$SNR_{in} = \frac{\left|a_{0,0}\right|^2 \sigma_s^2}{\sum_{k=1}^{M-1}\left|a_{0,k}\right|^2 \sigma_s^2 + \sigma_v^2} \tag{4.7}$$

After the ML-CFOC compensation, the signal power is σ_s^2, and the noise power is computed as:

$$\sum_{k=0}^{M-1}\left|a_{l,k}\right|^2 \frac{N_0}{2} = \frac{N_0}{2} \tag{4.8}$$

The SNR at the output of the ML-CFOC block is given by:

$$SNR_{out} = \frac{\sigma_s^2}{N_0} \tag{4.9}$$

Comparing the SNR in (4.7) with the SNR in (4.9), the SNR increases considerably since $\left|a_{0,0}\right|^2 < 1$. This is because the ML-CFOC collects the interference from other subcarriers into the desired subcarrier. This interference power becomes the signal power in the desired subcarrier. In addition, the SNR in (4.9) is independent of CFO, and is the same as the SNR of the received signal $x_l(n)$ for the system without CFO. Thus, the ML-CFOC removes the deleterious effects of CFO.

In summary, given the received signal vector $X(n)$, the maximum likelihood estimate of the $S(n)$ is to find the matrix A^{-1}. In the next section, the well-known

natural-gradient ICA algorithm will be applied to obtain A^{-1} to achieve maximum likelihood estimate as (4.6) shows.

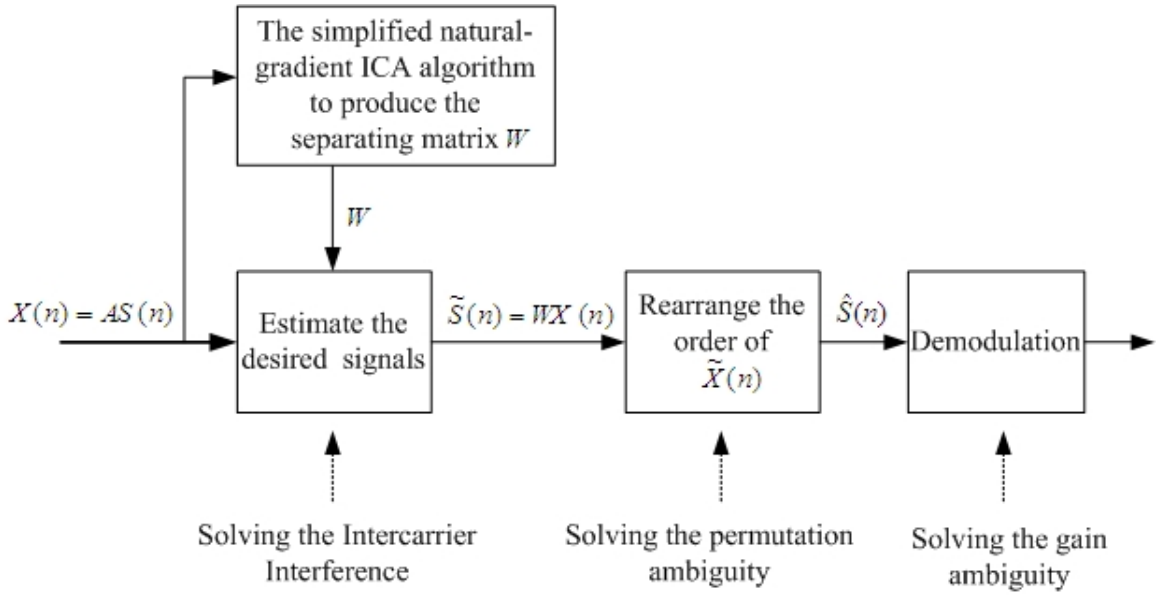

Figure 17: The proposed Maximum Likelihood Carrier Frequency Offset Correction (ML-CFOC) approach based on the simplified natural-gradient Independent Component Analysis (ICA) algorithm

4.2 Simplified Natural-Gradient Independent Component Analysis Algorithm

In most practical systems, the desired signals $s_k(n)'s$ are independent, complex-valued, zero-mean, non-Gaussian, and stationary. According to the Central Limit Theorem (CLT), the distribution of $x_l(n)$, which is the linear combination of $s_k(n)'s$ due to CFO, is more Gaussian than the distribution of $s_k(n)$. This property provides the

foundation for applying ICA to estimate A^{-1} from the $x_l(n)'s$. Therefore, ICA algorithms can be employed to determine the separation matrix W, which transforms $X(n)$ into $\tilde{S}(n)$. $\tilde{S}(n)$ is the estimate signal vector of $S(n)$ and suffers from the permutation and gain ambiguities. The separation matrix W should be found such that

$$\begin{aligned}\tilde{S}(n) &= [\tilde{s}_0(n),...,\tilde{s}_i(n),...,\tilde{s}_{K-1}(n)]^T \\ &= WX(n)\end{aligned} \tag{4.10}$$

where W is a K by M matrix, whose l th row and k th column element is denoted as $w_{l,k}$.

The natural-gradient ICA algorithm specified at Table 2 can be used to estimate W. Usually, a whitening preprocess is used in ICA algorithms. This makes the combination matrix unitary, which accelerates the convergence of the subsequent ICA algorithm. In this application, the ICI matrix A is already unitary as shown in (3.38). Thus, the whitening step is eliminated, resulting in a simplified ICA algorithm. The ML-CFOC approach employing the simplified natural-gradient ICA algorithm is shown in Fig.17.

Solving Permutation Ambiguity

The estimated signal vector $\hat{S}(n)$ without the permutation ambiguity is defined as:

$$\hat{S}(n) = [\hat{s}_0(n),...,\hat{s}_k(n),...,\hat{s}_{K-1}(n)]^T \tag{4.11}$$

In each row l of the matrix W, the element with the largest magnitude, $w_{l,k}$, is found. In (4.10), the row l of the matrix W recovers $\tilde{s}_l(n)$, which actually corresponds to the desired signal $s_k(n)$. Thus, the $\hat{s}_k(n)$ is given by:

$$\hat{s}_k(n) = \tilde{s}_l(n) \tag{4.12}$$

Solving Gain Ambiguity

After the ML-CFOC compensation, the $\hat{s}_k(n)$ is expressed as:

$$\hat{s}_k(n) = \beta_k h_k \hat{d}_k'(n) \tag{4.13}$$

where the unknown complex number β_k denotes the gain ambiguity, and $\hat{d}_k'(n)$ is the estimation of the transmitted signal $d_k'(n)$.

As expressed by (4.13), β_k can be absorbed into the channel transfer factor h_k. Thus, the gain ambiguity can be solved in the demodulation processing. For coherent-demodulation OFDM systems, the channel estimation can identify the value of $\beta_k h_k$ [88]. Differential-demodulation OFDM systems do not need channel knowledge, and the effects of β_k are canceled in the demodulation process.

The proposed ML-CFOC is summarized in Table 5.

Table 5
Outline of the proposed ML-CFOC

Task: Estimate the source signal vector $S(n)$ from their linear combination vector as:

$$X(n) = \mathbf{A}S(n) + V'(n).$$

Step 1. Initialize the separation matrix W.

Step 2. Obtain the $\widetilde{S}(n)$ as:

$$\widetilde{S}(n) = WX(n)$$

Step 3. Obtain the nonlinear vector $\widetilde{S}_{non}(n)$ as:

$$\widetilde{S}_{non}(n) = \left[f(\widetilde{s}_0(n)),..., f(\widetilde{s}_k(n))),..., f(\widetilde{s}_{K-1}(n)) \right]^T$$

where $f(\widetilde{s}_k(n)) = \left|\widetilde{s}_k(n)\right|^2 \widetilde{s}_k(n)$ is used.

Step 4. Use the natural-gradient ICA algorithm to update the separation matrix W.

$$W \leftarrow W + \mu\left(I - E\left[\widetilde{S}_{non}(n)\widetilde{S}^H(n)\right]\right)W$$

Step 5. Normalize W using

$$W \leftarrow W\left(W^H W\right)^{-1/2}$$

Step 6. Check the convergence of W. If the convergence is not reached, go back to **Step 3**. Otherwise, proceed to **Step 7**.

Step 7. Solve the permutation ambiguity.

Step 8.Solve the gain ambiguity.

4.3 Simulation Results

In this section, simulation results are presented to confirm the effectiveness of the proposed ML-CFOC . The simulation setting, shown in Table 6, is used throughout this chapter unless noted otherwise.

Simulation Example 1: Figure 18 shows the crosstalk error learning curve of the ML-CFOC under two different SNR levels, $SNR = 10dB$ and $SNR = 30dB$. Referring to Fig.18, the performance of the ML-CFOC degrades as the SNR decreases. The ML-CFOC converges after about 200 iterations. For the general W estimation case, the natural-gradient ICA algorithm converges in thousands of iterations. Thus, the computation complexity of the ML-CFOC is relatively low. This is because the separation matrix W only depends on the value of the relative CFO.

Simulation Example 2: Figure 19 shows the BER of the simulated OFDM system employing the proposed ML-CFOC for different values of relative CFO. For comparison, the BER of the same system without CFO compensation is also plotted. As expected, these two BER's are identical in the case of $e = 0$. This observation shows that the ML-CFOC does not degrade the system performance in the absence of CFO. For $-0.4 \le e \le 0.4$, the BER of the OFDM system employing the ML-CFOC is almost constant, and is the same as the BER in the case of $e = 0$. This result shows that the proposed ML-CFOC technique successfully removes the undesirable effects of the CFO.

Simulation Example 3: For different SNR values, the BER of the simulated OFDM system employing the proposed ML-CFOC and no CFO compensation is shown in Fig. 20. This figure illustrates that the ML-CFOC approach improves the system's performance over a wide range of SNR.

Table 6
Simulation parameters for the proposed ML-CFOC

Channel coding scheme	Convolutional coding
Coding rate	½
Decoding	Viterbi hard decoding
Modulation scheme	Differential Quadrature Phase Shift Keying (DQPSK)
The number of all subcarriers	8
The number of virtual subcarriers	0
The relative Carrier Frequency Offset	0.2
The total bandwidth	10MHz
Doppler frequency	100kHz
The fading channel	Two Rayleigh-fading taps, whose average path power is 0.38 and 0.62.
The number of processing OFDM symbols	10,000
Signal to Noise Ratio (SNR)	20dB
The number of Monte Carlo trial	100

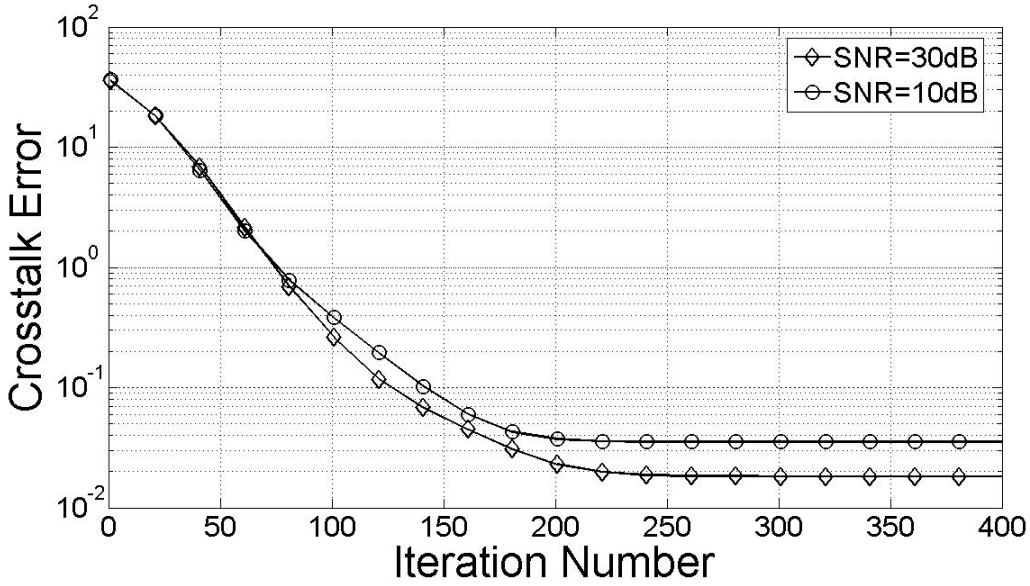

Figure 18: Crosstalk error evolution versus iteration number employing the proposed ML-CFOC under $SNR = 10dB$ and $SNR = 30dB$ for the relative CFO $e = 0.2$

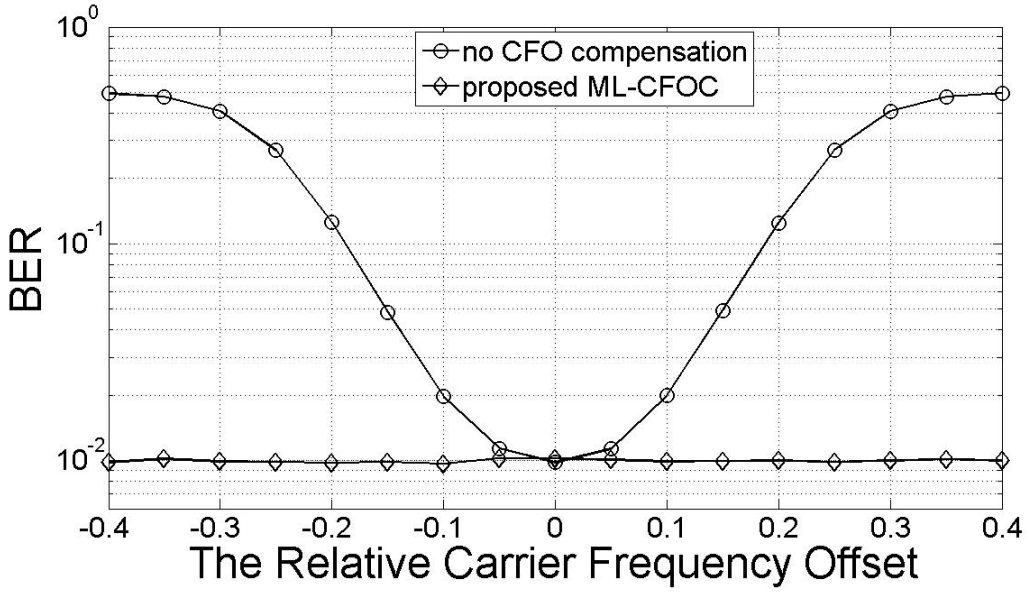

Figure 19: BER of the simulated OFDM system employing the proposed ML-CFOC and no CFO compensation versus the relative CFO under $SNR = 20dB$

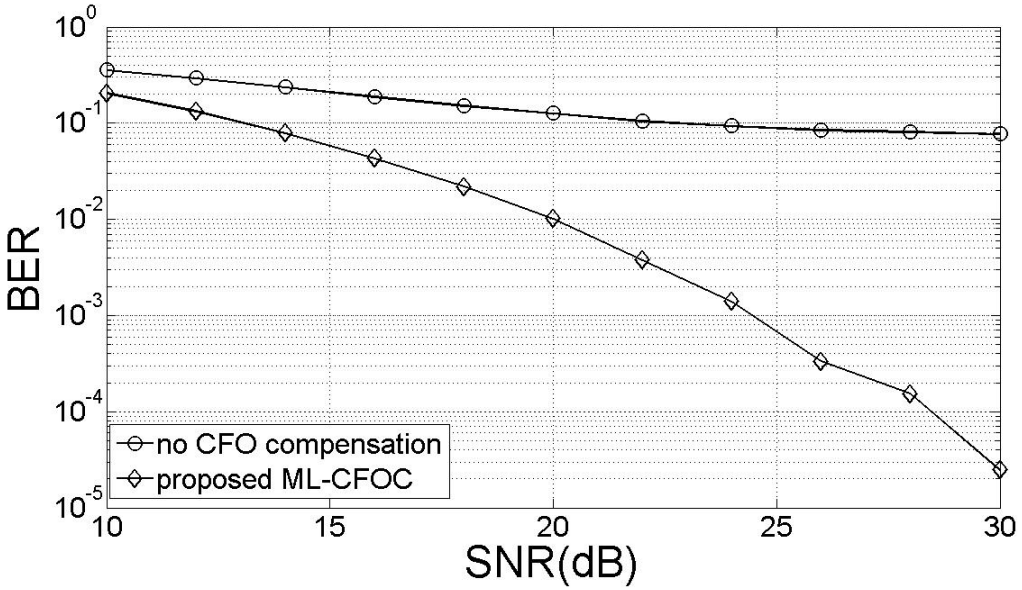

Figure 20: BER of the simulated OFDM system employing the proposed ML-CFOC and no CFO compensation versus SNR for the relative CFO $e = 0.2$

4.4 Conclusions

In this chapter, a novel Maximum Likelihood Carrier Frequency Offset Correction (ML-CFOC) approach based on Independent Component Analysis (ICA) is proposed. Computer simulations illustrate that the proposed ML-CFOC successfully compensates for a wide range of Carrier Frequency Offset (CFO) under different noise levels and over multipath fading channels. This performance improvement has been achieved at the expense of a modest increase in the computational requirements.

CHAPTER FIVE: HIGH-PERFORMANCE BLIND CARRIER FREQUENCY OFFSET ESTIMATOR FOR OFDM SYSTEMS

In this chapter, a novel Blind Carrier Frequency Offset Estimator (BCFOE) is proposed to identify Carrier Frequency Offset (CFO) in Orthogonal Frequency Division Multiplexing (OFDM) systems. The cost function in the proposed BCFOE is based on the fourth-order cumulant, Kurtosis. Both the gradient method and the curve-fitting method are employed to find the minimum of the cost function, which corresponds to the estimating CFO. Compared with the existing low-complexity blind CFO estimation technique [25, 78, 128], the BCFOE, for the same computational complexity, has better performance. Simulation results confirm the high-performance of the proposed BCFOE [73, 74].

This chapter is organized as follows. In Section 5.1, Kurtosis is used to construct the cost function of the BCFOE, which is optimized by the gradient method and the curve-fitting method. The performance and the computational complexity of the proposed BCFOE are compared with the blind CFO estimator [25, 78, 128] in Section 5.2. Simulation results are presented in Section 5.3. Finally, conclusions are drawn in Section 5.4.

5.1 Proposed Blind Carrier Frequency Offset Estimator

Estimation Scheme

As shown in chapter three, CFO destroys the orthogonality between subcarriers in OFDM systems, and thus introduces Intercarrier Interference (ICI). To recover the source signals $s_k(n)'s$ properly, the CFO, e, needs to be estimated and compensated before the Fast Fourier Transform (FFT) operation.

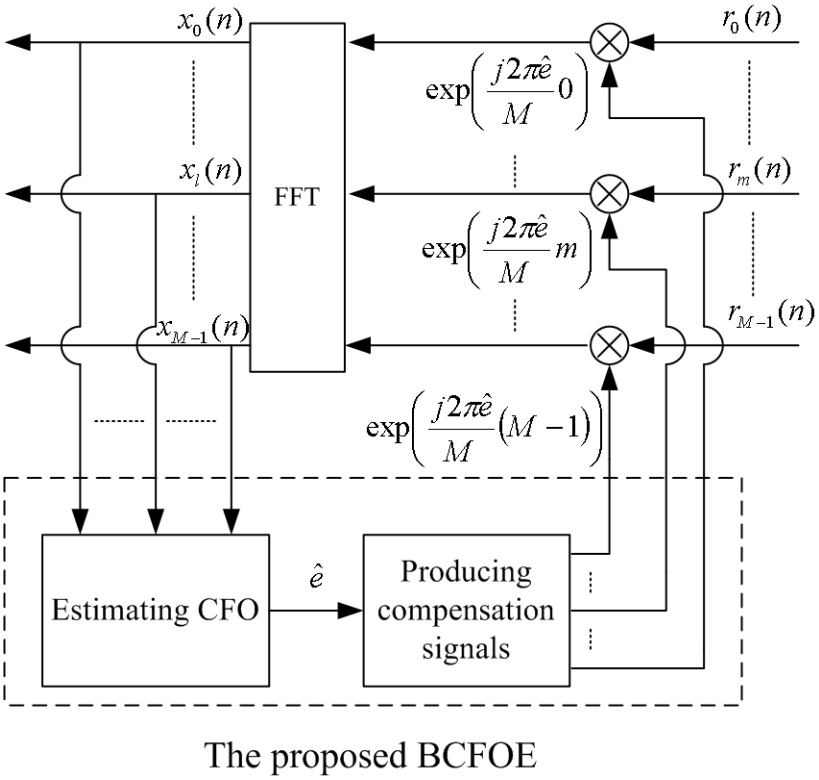

Figure 21: The block diagram of the proposed Blind Carrier Frequency Offset Estimator (BCFOE)

The proposed BCFOE is shown in Fig. 21. The $x_l(n)'s$ are fed into the proposed BCOFE to estimate e. The BCFOE is comprised of a cost function based on Kurtosis and an optimizing operation to find $\hat{e}$ that minimizes the cost function. Then, the $\hat{e}$ is used to correct the phase rotations caused by the e in the $r_m(n)'s$ as shown in (3.13).

The received signals $x_l(n)'s$ after FFT processing are given by:

$$\begin{aligned} x_l(n) &= \sum_{m=0}^{M-1} r_m(n) \exp\left(\frac{j2\pi m(\hat{e}-l)}{M} \right) \\ &= \sum_{k=0}^{K-1} a_{l.k} s_k(n) + v_l'(n), \quad l = 0,1,...,M-1 \end{aligned} \tag{5.1}$$

where the $a_{l.k}$ is the ICI coefficient given by:

$$a_{l.k} = \frac{\sin(\pi(k-l+\hat{e}-e))}{M \sin\left(\pi \frac{k-l+\hat{e}-e}{M} \right)} \exp\left(j\pi \left(\frac{M-1}{M} \right)(k-l+\hat{e}-e) \right) \tag{5.2}$$

As shown in chapter three, intuitively, the fourth-order statistical properties can be used to estimate the CFO. In the next section, Kurtosis, the fourth-order cumulant, is used to build the cost function of the BCFOE.

The Cost Function of the Proposed BCFOE

The variance and the fourth-order moment of the $s_k(n)'s$ are defined as:

$$E\left[|s_k(n)|^2 \right] = \sigma_s^2 \tag{5.3a}$$

and

$$E\left[|s_k(n)|^4 \right] = \gamma_s^4 \tag{5.3b}$$

In general, the $s_k(n)'s$ are sub-Gaussian signals with zero mean [5], and their Kurtoses are negative as:

$$\begin{aligned} Kurt(s_k(n)) &= E\left[\left|s_k(n)\right|^4\right] - 2\left(E\left[\left|s_k(n)\right|^2\right]\right)^2 - 2\left(E\left[s_k^2(n)\right]\right)^2 \\ &= \gamma_s^4 - 2\sigma_s^4 < 0 \end{aligned} \tag{5.4}$$

Assume that the source signals, $s_k(n)'s$, are independent. According to the Central Limit Theorem (CLT), the distribution of the linear combination of $s_k(n)'s$ is more Gaussian than the distribution of any individual $s_k(n)$. Thus, the distribution of $x_l(n)$ tends to be more non-Gaussian when the $\hat{e}$ approaches the e. When the perfect CFO estimation is achieved, i.e., $\hat{e} = e$, the distribution of the $x_l(n)$ is the most non-Gaussian.

According to [14], Kurtosis of a zero-mean, complex random variable is defined as:

$$Kurt(x_l(n)) = E\left[\left|x_l(n)\right|^4\right] - 2\left(E\left[\left|x_l(n)\right|^2\right]\right)^2 - \left|E\left[x_l(n)^2\right]\right|^2 \tag{5.5}$$

It is preferable to use all $x_l(n)'s$ to estimate CFO. The cost function of the proposed BCFOE is chosen as:

$$J(\hat{e}) = \sum_{l=0}^{M-1} Kurt\left(x_l(n)\right) \tag{5.6}$$

After mathematical manipulations, shown in Appendix C, (5.6) can be rewritten as:

$$J(\hat{e}) = a\cos\left(2\pi\left(\hat{e} - e\right)\right) + b \tag{5.7}$$

where a and b are constants defined as:

$$a = \frac{M^2 - 1}{3M^2}\left(\gamma_s^4 - 2\sigma_s^4\right)\left(\sum_{k=0}^{K-1}\left|h_k\right|^4\right) \tag{5.8}$$

and

$$b = \frac{2M^2+1}{3M^2}\left(\gamma_s^4 - 2\sigma_s^4\right)\left(\sum_{k=0}^{K-1}|h_k|^4\right) \tag{5.9}$$

From (5.4), it is clear that

$$a < 0 \tag{5.10}$$

The cost function given by (5.7) has a global minimum at $\hat{e} = e$. In fact, the cost function is a nonlinear function of $\hat{e}$.

In practice, the cost function given by (5.7) is evaluated over N OFDM symbols as:

$$J(\hat{e}) = \frac{1}{M}\sum_{l=0}^{M-1}\left[\frac{1}{N}\sum_{n=0}^{N-1}|x_l(n)|^4 - 2\left(\frac{1}{N}\sum_{n=0}^{N-1}|x_l(n)|^2\right)^2\right] \tag{5.11}$$

Proposed Gradient BCFOE

The gradient method is used to find $\hat{e}$, which minimizes the cost function in (5.11). If the initial value of $\hat{e}$ is chosen as zero, then the gradient method is guaranteed to converge such that the $\hat{e}$ approaches the e. The gradient of the cost function in (5.11) is given by:

$$\frac{\partial J(\hat{e})}{\partial \hat{e}} = \frac{4}{MN^2}\sum_{l=0}^{M-1}\left[\sum_{n=0}^{N-1}|x_l(n)|^2\,\mathrm{Re}\left(2\sum_{n'=0}^{N-1}x_l^*(n')\frac{\partial x_l(n')}{\partial \hat{e}} - N\times x_l^*(n)\frac{\partial x_l(n)}{\partial \hat{e}}\right)\right] \tag{5.12}$$

where

$$\frac{\partial x_l(n)}{\partial \hat{e}} = \sum_{m=0}^{M-1} r_m(n)\frac{j2\pi m}{M}\exp\left(\frac{j2\pi m(\hat{e}-l)}{M}\right) \tag{5.13}$$

Thus, the proposed gradient BCFOC is summarized in Table 7.

Table 7
Outline of the proposed gradient BCFOE

Task: Estimate the CFO from the received signals in the frequency domain $x_l(n)'s$, which are linear combinations of the source signals $s_k(n)'s$ as:

$$x_l(n) = \sum_{k=0}^{K-1} a_{l,k} s_k(n) + v_l'(n), \quad l = 0,1,...,M-1$$

Step 1. Choose the initial value $\hat{e} = 0$.

Step 2. Compute $x_l(n)$ and $\frac{\partial x_l(n)}{\partial \hat{e}}$ as:

$$x_l(n) = \frac{1}{\sqrt{M}} \sum_{m=0}^{M-1} r_m(n) \exp\left(\frac{j2\pi m(\hat{e} - l)}{M} \right)$$

and

$$\frac{\partial x_l(n)}{\partial \hat{e}} = \frac{1}{\sqrt{M}} \sum_{m=0}^{M-1} r_m(n) \frac{j2\pi m}{M} \exp\left(\frac{j2\pi m(\hat{e} - l)}{M} \right)$$

Step 3. Compute the gradient of the cost function as:

$$\frac{\partial J(\hat{e})}{\partial \hat{e}} = \frac{4}{MN^2} \sum_{l=0}^{M-1} \left[\sum_{n=0}^{N-1} |x_l(n)|^2 \operatorname{Re}\left(2 \sum_{n'=0}^{N-1} x_l^*(n') \frac{\partial x_l(n')}{\partial \hat{e}} - N \times x_l^*(n) \frac{\partial x_l(n)}{\partial \hat{e}} \right) \right]$$

Step 4. Update $\hat{e}$ as

$$\hat{e} \leftarrow \hat{e} - u \frac{\partial J(\hat{e})}{\partial \hat{e}}$$

Step 5. Check for convergence of $\hat{e}$. If so, go to step 2. Otherwise, stop the iteration.

Proposed Curve-Fitting BCFOE

Based on the exact form of the cost function in (5.7), the minimum of the cost function can be found using the curve-fitting method. Evaluate the cost function (5.11) at the points of $\hat{e} = 1/4$, $\hat{e} = 1/4$, and $\hat{e} = 1/4$, respectively, as:

$$\begin{aligned} J(1/4) &= a\cos\left(2\pi\left(1/4 - e\right)\right) + b \\ &= a\sin(2\pi e) + b \end{aligned} \tag{5.15}$$

$$\begin{aligned} J(0) &= a\cos(2\pi(0 - e)) + b \\ &= a\cos(2\pi e) + b \end{aligned} \tag{5.16}$$

$$\begin{aligned} J(-1/4) &= a\cos\left(2\pi\left(-1/4 - e\right)\right) + b \\ &= -a\sin(2\pi e) + b \end{aligned} \tag{5.17}$$

From (5.15), (5.16), and (5.17), the following two formulae are derived as:

$$\begin{aligned} \chi &= a\sin(2\pi e) \\ &= \frac{J(1/4) - J(-1/4)}{2} \end{aligned} \tag{5.18}$$

and

$$\begin{aligned} \gamma &= a\cos(2\pi e) \\ &= J(0) - \frac{J(1/4) + J(-1/4)}{2} \end{aligned} \tag{5.19}$$

From (5.18) and (5.19), the e is obtained as follows:

$$e = \begin{cases} \dfrac{1}{2\pi}\tan^{-1}\left(\dfrac{\chi}{\gamma}\right), & \text{when } \gamma < 0 \\ 0.5 - \dfrac{1}{2\pi}\tan^{-1}\left(\dfrac{\chi}{\gamma}\right), & \text{when } \gamma > 0, \text{ and } \chi < 0 \\ 0.5 + \dfrac{1}{2\pi}\tan^{-1}\left(\dfrac{\chi}{\gamma}\right), & \text{when } \gamma > 0, \text{ and } \chi > 0 \end{cases} \tag{5.20}$$

The proposed curve-fitting BCFOC algorithm is summarized in Table 8. The curve-fitting BCFOE has the lower computation complexity and is more attractive than the gradient BCFOE.

5.2 Comparison with the YG-CFO Estimator

In [25, 78, 128], the YG-CFO estimator exploits the fourth-order statistical properties of the $x_l(n)'s$ to estimate CFO. The YG-CFO estimator can uniquely identify the e in the range of -0.5 and 0.5. The cost function of the YG-CFO estimator was proposed as:

$$J_s(\hat{e}) = \frac{1}{MN}\sum_{l=0}^{M-1}\sum_{n=0}^{N-1}\left|x_l(n)\right|^4 \tag{5.21}$$

The gradient of the cost function in (5.21) was given by:

$$\frac{\partial J_s(\hat{e})}{\partial \hat{e}} = \frac{4}{MN}\sum_{l=0}^{M-1}\sum_{n=0}^{N-1}\left|x_l(n)\right|^2 \mathrm{Re}\left(x_l^*(n)\frac{\partial x_l(n)}{\partial \hat{e}}\right) \tag{5.22}$$

The gradient YG-CFO estimator was derived as the same as the gradient BCFOE; the curve-fitting YG-CFO estimator takes the same form as curve-fitting BCFOE. The computational cost of the YG-CFO estimator is low, and its performance is superior to the blind CFO estimator in [11]. However, the YG-CFO estimator does not consider noise effects. In the following, it will be shown that the proposed BCFOE outperforms the YG-CFO estimator, for the same computational complexity.

Table 8
Outline of the proposed curve-fitting BCFOE

Task: Estimate the source signal vector $S(n)$ from their linear combination vector

$$X(n) = \mathbf{A}S(n) + V'(n).$$

Step 1. Evaluate the cost function at the points of $\hat{e} = -1/4$, $\hat{e} = 1/4$, and $\hat{e} = 1/4$ to obtain the corresponding cost function values, $J(-1/4)$, $J(0)$, and $J(1/4)$.

Step 2. Compute two intermediate values as

$$\chi = \frac{J(1/4) - J(-1/4)}{2}$$

and

$$\gamma = J(0) - \frac{J(1/4) + J(-1/4)}{2}$$

Step 3. Compute the CFO estimate $\hat{e}$ as

If $\gamma < 0$, then

$$\hat{e} = \frac{1}{2\pi}\tan^{-1}\left(\frac{\chi}{\gamma}\right)$$

If $\gamma > 0$ and $\chi < 0$, then

$$\hat{e} = 0.5 - \frac{1}{2\pi}\tan^{-1}\left(\frac{\chi}{\gamma}\right)$$

If $\gamma > 0$ and $\chi > 0$, then

$$\hat{e} = 0.5 + \frac{1}{2\pi}\tan^{-1}\left(\frac{\chi}{\gamma}\right)$$

Performance Comparison between the BCFOE and the YG-CFO Estimator

In principle, all valid cost functions reach their minima when the model holds; in this sense, no one cost function is better than another. In practice, however, cost functions are only evaluated from finite data samples, which are corrupted by noises. Thus, some cost functions are more subjected to noise effects than others.

It is well known that Kurtosis of Gaussian noise is zero. Thus, given a non-Gaussian signal that is corrupted by additive Gaussian noise, applying Kurtosis in cost functions theoretically results in elimination of the noise effects. This feature of Kurtosis means that using Kurtosis to estimate a Gaussian-corrupted signal leads automatically to noise reduction.

Kurtosis is used in the cost function of the BCFOE algorithm as shown in (5.11). This is in contrast with the cost function of the YG-CFO estimator given by (5.21). Thus, the performance of the YG-CFO estimator is more degraded by Gaussian noise than that of the proposed BCFOE. That observation is confirmed by simulation results.

Computational Complexity Comparison between the Gradient BCFOE and the Gradient YG-CFO Estimator

The computational complexity here is measured in terms of real-number multiplications that a CFO estimator needs to optimize its cost function. Since both estimators need the values of $x_l(n)$ and/or $\frac{\partial x_l(n)}{\partial \hat{e}}$, computation loads to obtain these two values are not taken into account. Given the values of $x_l(n)$ and $\frac{\partial x_l(n)}{\partial \hat{e}}$, computing

$|x_l(n)|^2$ and $\mathrm{Re}\left(x_l^*(n) \frac{\partial x_l(n)}{\partial \hat{e}} \right)$ needs two real-number multiplications, respectively.

Computing $|x_l(n)|^4$ from $|x_l(n)|^2$ needs one real-number multiplication.

Computing the gradient of the BCFOE cost function in (5.12) needs $5MN$ real-number multiplications. Computing the gradient of the YG-CFO estimator's cost function, shown in (5.22), also needs $5MN$ real-number multiplications. Thus, the computational complexity of the gradient BCFOE is the same as the gradient YG-CFO estimator in terms of real-number multiplications.

Computational Complexity Comparison between the Curve-Fitting BCFOE and the Curve-Fitting YG-CFO Estimator

For the proposed curve-fitting BCFOE, computing $J(\hat{e})$ at one specific point $\hat{e}$ needs $(3N+1)M$ real-number multiplications, which approximately equals $3MN$. In the curve-fitting YG-CFO estimator, computing $J_s(\hat{e})$ at one specific point $\hat{e}$ requires $3MN$ real-number multiplications. Thus, the computational complexity of the curve-fitting BCFOE approximates the curve-fitting YG-CFO estimator in terms of real-number multiplications.

Table 9
Simulation parameters for the proposed BCFOE

Channel Coding Scheme	Convolutional Coding
Channel Coding Rate	$1/2$
Decoding	Viterbi Hard Decoding
Modulation scheme	QPSK or 16QAM
The total number of subcarriers	64
The number of virtual subcarriers	12
The relative Carrier Frequency Offset e	0.1
The total bandwidth	20MHz
Doppler frequency of the fading channel	200kHz
Multipath of the fading channel	6 Rayleigh-fading paths with exponentially decaying power
The number of processing OFDM symbols	20
Signal to Noise Ratio (SNR)	20dB
The number of Monte Carlo trial	1,000

5.3 Simulation Results

In this section, the performance of the proposed gradient and curve-fitting BCFOE is illustrated and compared with that of the corresponding YG-CFO estimators. The specification of the simulated OFDM system follows IEEE 802.11a [131]. The

simulated multipath fading channel has six independent, Rayleigh-fading paths. The average path power, $E\left[\left|h_p(n)\right|^2\right]$, $p = 0,1,...,5$, is the exponentially decaying function of the excess delay p, expressed as:

$$E\left[\left|h_p(n)\right|^2\right] = \frac{e^{-p/3}}{\sum_{q=0}^{5} e^{-q/3}}. \tag{5.23}$$

Quadrature Phase Shift Keying (QPSK) is used in simulation examples, which compute Mean Square Error (MSE) of the estimated CFO. For Simulation examples showing the BER of the simulated OFDM system, the exact channel parameters are utilized in the coherent demodulation. It was shown that the YG-CFO estimator can achieve almost optimal BER performance for QPSK-modulated OFDM systems [128]. Thus, 16-Quadrature Amplitude Modulation (16QAM) is used to show the BER of the simulated OFDM system since 16QAM-modulated OFDM systems are more sensitive to the CFO than QPSK-modulated OFDM systems. The simulation parameters shown in Table 9 are used throughout this chapter unless noted otherwise.

Proposed Gradient BCFOE

Simulation Example 1. Figure 22 shows the learning curves of the gradient BCFOE and the gradient YG-CFO estimator under two different SNR levels, $SNR = 0dB$ and $SNR = 30dB$. As shown in Fig.22, the gradient BCFOE has faster convergence properties. The performance of both approaches is degraded as the SNR is decreased. At the same noise level, the gradient BCFOE provides better performance.

Simulation Example 2. Figure 23 shows MSE of the gradient BCFOE and the gradient YG-CFO estimator versus the number of processing OFDM symbols. For both approaches, the MSE is dependent on the number of processing OFDM symbols. For the single OFDM symbol, MSEs of both estimators are the same, since the cost functions in (5.11) and (5.21) are equal when $N = 1$. However, with numerous processing OFDM symbols, the performance improvement of the BCFOE is demonstrated.

Simulation Example 3. The MSE of the gradient BCFOE and the gradient YG-CFO estimator versus SNR is illustrated in Fig. 24. Under different noise levels, the performance improvement employing the BCFOE is illustrated.

Simulation Example 4: Figure 25 shows the BER of the simulated system employing the gradient BCFOE, the gradient YG-CFO estimator, and perfect CFO compensation over a wide range of CFO conditions. Both algorithms can compensate CFO effects over a wide range of CFO. In fact, the BER compensated by the BCFOE is lower than that by the YG-CFO estimator.

Simulation Example 5: The BER of the simulated system employing the gradient BCFOE and the gradient YG-CFO estimator to retrieve and compensate for the CFO is given in Fig. 26. For comparison, the BER of the same system with perfect CFO compensation and no CFO compensation are also plotted. As expected, without CFO compensation, the system performance suffers serious degradation because of ICI. Better BER performance of the proposed BCFOE is maintained over a wide range SNR values, especially for high SNR values.

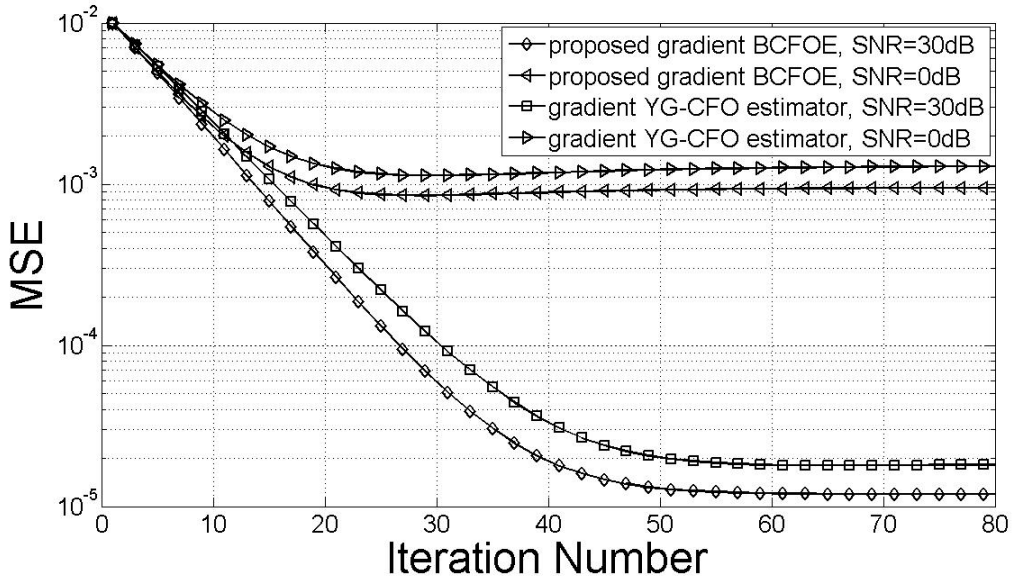

Figure 22: MSE evolution of the gradient BCFOE and the gradient YG-CFO estimator versus iteration number for the relative CFO $e = 0.1$

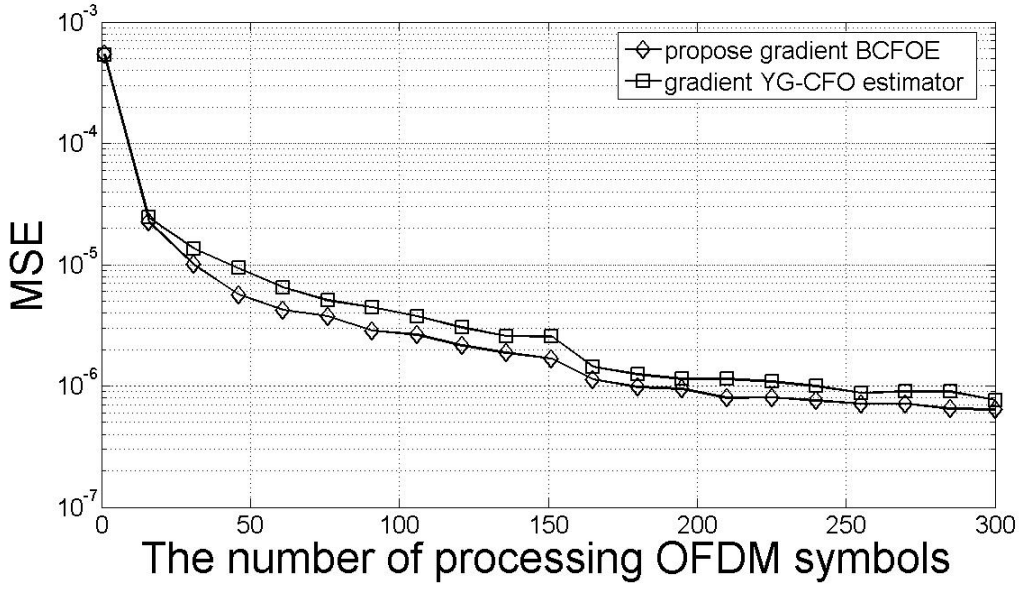

Figure 23: MSE of the gradient BCFOE and the gradient YG-CFO estimator versus the number of processing OFDM symbols under $SNR = 20dB$ for the relative CFO $e = 0.1$

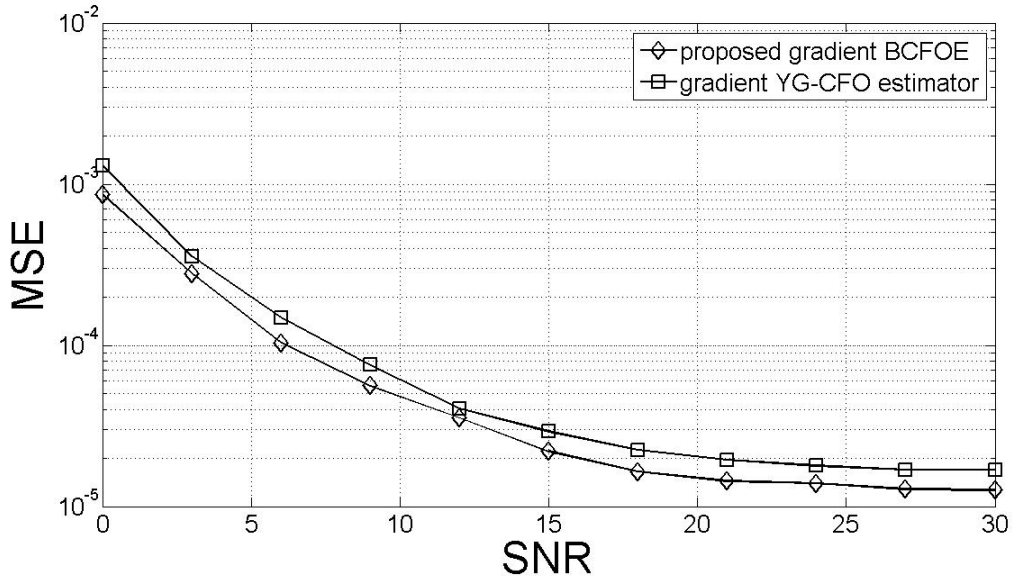

Figure 24: MSE of the gradient BCFOE and the gradient YG-CFO estimator versus SNR for the relative CFO $e = 0.1$

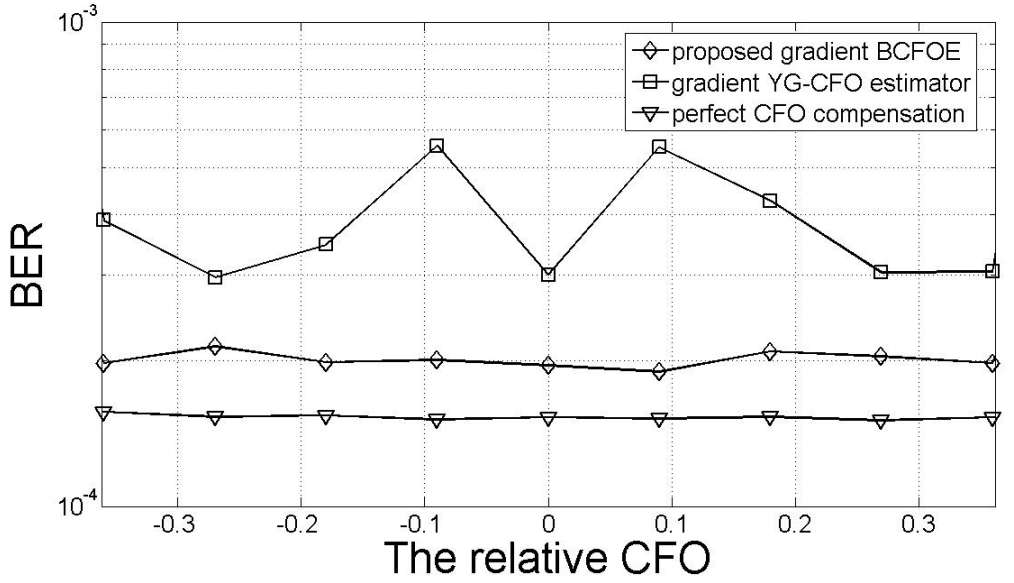

Figure 25: BER of the simulated system with the gradient BCFOE compensation, the gradient YG-CFO estimator compensation, and perfect CFO compensation versus the relative CFO under $SNR = 20dB$

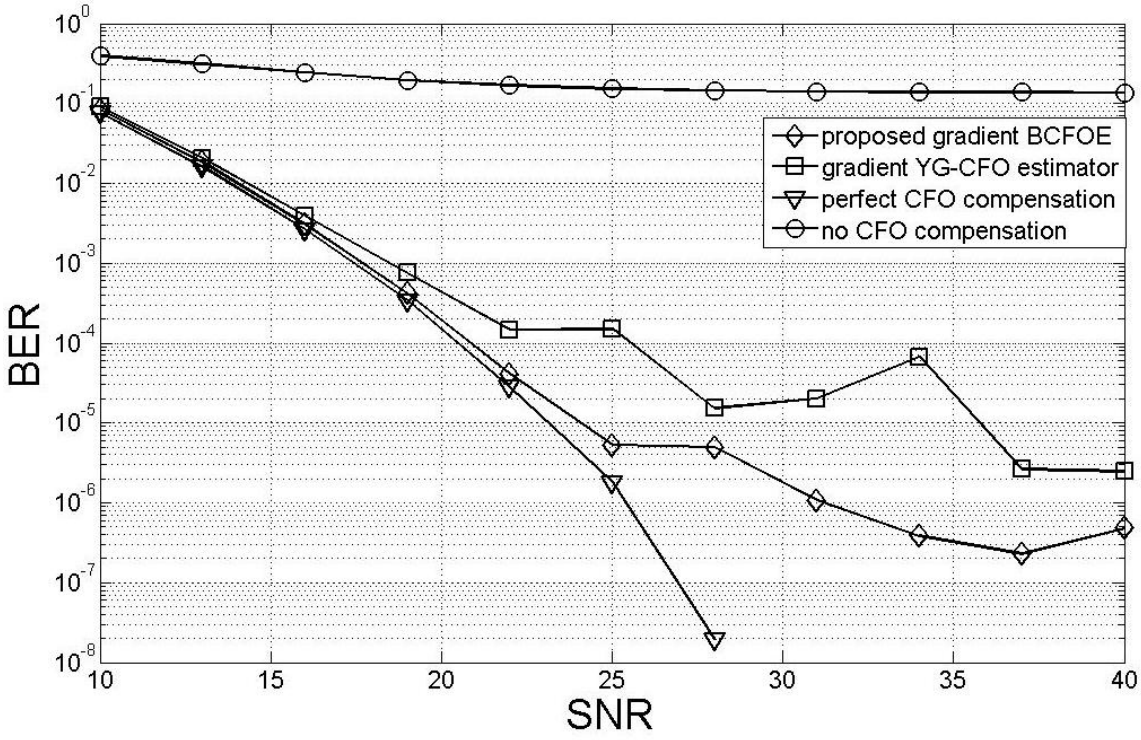

Figure 26: BER of the simulated system with the gradient BCFOE compensation, the gradient YG-CFO estimator compensation, perfect CFO compensation, and no CFO compensation versus SNR for the relative CFO $e = 0.1$

Proposed Curve-Fitting BCFOE

Simulation Example 1: Figure 27 shows the MSE of the proposed curve-fitting BCFOE and the curve-fitting YG-CFO estimator versus the number of processing OFDM symbols. For one processing OFDM symbol, the MSE of both CFO estimators is the same. This is because two cost functions shown in (5.11) and (5.21) are the same when $N = 1$. However, when processing more OFDM symbols, the performance improvement of the BCFOE is demonstrated in Fig.27.

Simulation Example 2: Figure 28 shows the MSE of the proposed curve-fitting BCFOE and the curve-fitting YG-CFO estimator versus SNR. The results illustrate the performance improvement employing the curve-fitting BCFOE for different noise levels.

Simulation Example 3: Figure 29 shows the BER of the 16QAM-modulated OFDM system employing the proposed curve-fitting BCFOE for different values of CFO. For comparison, the BER of the same system employing the curve-fitting YG-CFO estimator is also plotted. Both CFO estimators can compensate for CFO effects over a wide range of CFO. For the 16QAM-modulated OFDM system, perfect CFO compensation cannot be achieved by these two CFO estimators. However, the BER employing the curve-fitting BCFOE is much lower than that obtained using the curve-fitting YG-CFO estimator.

Simulation Example 4: Figure 30 shows the BER of the 16QAM-modulated OFDM system employing the proposed curve-fitting BCFOE, the curve-fitting YG-CFO estimator, perfect CFO compensation, and no CFO compensation for different Signal to Noise Ratio (SNR) values. It is clear that the proposed curve-fitting BCFOC outperforms the curve-fitting YG-CFO estimator over a wide range of SNR, especially at high SNR values.

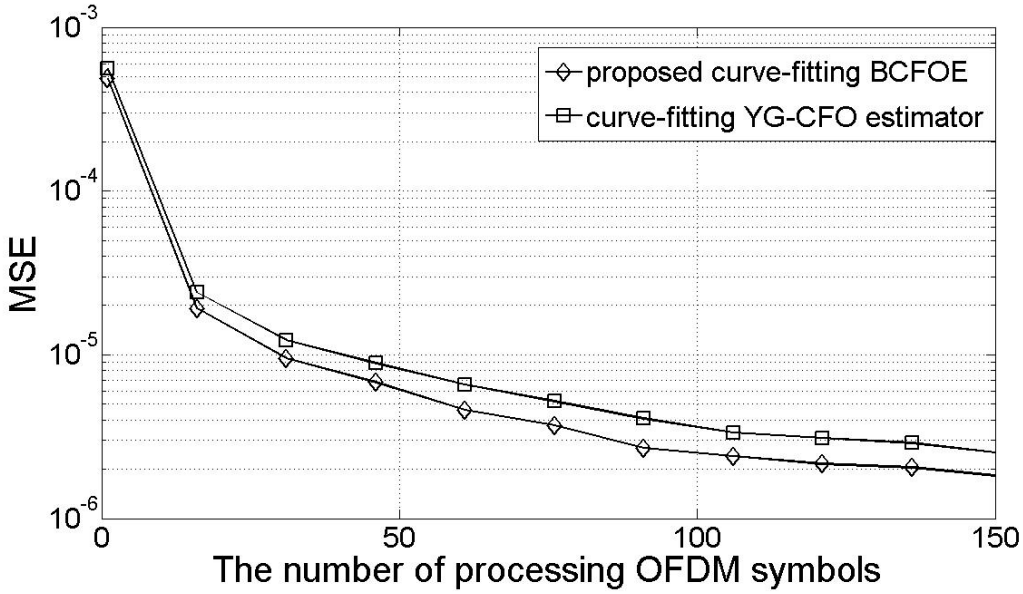

Figure 27: MSE of the curve-fitting BCFOE and the curve-fitting YG-CFO estimator versus the number of processing OFDM symbols under $SNR = 20dB$ for the relative CFO $e = 0.1$

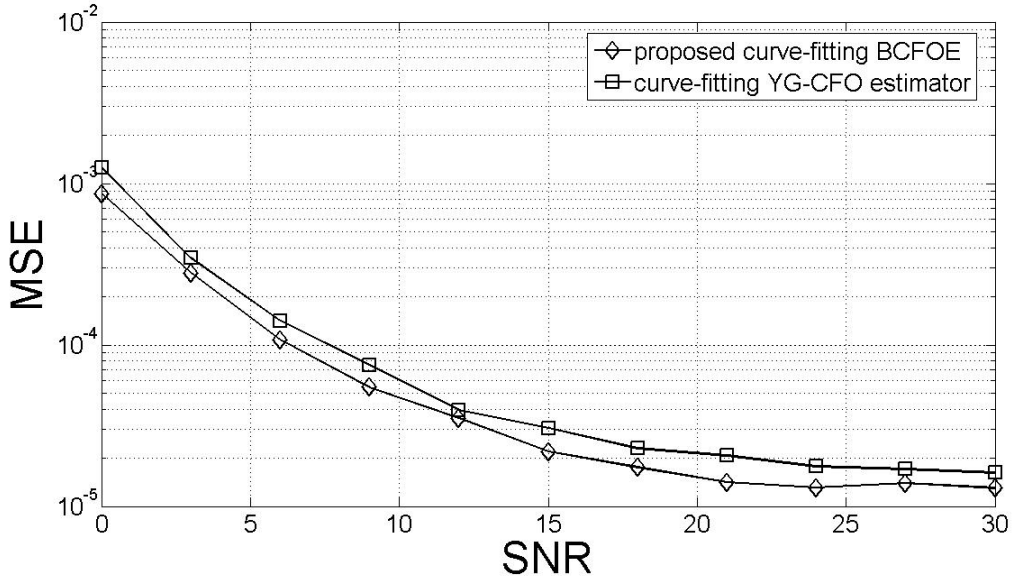

Figure 28: MSE of the curve-fitting BCFOE and the curve-fitting YG-CFO estimator versus SNR for the relative CFO $e = 0.1$

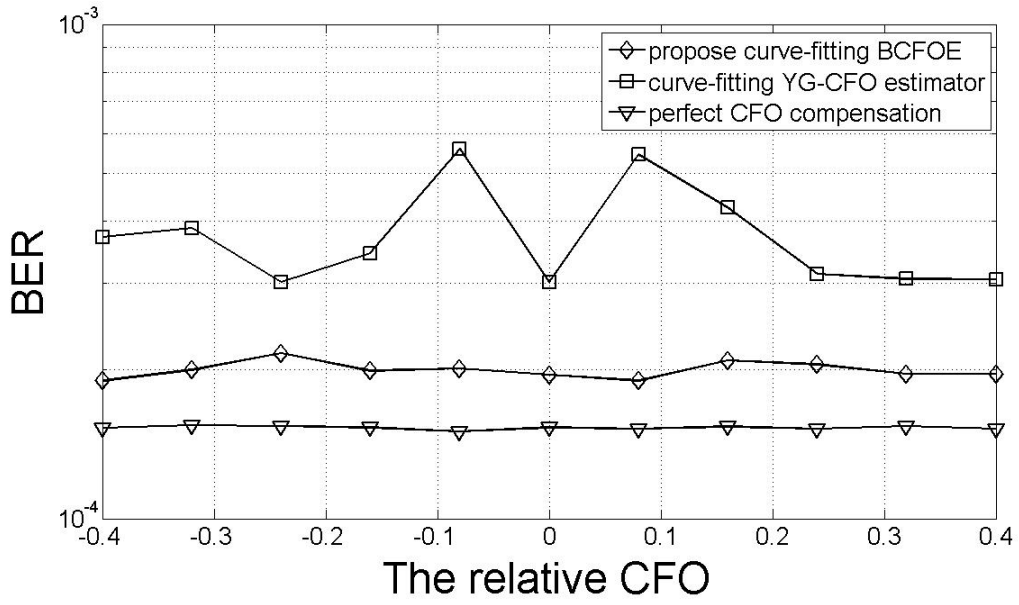

Figure 29: BER of the simulated OFDM system employing the curve-fitting BCFOE, the curve-fitting YG-CFO estimator, and perfect CFO compensation versus the relative CFO under $SNR = 20dB$

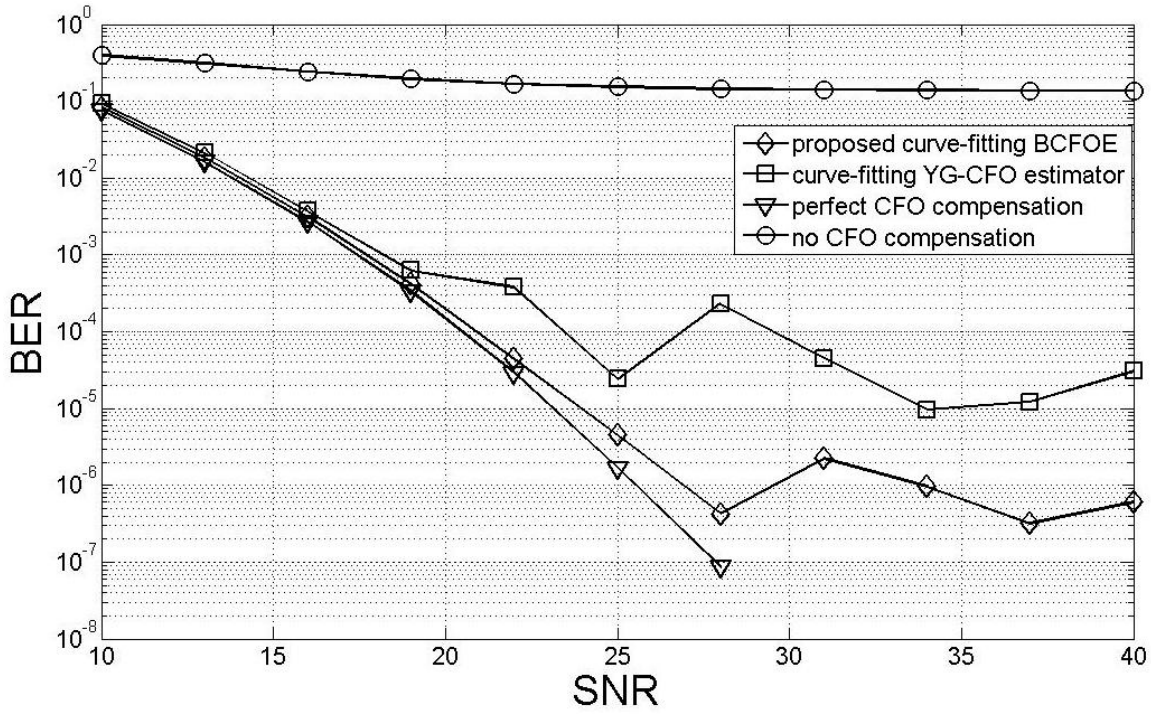

Figure 30: BER of the simulated OFDM system employing the curve-fitting BCFOE, the curve-fitting YG-CFO estimator, perfect CFO compensation, and no CFO compensation versus SNR for the relative CFO $e = 0.1$

5.4 Conclusions

In this chapter, a high-performance Blind Carrier Frequency Offset Estimator (BCFOE) is proposed for OFDM systems. The proposed BCFOE can identify the Carrier Frequency Offset (CFO) within the range of half subcarrier spacing. The BCFOE is based on Kurtosis, and has the same attractive computational properties as the YG-CFO estimator in [25, 78, 128]. However, the BCFOE achieves superior performance to the

YG-CFO estimator in the presence of noise. This has been confirmed by extensive simulations.

CHAPTER SIX: CONTRIBUTIONS AND FUTURE WORK

The research work presented in this dissertation examined the application of Blind Source Separation (BSS) via Independent Component Analysis (ICA) to wireless communications. This chapter summarizes key contributions of this research, and outlines some further research directions.

6.1 Major Contributions

The research presented in this dissertation contains the following key contributions.

In chapter two, a novel Frequency-Domain ICA (ICA-F) approach is proposed to separate and deconvolve digitally modulated signals traveling through frequency-selective, slow fading channels. In the ICA-F, the convolutive combination in the time domain is converted to multiple instantaneous combinations in the frequency domain. Then, the natural-gradient ICA algorithm is employed to separate the frequency components. Finally, the inherent permutation and gain ambiguities associated with ICA are successfully solved. Compared with existing time-domain approaches, the ICA-F is computationally efficient and possesses fast convergence. Simulation results confirm the effectiveness of the proposed ICA-F.

In chapter four, a novel Maximum Likelihood Carrier Frequency Offset Correction approach (ML-CFOC) is proposed for OFDM systems. The performance improvement of the ML-CFOC is achieved at the expense of a modest increase in the computational requirements without sacrificing the system bandwidth or increasing the hardware complexity. Simulation results illustrate the appreciable improvement in the Bit Error Rate (BER) over a wide range of CFO situations and noise levels employing the proposed ML-CFOC.

In chapter five, a high-performance Blind Carrier Frequency Offset Estimator (BCFOE) is proposed to identify CFO within the range of half subcarrier spacing. The cost function of the BCFOC is based on the fourth-order cumulant, Kurtosis. Both the gradient method and the curve-fitting method are used to optimize this cost function. The BCFOE achieves superior performance over the existing blind CFO estimator [25, 78, 128], referred to as the YG-CFO estimator, without increasing the computational complexity, sacrificing the system bandwidth, or increasing the hardware complexity. Extensive simulation results verify the superior performance of the proposed BCFOE in comparison with the YG-CFO estimator and the ML-CFOC technique.

6.2 Future Research Work

This research can be extended in many directions. The major topics are as follows.

Novel ICA Algorithms with Prior System Knowledge

In wireless communications, the receiver has prior knowledge about the source signals. This available information includes modulation scheme, discrete distribution, constant modulus, and Probability Density Function (PDF). This prior information should be incorporated into ICA algorithms in a suitable way to achieve optimal performance.

Frequency-Domain Fast-Convergent ICA Algorithms

As noted in chapter one, there are four kinds of fading channels:

- flat, slow fading channel
- frequency-selective, slow fading channel
- flat, fast fading channel
- frequency-selective, fast fading channel

Frequency-selective fading and fast fading are two major obstacles to applying ICA to wireless communications. In frequency-selective, fast fading channels, the combination model is convolutive and time-variant. This model is challenging and hard to solve. It would be interesting and useful to develop a fast-convergence ICA algorithm in the frequency domain to solve this combination model.

Blind Carrier Frequency Offset Estimation for MC-CDMA and MIMO-OFDM

Recently, a new Code Division Multiple Access (CDMA) system based on a combination of CDMA and OFDM signaling, Multicarrier-CDMA (MC-CDMA) [47, 88], has been proposed. Similar to an OFDM system, the MC-CDMA system is made up of a

series of orthogonal subcarriers. Unlike OFDM systems, where each subcarrier transmits a different symbol, MC-CDMA transmits the same data symbol over several subcarriers. The MC-CDMA transmitter can be implemented by concatenating a Direct Sequence CDMA (DS-CDMA) spreader and an OFDM transmitter. The input data sequence is first converted into a number of parallel data sequences. Then, each data sequence is multiplied by a spreading code. The data in the spreading bits are modulated into the baseband by IDFT and converted back to serial data. At the receiver, a coherent detection method is employed to successfully despread the signal. The received signal, after downconversion and digitization, is first coherently detected with DFT. Then, the received signal is multiplied by a gain factor. Equal Gain Combining (EGC) and Maximum Ratio Combining (MRC) are standard combining techniques used in MC-CDMA receivers.

In recent years, Multiple-Input Multiple-Output (MIMO) wireless technologies [93] have captured considerable research interest, given the capacity increase achievable with such schemes. MIMO exploits multiple antennas in both the transmitter and the receiver. In the transmitter, the high-speed data stream is encoded in time and space across multiple transmit antennas. In doing so, the same carrier is reused at each antenna. Signal processing is then used to decode the composite signals at the receiver. The spatial antenna processing is able to unravel the effects of complex multipath scattering, and fundamentally provides access to parallel independent propagation paths between the transmitter and the receiver. Thus, instead of having access to a single data pipe as with a

conventional wireless system design, a wireless system exploiting MIMO is able to capitalize on the presence of multiple parallel pipes, improving both the data rate and system capacity.

MIMO has now reached a certain level of maturity, and is being investigated in 3G systems. The combination of the two powerful techniques, MIMO and OFDM, results in MIMO-OFDM, which is very attractive, and has become a most promising broadband wireless technique [33, 116, 126].

Conventional OFDM, MC-CDMA, and MIMO-OFDM systems suffer from and require precise CFO estimation approaches. The proposed blind CFO estimators in this research may be extended to be applied in MC-CDMA and MIMO-OFDM systems.

Hybrid ICA Algorithm with Fast Convergence and High Accuracy

In chapter one, two typical ICA algorithms were introduced; they are the Fast fixed-point ICA (FastICA) algorithm [55, 56, 57] and the natural-gradient ICA algorithm [2, 3, 4]. The FastICA algorithm converges fast but has low accuracy. The natural-gradient ICA algorithm converges slow but has high accuracy. These two ICA algorithms are good candidates to compose a hybrid ICA algorithm, which is the combination of the FastICA algorithm and the natural-gradient ICA algorithm. The principle of the hybrid ICA algorithm is straightforward. In the hybrid ICA algorithm, the FastICA algorithm is first used to estimate the separating matrix W. Then, the estimated value of W is used as the initial value of the subsequent natural-gradient ICA algorithm.

The hybrid ICA algorithm inherits fast convergence of the FastICA algorithm and high accuracy of the natural-gradient ICA algorithm. In addition, the hybrid ICA algorithm is robust to local extremum. Even though the fixed-point ICA algorithm is trapped in a local extremum in some cases, the subsequent natural-gradient ICA algorithm can escape from this local extremum [75].

APPENDIX A:
FREQUENCY COMPONENTS OF INDEPENDENT RANDOM VARIABLES

Theorem A.1: If the random variables x and y are independent, then the random variables

$$z = g(x) \tag{A.1}$$

and

$$w = h(y) \tag{A.2}$$

are also independent [91].

This theorem states that functions of independent random variables are also statistically independent. In the proposed frequency-domain Independent Component Analysis (ICA-F), the source signals, $s_l(n)'s$, are independent, and their discrete Short-Time Fourier Transform (STFT), $s_l(r,k)'s$, are linear functions of the $s_l(n)'s$ as:

$$s_l(r,k) = \sum_{n=0}^{+\infty} s_l(n) win(rL-n) e^{-j2\pi k(rL-n)/K} \tag{A.3}$$

Thus, these frequency components $s_l(r,k)'s$ are also independent in each frequency bin, according to Theorem A.1.

APPENDIX B:
SUMMATIONS OF SECOND-ORDER AND FOURTH-ORDER ICI COEFFICIENTS

Theorem B.1: In [36], summations of inverse second-power and fourth-power of sine functions are given by:

$$\frac{1}{\sum_{m=0}^{M-1}\left|\sin\left(\frac{m+e}{M}\pi\right)\right|^2}=\frac{M^2}{\left|\sin(e\pi)\right|^2} \tag{B.1}$$

and

$$\frac{1}{\sum_{m=0}^{M-1}\left|\sin\left(\frac{m+e}{M}\pi\right)\right|^4}=\frac{M^4}{\left|\sin(e\pi)\right|^4}-\frac{2M^2\left(M^2-1\right)}{3\left|\sin(e\pi)\right|^2} \tag{B.2}$$

Theorem B.2: summation of inverse cross second-power of sine functions is given by:

$$\sum_{l=0}^{M-1}\frac{1}{\sin^2\left(\frac{m-l+e}{M}\pi\right)\sin^2\left(\frac{k-l+e}{M}\pi\right)}=\frac{2M^2}{\sin^2(e\pi)\sin^2\left(\frac{m-k}{M}\pi\right)},m\neq k \tag{B.3}$$

where M is a power of 2 as:

$$M=2^{M'} \tag{B.4}$$

Proof:

$$
\begin{aligned}
&\sum_{l=0}^{M-1}\frac{1}{\sin^2\left(\frac{m-l+e}{M}\pi\right)\sin^2\left(\frac{k-l+e}{M}\pi\right)}\\
&=\sum_{l=0}^{M/2-1}\frac{1}{\sin^2\left(\frac{m-l+e}{M}\pi\right)\sin^2\left(\frac{k-l+e}{M}\pi\right)}\\
&+\sum_{l=0}^{M/2-1}\frac{1}{\sin^2\left(\frac{m-l+e+M/2}{M}\pi\right)\sin^2\left(\frac{k-l+e+M/2}{M}\pi\right)}\\
&=\sum_{l=0}^{M/2-1}\frac{1}{\sin^2\left(\frac{m-l+e}{M}\pi\right)\sin^2\left(\frac{k-l+e}{M}\pi\right)}\\
&+\sum_{l=0}^{M/2-1}\frac{1}{\cos^2\left(\frac{m-l+e}{M}\pi\right)\cos^2\left(\frac{k-l+e}{M}\pi\right)}\\
&=\sum_{l=0}^{M/2-1}\frac{\left(\cos\left(\frac{m-l+e}{M}\pi\right)\cos\left(\frac{k-l+e}{M}\pi\right)+\sin\left(\frac{m-l+e}{M}\pi\right)\sin\left(\frac{k-l+e}{M}\pi\right)\right)^2}{\sin^2\left(\frac{m-l+e}{M}\pi\right)\sin^2\left(\frac{k-l+e}{M}\pi\right)\cos^2\left(\frac{m-l+e}{M}\pi\right)\cos^2\left(\frac{k-l+e}{M}\pi\right)}\\
&-\sum_{l=0}^{M/2-1}\frac{2\sin\left(\frac{m-l+e}{M}\pi\right)\sin\left(\frac{k-l+e}{M}\pi\right)\cos\left(\frac{m-l+e}{M}\pi\right)\cos\left(\frac{k-l+e}{M}\pi\right)}{\sin^2\left(\frac{m-l+e}{M}\pi\right)\sin^2\left(\frac{k-l+e}{M}\pi\right)\cos^2\left(\frac{m-l+e}{M}\pi\right)\cos^2\left(\frac{k-l+e}{M}\pi\right)}\\
&=2^4\cos^2\left(\frac{m-k}{M}\pi\right)\sum_{l=0}^{M/2-1}\frac{1}{\sin^2\left(\frac{m-l+e}{M/2}\pi\right)\sin^2\left(\frac{k-l+e}{M/2}\pi\right)}\\
&-2^3\sum_{l=0}^{M/2-1}\frac{1}{\sin\left(\frac{m-l+e}{M/2}\pi\right)\sin\left(\frac{k-l+e}{M/2}\pi\right)}
\end{aligned}
\tag{B.5}
$$

Successively repeating the above maneuver M' times gives the final form as:

$$\sum_{l=0}^{M-1}\frac{1}{\sin^2\left(\frac{m-l+e}{M}\pi\right)\sin^2\left(\frac{k-l+e}{M}\pi\right)}$$
$$=\frac{M^4}{\sin^4(e\pi)}\prod_{i=1}^{M'}\cos^2\left(\frac{m-k}{2^i}\pi\right) \tag{B.6}$$
$$-\sum_{i=1}^{M'}\frac{2^{4M'-2i+1}}{\sin((m+e)\pi)\sin((k+e)\pi)}\left[\prod_{l=i+1}^{M'}\cos^2\left(\frac{m-k}{2^l}\pi\right)\right]\left[\prod_{l=1}^{i-1}\cos\left(\frac{m-k}{2^l}\pi\right)\right]$$

Since $0 \le m,k \le M-1$, then

$$\prod_{i=1}^{M'}\cos^2\left(\frac{m-k}{2^i}\pi\right)=0 \tag{B.7}$$

The second term in the right hand of (B.6) can be written as

$$\sum_{i=1}^{M'}\frac{2^{4M'-2i+1}}{\sin((m+e)\pi)\sin((k+e)\pi)}\left[\prod_{l=i+1}^{M'}\cos^2\left(\frac{m-k}{2^l}\pi\right)\right]\left[\prod_{l=1}^{i-1}\cos\left(\frac{m-k}{2^l}\pi\right)\right]$$
$$=\frac{(-1)^{m+k+1}}{\sin^2(e\pi)\sin^2\left(\frac{m-k}{M}\pi\right)}$$
$$\sum_{i=1}^{M'}2^{4M'-2i+1}\sin^2\left(\frac{m-k}{M}\pi\right)\left[\prod_{l=i+1}^{M'}\cos^2\left(\frac{m-k}{2^l}\pi\right)\right]\left[\prod_{l=1}^{i-1}\cos\left(\frac{m-k}{2^l}\pi\right)\right] \tag{B.8}$$
$$=\frac{(-1)^{m+k+1}}{\sin^2(e\pi)\sin^2\left(\frac{m-k}{M}\pi\right)}\sum_{i=1}^{M'}2^{M'+1}\sin^2\left(\frac{m-k}{2^i}\pi\right)\left[\prod_{l=1}^{i-1}\cos\left(\frac{m-k}{2^l}\pi\right)\right]$$
$$=\frac{2M^2}{\sin^2(e\pi)\sin^2\left(\frac{m-k}{M}\pi\right)}$$

Hence, (B.6) can be simplified as (B.3).

Theorem B.3: Summation of ICI coefficients are given by:

$$\sum_{l=0}^{M-1}\left|a_{l,k}\right|^2=\frac{\sin^2(e\pi)}{M^2}\sum_{l=0}^{M-1}\frac{1}{\sin^2\left(\pi\frac{k-l-e}{M}\right)} \tag{B.9}$$
$$=1$$

$$\sum_{l=0}^{M-1}\left|a_{l,k}\right|^4 = \frac{\sin^4(e\pi)}{M^4}\sum_{l=0}^{M-1}\frac{1}{\sin^4\left(\pi\dfrac{k-l-e}{M}\right)}$$

$$= \frac{\sin^4(e\pi)}{M^4}\left(\frac{M^4}{\sin^4(e\pi)} - \frac{2M^2\left(M^2-1\right)}{3\sin^2(e\pi)}\right) \tag{B.10}$$

$$= 1 - \frac{2\left(M^2-1\right)\sin^2(e\pi)}{3M^2}$$

$$\sum_{l=0}^{M-1}\left|a_{l,k}\right|^2\left|a_{l,m}\right|^2 = \frac{\sin^4(e\pi)}{M^4}\sum_{l=0}^{M-1}\frac{1}{\sin^2\left(\pi\dfrac{k-l-e}{M}\right)\sin^2\left(\pi\dfrac{m-l-e}{M}\right)}$$

$$= \frac{\sin^4(e\pi)}{M^4}\times\frac{2M^2}{\sin^2(e\pi)\sin^2\left(\dfrac{m-k}{M}\pi\right)} \tag{B.11}$$

$$= \frac{1-\cos(2\pi e)}{M^2\sin^2\left(\dfrac{m-k}{M}\pi\right)}, k \neq m$$

APPENDIX C:
THE COST FUNCTION OF THE PROPOSED BLIND CARRIER FREQUENCY OFFSET ESTIMATOR

Since the $s_k(n)'s$ and the $v_l'(n)'s$ are mutually independent and zero mean, the following two conditions are valid.

$$E\left[s_k(n)s_{k'}^*(n)\right]=\begin{cases}\sigma_s^2, & k=k'\\ 0, & k\neq k'\end{cases} \tag{C.1}$$

and

$$\begin{aligned}E\left[s_k(n)v_l'^*(n)\right]&=E\left[s_k(n)\right]E\left[v_l'^*(n)\right]\\&=0\end{aligned} \tag{C.2}$$

$$\begin{aligned}E\left[\left|x_l(n)\right|^2\right]&=E\left[x_l(n)\times x_l^*(n)\right]\\&=E\left[\left(\sum_{k=0}^{K-1}a_{l.k}h_k s_k(n)+v_l'(n)\right)\times\left(\sum_{k=0}^{K-1}a_{l.k}h_k s_k(n)+v_l'(n)\right)^*\right]\\&=\sum_{k=0}^{K-1}\sum_{k'=0}^{K-1}a_{l.k}a_{l,k'}^*h_k h_{k'}^*E\left[s_k(n)s_{k'}^*(n)\right]+\sum_{k=0}^{K-1}a_{l.k}h_kE\left[s_k(n)v_l'^*(n)\right]+\\&\quad\sum_{k=0}^{K-1}a_{l,k}^*h_k^*E\left[s_k^*(n)v_l'(n)\right]+E\left[v_l(n)v_l'^*(n)\right]\end{aligned} \tag{C.3}$$

According to (C.1) and (C.2), (C.3) can be simplified as:

$$E\left[\left|x_l(n)\right|^2\right]=\sigma_s^2\sum_{k=0}^{K-1}\left|a_{l.k}\right|^2\left|h_k\right|^2+\sigma_v^2 \tag{C.4}$$

where σ_v^2 denotes the variance of the noise $v_l'(n)$.

$$\begin{aligned}\left(E\left[\left|x_l(n)\right|^2\right]\right)^2&=\sigma_s^4\sum_{k=0}^{K-1}\left|h_k\right|^4\left|a_{l,k}\right|^4+\sigma_s^4\sum_{k=0}^{K-1}\sum_{\substack{i=0\\k\neq i}}^{K-1}\left|h_k\right|^2\left|h_i\right|^2\left|a_{l,k}\right|^2\left|a_{l,i}\right|^2\\&+2\sigma_v^2\sigma_s^2\sum_{k=0}^{K-1}\left|h_k\right|^2\left|a_{l,k}\right|^2+\sigma_v^4\end{aligned} \tag{C.5}$$

$$
\begin{aligned}
&E\left[\left|x_l(n)\right|^4\right] = E\left[\left(x_l(n)\times x_l^*(n)\right)^2\right] \\
&= E\left[\left(\left(\sum_{k=0}^{K-1} a_{l.k}h_k s_k(n) + v_l'(n)\right)\times\left(\sum_{k=0}^{K-1} a_{l.k}h_k s_k(n) + v_l'(n)\right)^*\right)^2\right] \\
&= \sum_{k=0}^{K-1}\sum_{k'=0}^{K-1}\sum_{k''=0}^{K-1}\sum_{k'''=0}^{K-1} a_{l.k}a_{l,k'}^* a_{l.k''}a_{l,k'''}^* h_k h_{k'}^* h_{k''} h_{k'''}^* E\left[s_k(n)s_{k'}^*(n)s_{k''}(n)s_{k'''}^*(n)\right] + \\
&4\sigma_v^2\sigma_s^2\sum_{k=0}^{K-1}\left|a_{l.k}\right|^2\left|h_k\right|^2 + E\left[\left|v_l'(n)\right|^4\right]
\end{aligned}
\tag{C.6}
$$

where

$$
E\left[s_k(n)s_{k'}^*(n)s_{k''}(n)s_{k'''}^*(n)\right] = \begin{cases} \gamma_s^4, & k = k' = k'' = k''' \\ \sigma_s^4, & k = k' \neq k'' = k''' \\ \sigma_s^4, & k = k''' \neq k' = k'' \\ 0, & \text{otherwise} \end{cases}
\tag{C.7}
$$

Substituting (C.7) into (C.6) yields

$$
\begin{aligned}
&E\left[\left|x_l(n)\right|^4\right] = \gamma_s^4\sum_{k=0}^{K-1}\left|h_k\right|^4\left|a_{l,k}\right|^4 + 2\sigma_s^4\sum_{k=0}^{K-1}\sum_{\substack{i=0 \\ k\neq i}}^{K-1}\left|h_k\right|^2\left|h_i\right|^2\left|a_{l,k}\right|^2\left|a_{l,i}\right|^2 \\
&+ 4\sigma_s^2\sigma_v^2\sum_{k=0}^{K-1}\left|h_k\right|^2\left|a_{l,k}\right|^2 + \gamma_v^4
\end{aligned}
\tag{C.8}
$$

where γ_v^4 denotes the fourth-order moment of the $v_l'(n)$.

It is clear that

$$
E\left[x_l^2(n)\right] = 0
\tag{C.9}
$$

Since Kurtosis of a Gaussian noise equals zero, the following condition is valid.

$$
2\sigma_v^4 - \gamma_v^4 = 0
\tag{C.10}
$$

From (C.5), (C.8), and (C.9), Kurtosis of $x_l(n)$ can be expressed as:

$$
Kurt(x_l(n)) = \left(\gamma_s^4 - 2\sigma_s^4\right)\sum_{k=0}^{K-1}\left|h_k\right|^4\left|a_{l,k}\right|^4
\tag{C.11}
$$

Substituting (C.11) into (5.6) yields

$$\begin{aligned} J(\hat{e}) &= \left(\gamma_s^4 - 2\sigma_s^4\right)\left(\sum_{l=0}^{M-1}\left|a_{l,k}\right|^4\right)\sum_{k=0}^{K-1}\left|h_k\right|^4 \\ &= \left(\gamma_s^4 - 2\sigma_s^4\right)\left(\sum_{k=0}^{K-1}\left|h_k\right|^4\right)\frac{M^2-1}{3M^2}\cos\left(2\pi\left(\hat{e}-e\right)\right) + \left(\gamma_s^4 - 2\sigma_s^4\right)\left(\sum_{k=0}^{K-1}\left|h_k\right|^4\right)\frac{2M^2+1}{3M^2} \end{aligned} \tag{C.12}$$

Thus, (5.7) is obtained.

LIST OF REFERENCES

[1]. Robert Aichner, Herbert Buchner, Fei Yan, and Walter Kellermann, “Real-Time Convolutive Blind Source Separation Based on a Broadband Approach,” in Proc. of Fifth International Conference Independent Component Analysis and Blind Signal Separation, Granada, Spain, September 2004, pp. 840-848.

[2]. Shun-ichi Amari, Andrzej Cichocki, and H. H. Yang, “A New Learning Algorithm for Blind Signal Separation,” Advances in Neural Information Processing Systems, Vol. 8, pp. 757-763, 1996.

[3]. Shun-ichi Amari, “Natural Gradient Works Efficiently in Learning,” Neural Computation, Vol. 10, pp. 251-276, Feb. 1998.

[4]. Shun-ichi Amari, T-P. Chen, and Andrzej Cichocki, “Stability Analysis of Learning Algorithms for Blind Source Separation,” Neural Networks, Vol. 10, No. 8, pp. 1345–1351, August 1997.

[5]. Shun-ichi Amari, S. C. Douglas, Andrzej Cichocki, and H. H. Yang, “Multichannel Blind Deconvolution and Equalization Using the Natural Gradient,” in Proc. of Signal Processing Advance in Wireless Communication Workshop, Paris, France, 1997, pp. 101-104.

[6]. Shoko Araki, Ryo Mukai, Shoji Makino, Tsuyoki Nishikawa, and Hiroshi Saruwatari, “The Fundamental Limitation of Frequency Domain Blind Source

Separation for Convolutive Mixtures of Speech," IEEE Trans. on Speech and Audio Processing, Vol. 11, No. 2, pp. 109-116, March 2003.

[7]. Jean Armstrong, "Analysis of New and Existing Methods of Reducing Intercarrier Interference Due to Carrier Frequency Offset in OFDM," IEEE Trans. on Communications, Vol. 47, No. 3, pp. 365-369, March 1999.

[8]. Futoshi Asano, Shiro Ikeda, Michiaki Ogawa, Hideki Asoh, and Nobuhiko Kitawaki, "Combined Approach of Array Processing and Independent Component Analysis for Blind Separation of Acoustic Signals," IEEE Trans. on Speech and Audio Processing, Vol.11, No.3, pp. 204-215, May 2003.

[9]. Samir Attallah, "Blind Estimation of Residual Carrier Offset in OFDM Systems," IEEE Signal Processing Letters, Vol. 11, No. 2, pp. 216-219, Feb. 2004.

[10]. Ahmad R. S. Bahai, and Burton R. Saltzberg, Multi-Carrier Digital Communications Theory and Applications of OFDM, Kluwer Academic Publishers, 1999.

[11]. Jan-Jaap van de Beek, Magnus Sandell, and Per Ola Borjesson, "ML Estimation of Time and Frequency Offset in OFDM Systems," IEEE Trans. on Signal Processing, Vol.45, No.7, pp. 1800-1805, July 1997.

[12]. A.J. Bell, and T. J. Sejnowske, "An Information Maximization Approach to Blind Separation and Blind Deconvolution," Neural Computation, Vol.7, pp. 1129-1159, 1995.

[13]. Philip A. Bello, “Characterization of Randomly Time-Variant Linear Channels,” IEEE Trans. on Communications Systems, Vol.11, No.4, pp. 360-393, December 1963.

[14]. E. Bingham, and A. Hyvarinen, “A Fast Fixed-Point Algorithm for Independent Component Analysis of Complex-Valued Signals,” International Journal of Neural Systems, Vol.10, No.1, pp. 1-8, 2000.

[15]. John A. C. Bingham, “Mutlicarrier Modulation for Data Transmission: An Idea Whose Time Has Come,” IEEE Communications Magazine, Vol. 28, No. 5, pp. 5-14, May 1990.

[16]. V. Capdevielle, Ch. Serviere, and J. L. Lacoume, “Blind Separation of Wide-Band Sources in the Frequency Domain,” in Proc. of International Conference on Acoustics, Speech, and Signal Processing, Detroit, USA, May 1995, pp. 2080-2083.

[17]. Jean-Francois Cardoso, “Blind Signal Separation: Statistical Principles,” Proceedings of THE IEEE, Vol. 86, No.10, pp 2009-2025, Oct. 1998.

[18]. Jean-Francois Cardoso, “High-Order Contrasts for Independent Component Analysis,” Neural Computation, Vol. 11, pp 157-192, 1999.

[19]. Jean-Francois Cardoso, and Beate Hvam Laheld, “Equivariant Adaptive Source Separation,” IEEE Trans. on Signal Processing, Vol. 44, No.12, pp. 3017-3030, Dec. 1996.

[20]. Vasu Chakravarthy, Abel S. Nunez, James P. Stephens, Arnab K. Shaw, and Michael A. Temple, “TDCS, OFDM, and MC-CDMA: A Brief Tutorial,” IEEE Radio Communications, Vol. 43, No. 9, pp. S11- S16, September 2005.

[21]. Robert W. Chang, “Synthesis of Band-Limited Orthogonal Signals for Multichannel Data Transmission,” Bell System Tech. Journal, Vol. 45, pp. 1775-1796, Dec. 1966.

[22]. Biao Chen, and Hao Wang, “Blind Estimation of OFDM Carrier Frequency Offset via Oversampling,” IEEE Trans. on Signal Processing, Vol. 52, No. 7, pp. 2047-2057, July 2004.

[23]. Binning Chen, and Athina P. Petropulu, “Frequency Domain Blind MIMO System Identification Based on Second- and Higher-Order Statistics,” IEEE Trans. on Signal Processing, Vol. 49, No. 8, pp.1677-1688, August 2001.

[24]. Andrzej Cichocki, and Shun-ichi Amari, Adaptive Blind Signal and Image processing: learning Algorithms and Applications, John Wiley & Sons, 2002.

[25]. Wonzoo Chung, and C. Richard Johnson, “Blind Carrier Frequency Offset Synchronization for OFDM Systems based on High Order Statistics,” in Proc. of Conference of on Information Science and Systems, Princeton, NJ, USA, March 2002, pp. 624-629.

[26]. Leonard J. Cimini, “Analysis and Simulation of a Digital Mobile Channel Using Orthogonal Frequency Division Multiplexing,” IEEE Trans. on Communications, Vol. 33, No. 7, pp. 665-675, July 1985.

[27]. Pierre Comon, “Independent Component Analysis, A new Concept,” Signal Processing, Vol. 36, No. 3, pp. 287-314, April 1994.

[28]. Ronald E. Crochiere, and Lawrence R. Rabiner, Multirate Digital Signal Processing, Prentice-Hall, Englewood Cliffs, New Jersey, 1983.

[29]. Adriana Dapena, Monica F. Bugallo, and Luis Castedo, “Separation of Convolutive Mixtures of Temporally-White Signals: A Novel Frequency-Domain Approach,” in Proceeding of Third International Conference on Independent Component Analysis and Blind Signal Separation, San Diego, California, USA, December 2001, pp. 179-184.

[30]. Adriana Dapena, and Luis Castedo, “Blind source Separation in the Frequency Domain: A novel Solution to the Amplitude and the Permutation Indeterminacies,” in Proceeding of International Work-Conference on Artificial Neural Networks, Granada, Spain , June 2001, pp. 603-610.

[31]. Konstantinos I. Diamantaras, “Blind Separation of Multiple Binary Sources Using a Single Linear Mixture,” in Proceedings of IEEE International Conference Acoustics, Speech, and Signal Processing, Istanbul, Turkey, June 2000, pp. 2889-2892.

[32]. Scott C. Douglas, “Blind Source Separation: Criteria, Algorithms, and Applications,” Tutorial 9, IEEE International Conference on Acoustics, Speech, and Signal Processing, Orlando, Florida, USA, May 2002.

[33]. Christian Dubuc, David Starks, Tim Creasy, and Yong Hou, “A MIMO-OFDM Prototype for Next-Generation Wireless WANS,” IEEE Communications Magazine, Vol. 42, No. 12, pp. 82- 87, Dec. 2004.

[34]. Carl Eklund, Roger B. Marks, Kenneth L. Stanwood, and Stanley Wang, “IEEE Standard 802.16: A Technical Overview of the WirelessMAN™ Air Interface Broadband Wireless Access,” IEEE Communications Magazine, Vol.40, No.6, pp. 98-107, June 2002.

[35]. Bernard Le Floch, Michel Alard, and Claude Berrou, “Coded Orthogonal Frequency Division Multiplex,” Proceedings of THE IEEE, Vol. 83, No. 6, pp. 982-996, June 1995.

[36]. L. A. Gardner Jr., “Problem 69-14, Sums of Inverse Power of Cosine,” Solution of by M. E. Fisher, SIAM Review, Vol. 13, pp. 116-119, 1971.

[37]. M. Ghogho, A. Swami, and G. B. Giannakis, “Optimized Null-Subcarrier Selection for CFO Estimation in OFDM over Frequency-Selective Fading Channels,” in Proc. of IEEE GLOBECOM, San Antonio, TX, USA, Nov. 2001, pp. 202-206.

[38]. M. Ghogho, and A. Swami, “Blind Frequency-Offset Estimator for OFDM Systems Transmitting Constant-Modulus Symbols,” IEEE Communications Letters, Vol. 6, No. 8, pp. 343-345, August 2002.

[39]. Arunabha Ghosh, David R. Wolter, Jeffrey G. Andrews, and Runhua Chen, “Broadband Wireless Access with WiMax/802.16: Current Performance

Benchmarks and Future Potential," IEEE Communications Magazine, Vol. 43, No. 2, pp. 129- 136, Feb. 2005.

[40]. Georgios B. Giannakis, Yingbo Hu, Petre Stoica, and Lang Tong, Signal Processing Advances in Wireless and Mobile Communications Volume 1: Trends in Channel Estimation and Equalization, Prentice Hall, 2002.

[41]. Georgios B. Giannakis, Yingbo Hu, Petre Stoica, and Lang Tong, Signal Processing Advances in Wireless and Mobile Communications Volume 2: Trends in Single- and Multi-User Systems, Prentice Hall, 2002.

[42]. Xavier Giannakopoulos, Juha Karhunen, and Erkki Oja, "An Experimental Comparison of Neural Algorithm for Independent Component Analysis and Blind Separation," Int. Journal of Neural Systems, Vol. 9, No. 2, pp. 99-114, April 1999.

[43]. Dominique N. Godard, "Self-Recovering Equalization and Carrier Tracking in Two-Dimensional Data Communication System," IEEE Trans. on Communications, Vol.28, No.11, pp. 1867-1875, Nov. 1980.

[44]. Robert M. Gray. (2000, August). Toeplitz and Circulant Matrices: A Review. [Online]. Available: http://www-ee.stanford.edu/~gray/toeplitz.pdf.

[45]. Olivier Grellier, and Pierre Comon, "Blind Separation of Discrete Sources," IEEE Signal Processing Letters, Vol. 5, No. 8, pp.212-214, August 1998.

[46]. Erik Haas, and Stefan Kaiser, “Analysis of Two-Dimensional Differential Demodulation for OFDM,” in Proc. of IEEE Global Telecommunications Conf., Nov./Dec. 2000, pp. 751–755.

[47]. Shinsuke Hara, and Ramjee Prasad, “Overview of Multicarrier CDMA,” IEEE Communications Magazine, Vol. 35, No. 12, pp. 126-133, December 1997.

[48]. Homayoun Hashemi, “The Indoor Radio Propagation Channel,” Proceedings of The IEEE, Vol. 81, No. 7, pp. 943-968, July 1993.

[49]. Simon Haykin, Adaptive Filter Theory, Fourth Edition, Prentice Hall, 2001.

[50]. Simon Haykin, Unsupervised Adaptive Filtering Volume 1: Blind Source Separation, John Wiley & Sons, Inc., New York, 2000.

[51]. Meng-Han Hsieh, and Che-Ho Wei, “A Low-Complexity Frame Synchronization and Frequency Offset Compensation Scheme for OFDM Systems over Fading Channels,” IEEE Trans. on Vehicular Technology, Vol. 48, No. 5, pp.1596-1609, Sep. 1999.

[52]. Yiteng Huang, and Jacob Benesty, Audio Signal Processing for Next-Generation Multimedia Communication Systems, Kluwer Academic Publishers, 2004.

[53]. Aapo Hyvarinen, Juha Karhunen and Erkki Oja, Independent Component Analysis, John Wiley & Sons, Inc., 2001.

[54]. Aapo Hyvarinen, and Erkki Oja, “Independent Component Analysis: Algorithm and Applications,” Neural Networks, Vol. 13, pp. 411-430, 2000.

[55]. Aapo Hyvarinen, and Erkki Oja, “A Fast Fixed-Point Algorithm for Independent Component Analysis,” Neural Computation, Vol. 9, pp. 1483-1492, 1997.

[56]. Aapo Hyvarinen, “Fast and Robust Fixed-Point Algorithm for Independent Component Analysis,” IEEE Trans. on Neural Network, Vol. 10, No.3, pp. 626-634, May 1999.

[57]. Aapo Hyvarinen, “The Fixed-Point Algorithm and Maximum Likelihood Estimation for Independent Component Analysis,” Neural Processing Letters, Vol. 10, No. 1, pp. 1-5, August 1999.

[58]. Mohamed Ibnkahla, Signal Processing for Mobile Communications Hand book, CRC Press, Boca Raton, Florida, USA, 2005.

[59]. Shiro Ikeda, and Noboru Murata, “A Method of ICA in Time-Frequency Domain,” in Proceedings of International Workshop on Independent Component Analysis and Blind Signal Separation, Aussions, France, January 1999, pp. 365-371.

[60]. C. Richard Johnson, Philip Schniter, Thomas J. Endres, James D. Behm, Donald R. Brown, and Raul A. Casas, “Blind Equalization Using the Constant Modulus Criterion: A Review,” Proceedings of The IEEE, Vol. 86, No. 10, pp. 1927-1950, October 1998.

[61]. Steven M. Kay, Fundamentals of Statistical Signal Processing: Estimation Theory, Prentice Hall, Englewood Cliffs, New Jersey, 1993.

[62]. Ivica Kostanic, Independent Component Analysis Based Interference Reduction in Cellular Systems with Co-Channel Interference, Ph.D. dissertation, University of Central Florida, Spring 2003.

[63]. Ivica Kostanic, and Wasfy Mikhael, “Independent Component Analysis Based QAM Receiver,” Digital Signal Processing, Vo.14, No.3, pp. 241-252, May 2004.

[64]. Russel H. Lambert, Multichannel Blind Deconvolution: FIR Matrix Algebra and Separation of Multipath Mixtures, Ph.D. dissertation, University of South California, 1996.

[65]. Hui Liu, and Ufuk Tureli, “A High-Efficiency Carrier Estimator for OFDM Communications,” IEEE Communication Letters, Vol. 2, No. 4, pp. 104-106, April 1998.

[66]. Yuan Liu, and Wasfy Mikheal, “Blind Source Separation for Frequency Dependent Channels,” in Proceeding of The 46th IEEE International Midwest Symposium On Circuit and System, Cairo, Egypt, Dec. 2003 (Top Ten Contributions over 500 papers).

[67]. Yuan Liu, and Wasfy Mikhael, “Practical Frequency Domain ICA Algorithm Capable of Solving Permutation and Gain Ambiguities for Digital Communication System,” IEE Electronics Letters, Vol. 40, No.13, pp. 839-840, June 2004.

[68]. Yuan Liu, and Wasfy Mikheal, “Frequency-Domain Independent Component Analysis for MIMO Systems over Frequency-Selective Channels,” WSEAS Transactions on Signal Processing, Vol. 1, No. 3, pp. 411-418, December 2005.

[69]. Yuan Liu, and Wasfy Mikheal, “A Novel Frequency-Domain Independent Component Analysis Approach for Wireless Communications,” in Proceeding of 4th WSEAS International Conference on Electronics, Control, and Signal Processing, Miami, Florida, USA, Nov. 2005, pp. 187-192.

[70]. Yuan Liu, and Wasfy Mikheal, “A Novel Intercarrier Interference Cancellation Approach based on BSS in OFDM,” in Proceeding of The 41st Space Congress, Cape Canaveral, Florida, USA, April 2004.

[71]. Yuan Liu, and Wasfy Mikheal, “A Blind Intercarrier Interference Cancellation Approach in Differential Modulation OFDM Communication Systems,” in Proceeding of IASTED International Conference on Circuits, Signal, and Systems, Tampa, Florida, USA, Dec. 2004, pp. 178-181.

[72]. Yuan Liu, and Wasfy Mikheal “A Blind Maximum Likelihood Carrier Frequency Offset Correction Approach for OFDM Systems over Multipath Fading Channels,” submitted in Sep. 2005 to the Journal of Circuits, Systems, and Signal Processing.

[73]. Yuan Liu, and Wasfy Mikheal, “Blind Carrier Frequency Offset Estimation for OFDM Systems Based on Kurtosis,” in Proceeding of The 48th IEEE

International Midwest Symposium On Circuit and System, Cincinnati, Ohio, USA, August 2005.

[74]. Yuan Liu, and Wasfy Mikheal, “High-Performance Blind Carrier Frequency Offset Estimation for OFDM Systems,” submitted in August 2005 to the Journal of Circuits, Systems, and Computers.

[75]. Yuan Liu, and Wasfy Mikheal, “A Hybrid Independent Component Analysis Algorithm with Fast Convergence and High Accuracy,” under preparation.

[76]. V. Lottici, M. Luise, M. Marselli, and R. Reggiannimi, ”Blind Subcarrier Frequency Ambiguity Resolution for OFDM Signals over Selective Channels,” IEEE Trans. on Communications, Vol. 52, No. 9, pp. 1532-1537, Sep. 2004.

[77]. Marco Luise, and Ruggero Reggiannini, “Carrier Frequency Acquisition and Tracking for OFDM Systems,” IEEE Trans. on Communications, Vol. 44, No. 11, pp.1185-1191, Nov. 1996.

[78]. Marco Luise, Marco Marselli, and Ruggero Reggiannini, “Low-Complexity Blind Carrier Frequency Recovery for OFDM signals Over Frequency-Selective Radio Channels,” IEEE Trans. on Communications, Vol. 50, No. 7, pp.1182-1188, July 2002.

[79]. Odile Macchi, and Eric Moreau, “Adaptive Unsupervised Separation of Discrete Sources,” Signal Processing, Vol. 73, No.1-2, pp. 49-66, January 1999.

[80]. Ali Mansour, Allan Kardec Barros, and Noboru Ohnishi, “Blind Separation of Sources: Methods, Assumptions and Applications,” IEICE Trans. Fundamentals, Vol. E83-A, No. 8, pp. 1498 – 1512, August 2003.

[81]. Ali Mansour, and Mitsuru Kawamoto, “ICA Papers Classified According to their Application and Performance,” IEICE Trans. Fundamentals, Vol. E86-A, No. 3 pp. 620 – 633, March 2003.

[82]. Heinz Mathis, Marcel Joho, and George S. Moschytz, “A Simple Threshold Nonlinearity for Blind Separation of Sub-Gaussian Signals,” in Proceeding of IEEE International Symposium on Circuits and Systems, Geneva, Switzerland, May 2000, pp. 489-492.

[83]. Cristina Mejuto, Adriana Dapena, and Luis Castedo, “Frequency-Domain Informax for Blind Separation of Convolutive Mixtures,” in Proc. of International Workshop on Independent Components Analysis and Blind Signal Separation, Helsinki, Finland, June 2000, pp. 315-320.

[84]. Paul H. Moose, “A Technique for Orthogonal Frequency Division Multiplexing Frequency Offset Correction,” IEEE Trans. on Communications, Vol. 42, No. 10, pp. 2908-2914, Oct. 1994.

[85]. M. Morelli, A. N. D’Andrea, and U. Mengali, “Frequency Ambiguity Resolution in OFDM Systems,” IEEE Communications Letters, Vol. 4, No. 4, pp. 134-136, April 2000.

[86]. Noboru Murata, Shiro Ikeda, and Andreas Ziehe, “An Approach to Blind Source Separation Based on Temporal Structure of Speech Signals,” Neurocomputing, Vol. 41, pp. 1-24, 2001.

[87]. S. Hamid Nawab, and Thomas F. Quatieri, “Short-Time Fourier Transform,” In Advanced Topics on Signal Processing, edited by Jae S. Jim, and Alan V. Oppenheim, pp. 289-337, Prentice Hall, New Jersey, USA, 1988.

[88]. Richard van Nee, and Ramjee Prasad, OFDM for Wireless Multimedia Communications, Artech House Publisher, 2000.

[89]. Alvan V. Oppenheim, Ronald W. Schafer, and John R. Buck, Discrete-Time Signal Processing, Prentice Hall, New Jersey, USA, 1999.

[90]. Petteri Pajunen, “Blind Source Separation using algorithm information theory,” Neural Computation Vol.22, pp 35-48, 1998.

[91]. Athanasios Papoulis, and Pillai, S., Unnikrishna, Probability, Random Variables, and Stochastic Processes, fourth Edition., McGraw Hill, 2002.

[92]. Hyung-Min Park, Ho-Young Jung, Te-Won Lee, and Soo-Young Lee, “Subband-based Blind Signal Separation for Noisy Speech Recognition,” IEE Electronics Letters, Vol. 35, No. 23, pp. 2011-2012, November 1999.

[93]. Arogyswami J. Paulraj, Dhananjay A. Gore, Rohit U. Nabar, and Helmut Bolcskei, “An Overview of MIMO Communications – A Key to Gigabit Wireless,” Proceedings of THE IEEE, Vol.92, No. 2, pp. 198-218, Feb. 2004.

[94]. Thierry Pollet, Mark Van Bladel, and Marc Moeneclaey, “BER Sensitivity of OFDM System to Carrier Frequency Offset and Wiener Phase Noise,” IEEE Trans. on Communications, Vol. 43, No. 2/3/4, pp. 191-193, Feb./March/April 1995.

[95]. K. J. Pope, and R.E. Bogner, “Blind Signal Separation I: Linear, Instantaneous Combinations,” Digital Signal Processing, Vol. 6, pp 5-16, 1996.

[96]. K. J. Pope, and R.E. Bogner, “ Blind Signal Separation II: Linear, Convolutive Combinations,” Digital Signal Processing, Vol. 6, pp 17-28, 1996.

[97]. John G. Proakis, Digital Communication, Fourth Edition, McGraw-Hill, 2001.

[98]. John G. Proakis, and Dimitris G. Manolakis, Digital Signal Processing: Principles, Algorithm, and Applications, Third Edition, Prentice Hall, 1996.

[99]. Kamran Rahbar, and James P. Reilly, “A New Frequency Domain Method for Blind Source Separation of Convolutive Audio Mixtures,” online source, http://www.ece.mcmaster.ca/~reilly/assp_02_daft8.pdf.

[100]. Theodore S. Rappaport, Wireless Communication: Principle and Practice, Prentice Hall, 1996.

[101]. C. Reiners, and H. Rohling, “Multicarrier Transmission Technique in Cellular Mobile Communications Systems,” in Proc. of IEEE 44th Vehicular Technology Conf., Stockholm, Sweden, June 1994, pp. 1645-1649.

[102]. Hermann Rohling, Thomas May, Karsten Bruninghaus, and Rainer Grunheid, "Broad-band OFDM Radio Transmission for Multimedia Application," Proceedings of THE IEEE, Vol. 87, No. 10, pp. 1778-1789, Oct. 1999.

[103]. Giovanni Santella, "A Frequency and Symbol Synchronization System for OFDM Signals: Architecture and Simulation Results," IEEE Trans. On Vehicular Technology, Vol. 49, No.1, pp. 254-275, January 2000.

[104]. Hikmet Sari, Georges Karam, and Isabelle Jeanclaude, "Transmission Technique for Digital Terrestrial TV Broadcasting," IEEE Communications Magazine, Vol. 33, No.2, pp. 100-109, February 1995.

[105]. Hiroshi Sawada, Ryo Mukai, Shoko Araki, and Shoji Makino, "A Robust and Precise Method for Solving the Permutation Problem of Frequency-Domain Blind Source Separation," IEEE Trans. on Speech and Audio Processing, Vol.12, No.5, pp. 530-538, September 2004.

[106]. T. M. Schmidl, and D. C. Cox, "Robust Frequency and Timing Synchronization for OFDM," IEEE Trans. on Communications, Vol. 45, No. 12, pp.1613-1621, Dec. 1997.

[107]. T. M. Schmidl, and D. C. Cox, "Blind Synchronisation for OFDM," IEE Electronics Letters, Vol.33, pp.113-114, Feb. 1997.

[108]. Daniel W. E. Schobben, and Piet C. W. Sommen, "A Frequency Domain Blind Signal Separation Method Based on Decorrelation," IEEE Trans. on Signal Processing, Vol 50, No 8, pp. 1855-1865, Aug. 2000.

[109]. Ch. Serviere, and V. Capdevielle “Blind Adaptive Separation of Wide-Band Sources,” in Proceeding of IEEE International Conference on Acoustic, Speech, and Signal Processing (ICASSP) Atlanta, Georgia, USA, 1996, pp. 2698-2701.

[110]. Ch. Serviere, “Feasibility of Source Separation in Frequency Domain,” in Proceedings of IEEE International Conference on Acoustics, Speech, and Signal Processing, Seattle, Washington, USA, May 1998, pp. 2085–2088.

[111]. Bernard Sklar, Digital Communications: Fundamental and Application, Second Edition, Prentice Hall, 2001.

[112]. Bernard Sklar, “Rayleigh Fading Channels in Mobile Digital Communication Systems Part I: Characterization,” IEEE Communications Magazine, Vol.35, No. 9, pp. 136-146, September 1997.

[113]. Bernard Sklar, “Rayleigh Fading Channels in Mobile Digital Communication Systems Part II: Mitigation,” IEEE Communications Magazine, Vol.35, No. 9, pp. 148-155, September 1997.

[114]. Paris Smaragdis, “Blind Separation of Convolved Mixtures in the Frequency Domain,” Neurocmputing, Vol. 22, pp. 21-34, 1998.

[115]. Paris Smaragdis, Information Theoretic Approaches to Source Separation, Masters Thesis, Massachusetts Institute of Technology, http://web.media.mit.edu/~paris/ica.html.

[116]. Gordon L. Stuber, John R. Barry, Steve W. Mclaughlin, Ye Li, Mary Ann Ingram, and Thomas G. Pratt, "Broadband MIMO-OFDM Wireless Communications," Proceedings of The IEEE, Vol.92, No. 2, pp. 271-294, Feb. 2004.

[117]. John Terry, and Juha Heiskala, OFDM Wireless LANs: A Theoretical and Practical Guide, Sams Publishing, Indianapolis, Indiana, USA, 2002.

[118]. Lang Tong, Ruey-wen Liu, Victor C. Soon, and Yih-Fang Huang, "Indeterminacy and Identifiability of Blind Identification," IEEE Trans. on Circuits and Systems, Vol. 38, No. 5, pp. 499-509, May 1991.

[119]. Kari Torkkola, "Blind Separation of Radio Signals in Fading Channels," Advances in Neural Information Processing Systems, Vol.10, , pp.756-762, Dec. 1997.

[120]. Kari Torkkola, "Blind Signal Separation in Communications: Making Use of Known Signal Distributions," in Proceeding of IEEE DSP Workshop, Bryce Canyon, UT, USA, August 1998.

[121]. Ufuk Tureli, Hui Liu, and Michael D. Zoltowski, "OFDM Blind Carrier Offset Estimation: ESPRIT," IEEE Trans. on Communication, Vol. 48, No. 9, pp. 1459-1461, Sep. 2000.

[122]. Ufuk Tureli, Didem Kivanc, and Hui Liu, "Experimental and Analytical Studies on a High-Resolution OFDM Carrier Frequency Offset Estimator," IEEE Trans. on Vehicular Technology, Vol. 50, No. 2, pp. 629 – 643, March 2001.

[123]. Ehud Weistein, Meir Feder, and Alan V. Oppenheim, “Multi-Channel Signal Separation by Decorrelation,” IEEE Trans. on Speech and Audio Processing, Vol. 1, No. 4, pp. 405 - 413. October 1993.

[124]. S. B. Weistein, and Paul M. Ebert, “Data Transmission by Frequency-Division Multiplexing Using the Discrete Fourier Transform,” IEEE Trans. on Communications Technology, Vol. 19, No. 5, pp. 628-634, October 1971.

[125]. Bernard Widow, and Samuel D. Stearns, Adaptive Signal Processing, Prentice Hall, 1985.

[126]. Hongwei Yang, “A road to Future Broadband Wireless Access: MIMO-OFDM-Based Air Interface,” IEEE Communications Magazine, Vol.43, No.1, pp.53-60, January 2005.

[127]. Tianyu Yang, General Interference Suppression Techniques for Diversity Wireless Receivers In Fading Channels Based on Independent Component Analysis, Ph.D. dissertation, University of Central Florida, Fall 2004.

[128]. Yingwei Yao, and Georgios B. Giannakis, “Blind Carrier Frequency Offset Estimation in SISO, MIMO and Multiuser OFDM Systems,” IEEE Trans. On Communications, Vol. 53, No. 1, pp. 173-183, Jan. 2005.

[129]. Yuping Zhao, and Sven-Gustav Haggman, “Intercarrier Interference Self-Cancellation Scheme for OFDM Mobile Communication System,” IEEE Trans. on Communications, Vol. 49, No. 7, pp.1185-1191, July 2001.

[130]. William Y. Zou, and Yiyan Wu, “COFDM: An Overview,” IEEE Trans. on Broadcasting, Vol. 41, No. 1, pp.1-8, March 1995.

[131]. IEEE, “Supplement to IEEE Standard for Information Technology - Telecommunications and Information Exchange Between Systems – Local and Metropolitan Area Network – Specific Requirements – Part 11: Wireless LAN MAC and PHY Layer Specifications: High-Speed Physical Layer in the 5GHZ Band,” P802.11a/D7.0, July 1999.

[132]. IEEE, “IEEE Standard for Local and metropolitan area networks – Part 16: Air Interface for Fixed Broadband Wireless Access Systems,” IEEE Std. 802.16, October 2004.